AFRL-RV-PS-
TR-2015-0109

NASCAP-2K VERSION 4.2 SCIENTIFIC DOCUMENTATION

V. A. Davis and M. J. Mandell

Leidos, Inc
10260 Campus Point Drive, Mailstop C4
San Diego, CA 92121

31 October 2014

Technical Report

AIR FORCE RESEARCH LABORATORY
Space Vehicles Directorate
3550 Aberdeen Ave SE
AIR FORCE MATERIEL COMMAND
KIRTLAND AIR FORCE BASE, NM 87117-5776

DTIC COPY

NOTICE AND SIGNATURE PAGE

Using Government drawings, specifications, or other data included in this document for any purpose other than Government procurement does not in any way obligate the U.S. Government. The fact that the Government formulated or supplied the drawings, specifications, or other data does not license the holder or any other person or corporation; or convey any rights or permission to manufacture, use, or sell any patented invention that may relate to them.

This report was cleared for public release by the 377 ABW Public Affairs Office and is available to the general public, including foreign nationals. Copies may be obtained from the Defense Technical Information Center (DTIC) (http://www.dtic.mil).

AFRL-RV-PS-TR-2015-0109 HAS BEEN REVIEWED AND IS APPROVED FOR PUBLICATION IN ACCORDANCE WITH ASSIGNED DISTRIBUTION STATEMENT.

//SIGNED//	//SIGNED//
Adrian Wheelock	Glenn M. Vaughan, Colonel, USAF
Project Manager, AFRL/RVBXR	Chief, Battlespace Environment Division

This report is published in the interest of scientific and technical information exchange, and its publication does not constitute the Government's approval or disapproval of its ideas or findings.

REPORT DOCUMENTATION PAGE

Form Approved
OMB No. 0704-0188

1. REPORT DATE *(DD-MM-YYYY)*	**2. REPORT TYPE**	**3. DATES COVERED** *(From - To)*
31-10-2014	Technical Report	19 Sep 2011 to 31 Oct 2014

4. TITLE AND SUBTITLE
Nascap-2k Version 4.2 Scientific Documentation

5a. CONTRACT NUMBER
FA9453-11-C-0262

5b. GRANT NUMBER

5c. PROGRAM ELEMENT NUMBER
62601F

6. AUTHOR(S)
V. A. Davis and M. J. Mandell

5d. PROJECT NUMBER
1010

5e. TASK NUMBER
PPM00012836

5f. WORK UNIT NUMBER
EF003277

7. PERFORMING ORGANIZATION NAME(S) AND ADDRESS(ES)
Leidos, Inc.
10260 Campus Point Drive, Mailstop C4
San Diego, CA 92121

8. PERFORMING ORGANIZATION REPORT NUMBER

9. SPONSORING / MONITORING AGENCY NAME(S) AND ADDRESS(ES)
Air Force Research Laboratory
Space Vehicles Directorate
3550 Aberdeen Avenue SE
Kirtland AFB, NM 87117-5776

10. SPONSOR/MONITOR'S ACRONYM(S)
AFRL/RVBXR

11. SPONSOR/MONITOR'S REPORT NUMBER(S)
AFRL-RV-PS-TR-2015-0109

12. DISTRIBUTION / AVAILABILITY STATEMENT
Approved for public release; distribution is unlimited. (377ABW-2015-0419 dtd 28 May 2015)

13. SUPPLEMENTARY NOTES

14. ABSTRACT

Nascap-2k is a spacecraft charging and plasma interactions code designed to be used by spacecraft designers, aerospace and materials engineers, and space plasma environments experts to study the effects of both the natural and spacecraft-generated plasma environments on spacecraft systems.

This document describes the physics and numeric models used in the surface charging, potential solution, and particle tracking portions of the code.

15. SUBJECT TERMS
Nascap-2k, Spacecraft Charging, Space Environment

16. SECURITY CLASSIFICATION OF:			**17. LIMITATION OF ABSTRACT**	**18. NUMBER OF PAGES**	**19a. NAME OF RESPONSIBLE PERSON**
a. REPORT	**b. ABSTRACT**	**c. THIS PAGE**			Adrian Wheelock
Unclassified	Unclassified	Unclassified	Unlimited	94	**19b. TELEPHONE NUMBER** *(include area code)*

This page is intentionally left blank.

TABLE OF CONTENTS

LIST OF FIGURES

Page

This page is intentionally left blank.

1 INTRODUCTION

Nascap-2k is a spacecraft charging and plasma interactions code designed to be used by spacecraft designers, aerospace and materials engineers, and space plasma environments experts to study the effects of both the natural and spacecraft-generated plasma environments on spacecraft systems.

Designers of spacecraft for government, commercial, and research purposes require advanced modeling capabilities to guide the design of satellites that can survive and operate properly in the natural environment. Computer modeling of flight experiments (such as SCATHA (Spacecraft Charging at High Altitude),[1] the SPEAR (Space Power Experiments Aboard Rockets)[2,3] series, and CHAWS (Charging Hazards and Wake Studies)[4]) has demonstrated excellent ability to predict both steady-state and dynamic interactions between high-voltage spacecraft and the ambient plasma. This ability was also extended to inherently dynamic problems involving three-dimensional space charge sheath formation, current flow in the quasi-neutral presheath, breakdown phenomena, plasma kinetics, ionization processes, and the effect of unsteady processes on spacecraft charging.

Nascap-2k encapsulates the knowledge gained in these efforts as well as in modeling spacecraft with unique requirements and destined for disparate environments. This gives the spacecraft designer quality modeling capabilities by taking advantage of the present understanding of the pertinent phenomena, employing advanced algorithms, and implementing a state-of-the-art user interface, including three-dimensional post-processing graphics.

The core capabilities of *Nascap-2k* are as follows:

- Define spacecraft surfaces and geometry and the structure of the computational space surrounding the spacecraft.
- Solve for time-dependent potentials on spacecraft surfaces.
- Solve the electrostatic potential around the object, with flexible boundary conditions on the object and with space-charge computed either fully by particles, fully analytically, or in a hybrid manner.
- Generate, track, and otherwise process particles of various species, represented as macro-particles, in the computational space.
- View surface potentials, space potentials, particle trajectories, and time-dependent potentials and currents.

Nascap-2k calculates surface charging in tenuous plasma environments, such as geosynchronous earth orbit (GEO) and interplanetary (Solar Wind) environments, using the Boundary Element Method[5] (BEM). The Boundary Element Method facilitates calculation of surface electric fields (which limit the emission of photoelectrons and secondary electrons) without the need to grid the space surrounding the spacecraft. It also enables *Nascap-2k* to anticipate electric field changes due to surface charging, resulting in a smoother and more stable charging simulation.

Nascap-2k uses a high-order, finite-element representation for the electrostatic potential that ensures electric fields are strictly continuous throughout space. The electrostatic potential solver

uses a finite element/conjugate gradient technique to solve for the potentials and fields on the spacecraft surface and throughout the surrounding space. Space charge density models presently include Laplacian, Linear, Nonlinear, Frozen Ions, Consistent with Ion Density, Full PIC (Particle-in-Cell), and Hybrid PIC.

Particle tracking is used to simulate sheath currents, to study detector response, or to generate space charge evolution for dynamic calculations. *Nascap-2k* generates macroparticles (each of which represents a collection of particles) at a sheath boundary, the problem boundary, specified surface elements, throughout all space, or at user-specified locations. Particles are tracked for a specified amount of time, with the timestep automatically subdivided at each step of each particle to maintain accuracy. The current to each surface element of the spacecraft and optionally through each volume element is recorded for further processing.

Nascap-2k User's Manual is the primary document on the use of the code. This document, *Nascap-2k Scientific Documentation*, describes the physics and numeric models used in the surface charging, potential solution, and particle tracking portions of the code. Section 2, Physical Models, describes the physics models included in the code. Section 3, Numeric Models, describes the implementation.

2 PHYSICAL MODELS

Nascap-2k incorporates physical models appropriate to both tenuous (e.g., GEO orbit or interplanetary missions) and dense (e.g., LEO orbit) plasma environments. The code solves for environmentally-induced time-dependent potentials on spacecraft surfaces, the electrostatic potential about the object, and the resulting charged particle motion.

Time-dependent surface currents are computed using orbit limited currents in tenuous plasma, tracked currents and/or analytic approximations in dense plasma, or a combination in intermediate environments.

The electrostatic potential solver uses a conjugate gradient technique with flexible boundary conditions to solve Poisson's equation for the potentials and fields throughout the computational space. Several analytic and numeric space charge density models are available.

Particle tracking is used to study sheath currents, to study detector response, to generate steady-state charge densities, and to generate space charge evolution for dynamic calculations.

2.1 Surface Charging from Orbit Limited Currents

Spacecraft surface charging is the accumulation of charge on spacecraft surfaces. As illustrated in Figure 1, several different current components can contribute to the charging.[6,7,8,9] First there are the incident charged particles. The impact of high-energy electrons and ions causes the ejection of secondary electrons into space. Incident electrons can also be reflected as backscatter. In sunlight, solar ultraviolet radiation generates low-energy photoelectrons which are ejected from the surface. Due to the low mass of electrons, the incident electron current is generally higher than the ion current. By itself, this would lead to negative charging. However, with the inclusion of the other terms, all of which contribute positive current, the net charge can be either positive or negative.

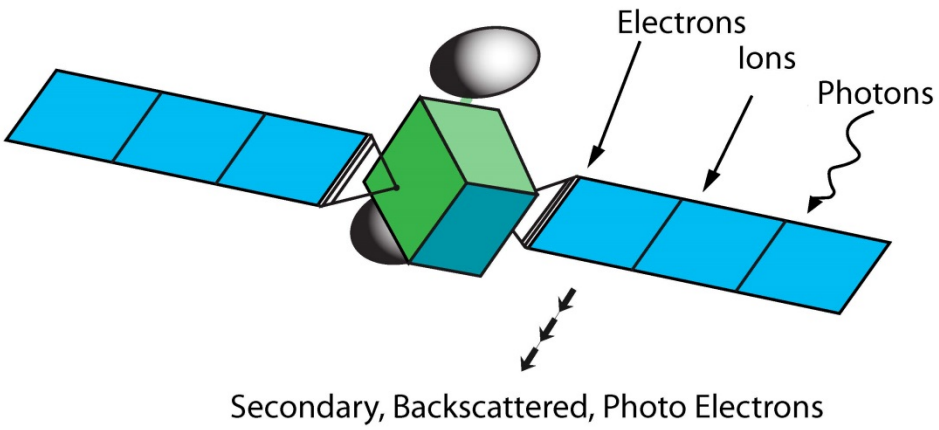

Figure 1. High Negative Potentials Can Result from the Accumulation of Charge on Spacecraft Surfaces.

The rest of the spacecraft influences the potential and local electric field of each surface. Each conductor and each insulating spacecraft surface collects current from the plasma and is capacitively and resistively coupled to the other conductors and other surfaces. Additionally, some spacecraft have current sources, such as electron and ion guns, that contribute to the net current. *Nascap-2k* uses the spacecraft geometry, surface materials, plasma environment, and sun intensity and direction to calculate the time history of the surface potentials, electric fields, and fluxes.

If the net current is initially negative or positive, the exposed surface begins to acquire a negative or positive potential respectively. As the magnitude of the potential increases, the net current is attenuated, until it eventually approaches zero and the surface potential reaches its equilibrium value. Negative potentials as high as ten kilovolts have been observed during geosynchronous substorms and over one kilovolt during auroral precipitation events. Because positive currents generally result from emission of low energy secondary electrons and photoelectrons, the positive potentials that can be attained are relatively modest. As soon as the surface reaches a potential greater than that of the emitted electrons they are re-attracted to the surface, so their contribution to the current is suppressed. The equilibrium potential is determined by the suppression of low energy electron emission due to the surface's own electric field. A similar suppression effect may occur due to the electric fields of neighboring negative charged surfaces. This effect is the primary reason that accurate spacecraft surface charging calculations are inherently three dimensional.

Positive potentials up to 100 V are possible in environments where the plasma current is small compared with the photo current (outer magnetosphere and in the solar wind). In these environments, the small incident plasma current is balanced by escape of the high energy tail of the photoelectron energy distribution, even though the bulk of the emitted photoelectrons return to the surface.

Nascap-2k models the spacecraft as a collection of surfaces that are either conductive or are a dielectric film over a conductive substrate. The conductive surfaces and substrates can be at the same potential or biased with respect to each other.

2.1.1 Plasma Environment

In the orbit limited approximation of the current incident on a surface, the flux is calculated as that incident on a sphere of the same potential and depends only on the surface potential, and optionally an angle with respect to the direction of flow. This approximation applies if any charged particle far from the spacecraft can reach the surface, that is, there are no excluded orbits. For spacecraft this is generally true if the Debye length is long compared with the spacecraft size and the spacecraft is essentially convex with no self-shading. Calculations using the "Surface Charging" with "Analytic Currents" option use this approximation for both species, and calculations using the "Surface Charging" with "Tracked Ions and Analytic Electron Currents" option use this approximation for electron currents.

The analytic current density to a surface at potential ϕ is given by integrating over the distribution function.

$$j = q\int_L^\infty \frac{2Ee^2}{m^2}\left(\frac{E}{E \pm \phi}\right) f(E \pm \phi)dE = q\int_L^\infty \left(\frac{E}{E \pm \phi}\right) F(E \pm \phi)dE \tag{1}$$

Where the integration variable E represents the energy at the surface, the integration limit L is 0 for the repelled species and $|\phi|$ for the attracted species, the fraction in parentheses represents the orbit limited enhancement or reduction of current, the upper sign is for ions and the lower sign is for electrons, f(E) is the distribution function at infinity, and F(E) is the flux at infinity. Depending on the model selected, the flux is given by one of the following formulas in which the particle energy E and the temperature θ are measured in electron volts, and the surface potential ϕ is measured in volts.

Maxwellian

$$F(E) = \sqrt{\frac{e}{2\pi\theta m}}\frac{E}{\theta} n \exp\left(-\frac{E}{\theta}\right) \tag{2}$$

Double Maxwellian

$$F(E) = \sqrt{\frac{e}{2\pi\theta_1 m}}\frac{E}{\theta_1} n_1 \exp\left(-\frac{E}{\theta_1}\right) + \sqrt{\frac{e}{2\pi\theta_2 m}}\frac{E}{\theta_2} n_2 \exp\left(-\frac{E}{\theta_2}\right) \tag{3}$$

Fontheim (electrons only)

This distribution is used to model auroral electrons.

$$F(E) = \pi\zeta_{max} E \exp\left(-\frac{E}{\theta}\right) + \pi\zeta_{gauss} E \exp\left(-\left(\frac{E_o - E}{\Delta_{gauss}}\right)^2\right) + \pi\zeta_{power} E^{-\alpha} H(E < E_U) H(E > E_L) \tag{4}$$

where H is the Heaviside step function and E_L and E_U are upper and lower energy limits.

Kappa

$$F(E) = \sqrt{\frac{e}{2\pi\kappa\theta m}}\frac{E}{\kappa\theta} n \left(\frac{\Gamma(\kappa+1)}{\Gamma\left(\kappa-\frac{1}{2}\right)}\right)\left(1+\frac{E}{\kappa\theta}\right)^{-\kappa-1} \tag{5}$$

Convected Maxwellian

This distribution is used to model a flowing plasma.

$$F(E,\chi) = \sqrt{\frac{e}{2\pi\theta m}}\frac{E}{\theta} n \exp\left(-\frac{E + mU^2/2 - \sqrt{Em/2}U\cos\chi}{\theta}\right) \tag{6}$$

where U is the velocity of the plasma in the spacecraft frame of reference and χ is the angle between the flow vector and the incident velocity at infinity, which can be related to the velocity at which the particle strikes the surface. In this case, obtaining the flux to the surface requires integrating over angle as well as energy.

Measured

This option should be used with extreme caution as inadequately characterized environments can lead to numeric instabilities or unphysical results.

$$F(E) = \sum_i f_i(E) \text{ where } f_i(E) = \begin{cases} F_i \text{ for } E_i < E < E_{i+1} \\ 0 \text{ otherwise} \end{cases} \tag{7}$$

2.1.2 Secondary and Backscattered Current

The secondary and backscattered currents are given by

$$j_{s,b} = q\int_L^\infty Y^{s,b}(E)\left(\frac{E}{E\pm\phi}\right)F(E\pm\phi)dE \tag{8}$$

where $Y^{s,b}$ is the number of secondary or backscattered (respectively) electrons per incident charged particle (after accounting for the angular distribution of the incident particles) and F is the flux at infinity of the appropriate incident charged particle.

We take the spectrum of emitted secondary electrons to be a Maxwellian characterized by a temperature of 2 eV. It follows that the effective secondary electron current from surfaces at positive potentials is reduced by a factor of exp(-ϕ/2) relative to Equation (8). If the surface potential is negative, the secondary electron current can still be reduced by an electron-attracting

$(\mathbf{E}\cdot\mathbf{n}>0)$ electric field caused by other, more negative surfaces, by negative potentials in a nearby wake, or by the space charge of the emitted electrons themselves.

2.1.3 Photocurrent

For surfaces at negative potentials, the photocurrent depends on the surface material, angle of incident sunlight, and distance from the sun. As with secondaries, the photoelectron spectrum is by default taken to be a Maxwellian characterized by a temperature of 2 eV, so that current escaping from surfaces at positive potentials is reduced by a factor of exp(-ϕ/2).

Spacecraft in the solar wind normally charge to positive potential (a few volts to tens of volts) to reduce the emitted photoelectron current to balance a very low incident current of ambient electrons. Unlike geosynchronous substorm charging, where the spacecraft goes negative, determining how positive the spacecraft charges requires knowledge of the high-energy portion of the photoelectron spectrum. To override the default, the user can supply this spectrum as either a table or as the sum of exponentials of the form $Ae^{-E/\theta}$.

In magnetospheric or interplanetary space the space charge near a photoemitting surface is dominated by photoelectrons. This causes the potential to decrease with distance from the surface until loss of returning electrons together with spatial divergence reduces the photoelectron density to the order of the ambient plasma density. Both close (~0.1 AU) to the sun where photoemission is high and on a very large spacecraft (e.g., Solar Sail) for which divergence is low, the potential some distance from the surface can reach negative values. When this is the case, the minimum energy for photoelectron escape is increased beyond the surface potential. The barrier reduces the net photocurrent and lowers the surface potential. This problem was studied analytically by Guernsey and Fu,[10] and, more recently, numerically by Ergun *et al.*[11]

When the user requests that this space charge limiting of photocurrent be included in the surface potential calculation, the code computes a barrier height. If the space charge barrier exceeds the surface potential, the code reduces the net photocurrent and the secondary electron current. In addition to the photoemission current and the ambient plasma density, the preliminary *Nascap-2k* model depends on the effective radius of curvature of the surface element (estimated by ϕ/E, where E is the electric field [calculated using the boundary element method for the spacecraft at uniform potential ϕ] and constrained to be between 0.3 m to 2.0 m) and the shape of the photoemission spectrum (taken to be $J = 53e^{-E/1.6} + 21e^{-E/3} + 4e^{-E/8.9}$ [12]). The effect of this algorithm on large, flat surfaces is to reduce the effective photoemission current from the interior of the surface (where effective radius of curvature is large) but not near the edges (where the effective radius of curvature is small).

2.1.4 Other Current Sources

Conduction Current through Insulators

In surface charging calculations, the charge deposition thickness is short compared with the thickness of the insulator layer, and therefore, the electric field is spatially uniform throughout the layer and current is conducted through it. (Note: the range of a 40 keV electron in aluminum is ~15 microns [~ 0.0006 inches].) For insulating surface elements, the current through the layer

to the underlying conductive substrate is given as a function of the conductivity and thickness of the layer by Ohm's Law:

$$j_{conduction} = \frac{\Delta\phi}{\rho d} \tag{9}$$

where $\Delta\phi$ is the difference in potential between the surface and the conductive substrate and ρ and d are the resistivity and thickness of the layer respectively.

Surface Conductivity

Nascap-2k accounts for current flowing along surfaces. Current flows between insulating surface elements of a common material and with a common edge, transporting charge over a wide expanse of such material. The surface element to surface element conductivity is proportional to the length of the common edge and inversely proportional to the sum of the centroid-to-edges distances. For a surface element i having a common edge with j, $R_i = (d_i/l_{ij})\,\rho$, where ρ is the surface resistivity, d_i is the distance from the centroid of surface element i to the center of the common edge, and l_{ij} is the length of the common edge. The surface conductance across the edge between adjoining surface elements i and j is

$$\text{Conductivity} = \frac{1}{R_i + R_j}. \tag{10}$$

A surface can be grounded by a strip at an element edge (grounding edge) or by a circular contact located at a node (grounding node).

Charged Particle Emission

Nascap-2k also allows for the inclusion of the current due to charged particle emission from a conductor (e.g., an electron gun). This capability is accessed by editing the script.

2.1.5 Timescales

Charged particles with energies below 50 keV penetrate less than a hundred microns into the spacecraft skin. While the time for the entire spacecraft to achieve net current balance is typically several milliseconds, the time for each surface to achieve its own equilibrium potential is thousands of times longer. The development of differences between the potentials of different surfaces is referred to as differential charging.

The rate of absolute charging is determined by the capacitance of the spacecraft to infinity, while the rate of differential charging is determined by the capacitance across the insulator layer. *Nascap-2k* does *not* take the presence of a plasma into account when computing the capacitance to space. The rate of change of the potential on a sphere is given by

$$\frac{d\phi}{dt} = \frac{1}{4\pi\varepsilon_o}\frac{I}{R} = \frac{JR}{\varepsilon_o} \tag{11}$$

where I is the current to the sphere, J is the current density to the sphere surface, and R is the sphere radius. For a 1-meter sphere and a net current of 1 $\mu A\ m^{-2}$, the sphere begins to charge at a rate of 100 $kV\ s^{-1}$. As the sphere charges toward its steady-state (zero net current) potential, the net current decreases toward zero as electrons are repelled. Therefore, the charging rate decreases with time.

The rate of change of the difference in potential across a dielectric layer is given by

$$\frac{d\phi}{dt} = \frac{Jd}{\varepsilon_o} \tag{12}$$

where d is the thickness of the layer. A 100 μm layer with the same incident current density charges at a rate of 10 $V\ s^{-1}$. In this representative example, differential charging takes place 10^4 times more slowly than absolute charging.

2.1.6 Shadowing

A surface element is shadowed from the sun if, either

(1) Its normal points anti-sunward, or
(2) Its centroid lies behind the projection of another sun-facing surface.

Shadowing from the ram flow is handled in the same manner.

2.1.7 Circuit Model

Figure 2 shows a circuit diagram for a spacecraft with one insulating surface element and exposed conducting surfaces. The widely differing capacitances of surfaces to infinity, C_A and C_S and of the surface to spacecraft ground, C_{AS}, make this a complex numeric problem.

$$C_{AS} = \varepsilon\varepsilon_0 \frac{S}{d} \approx S \times 10^{-6} \quad \text{Farad} \tag{13}$$

$$C_A \approx C_S \approx 4\pi\varepsilon_0 R\left(\frac{S}{4\pi R^2}\right) \approx \left(\frac{S}{R}\right) \times 10^{-11}\ \text{Farad} \tag{14}$$

where ε, d, and S are the dielectric constant, thickness (m), and surface area (m^2) of the insulating surface element, and R is the radius of a sphere approximating the size of the spacecraft. The potentials as a function of time are computed using implicit time integration of the charging equations, which relate the derivative of the potential, **Φ**, with time to the current, **I**.

$$\mathbf{C}_A\dot{\mathbf{\Phi}}_A + \mathbf{C}_{AS}\left(\dot{\mathbf{\Phi}}_A - \dot{\mathbf{\Phi}}_S\right) = \mathbf{I}_A$$
$$-\mathbf{C}_{AS}\left(\dot{\mathbf{\Phi}}_A - \dot{\mathbf{\Phi}}_S\right) + \mathbf{C}_S\dot{\mathbf{\Phi}}_A = \mathbf{I}_A$$

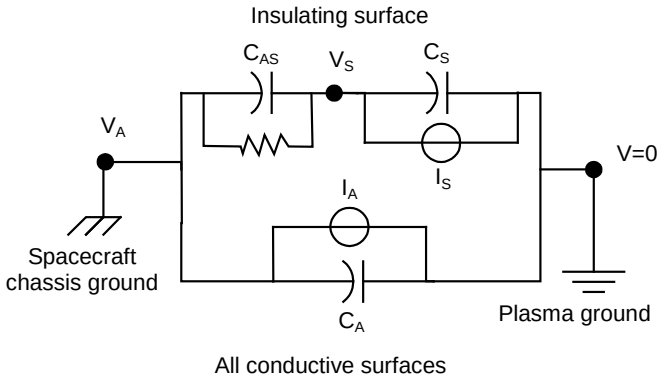

Figure 2. Circuit Model of a Spacecraft with One Insulating Surface Element.

The multi-surface problem is solved by linearizing the currents and inverting the matrix.

$$\mathbf{C}\dot{\mathbf{\Phi}} = \mathbf{I}(\mathbf{\Phi}) \tag{15}$$

2.2 Material Properties

The properties of the spacecraft surface materials determine the charging rates and equilibrium surface potentials. *Nascap-2k* uses the models of secondary electrons due to incident electrons, secondary electrons due to incident ions, backscattered electrons, and photoelectrons originally developed for NASCAP/GEO.[13]

2.2.1 Secondary Electron Emission Due to Electron Impact

Secondary electrons are those emitted from a surface with energies below 50 eV in response to energy deposited near the surface by incident electrons. Their energy distribution is usually peaked below 10 eV. The secondary yield, Y_{ee}, is the ratio of primary to secondary electron current.

$$Y_{ee} = \frac{\text{emitted secondary current due to electron impact}}{\text{primary electron current}} \tag{16}$$

A typical curve is shown in Figure 3.

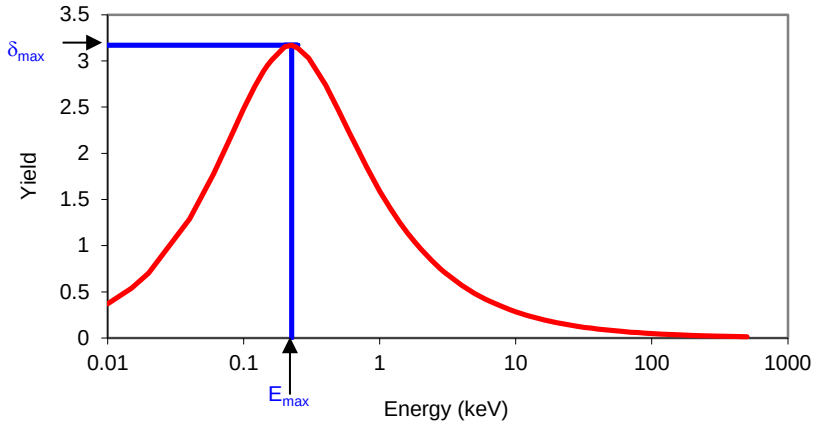

Figure 3. Electron Secondary Yield as a Function of Incident Energy.

The secondary electron emission yield can be calculated using the empirical formula[14]:

$$Y_{ee}(\psi) = C\int_0^R \left|\frac{dE}{dx}\right| e^{-\alpha x \cos\psi} dx \tag{17}$$

where x is the path length of penetration of a primary electron beam into the material, R is the "range," or maximum penetration length, and ψ is the angle of incidence of the primary electron.

This equation is based on a simple physical model[15]:

1. The number of secondary electrons produced by the primary beam at a distance x is proportional to the energy loss of the beam or "stopping power" of the material, $S(E) = \left|\frac{dE}{dx}\right|$.

2. The fraction of the secondaries that migrate to the surface and escape decreases exponentially with depth ($f = e^{-\alpha x \cos\psi}$). Thus only secondaries produced within a few multiples of the distance $1/\alpha$ (the depth of escape) from the surface contribute significantly to the observed yield.

The stopping power for incident electrons of energy E is related to the range of these electrons through the equation

$$S(E) = \left|\frac{dE}{dx}\right| = \left|\frac{dR}{dE}\right|^{-1} \tag{18}$$

The usual formulation for the range is that it increases with the energy, E of the incident electrons in a way that approximates a simple power law[16]:

$$R = bE^q \tag{19}$$

where q is a bit less than 2 for electrons with energy $\lesssim$ 300 keV. Because the primary beam loses energy as it passes through the material, E and $S(E_o, x)$ depend on the path length x, where E_o is the initial electron energy. The stopping power can be written as

$$S(E_o, x) = \left|\frac{dE}{dx}\right| = \left|\frac{dR}{dE}\right|^{-1} = \frac{1}{qb}\left(\frac{b}{R - x}\right)^{1-1/q} \tag{20}$$

Figure 4 shows $S(E_o, x)$ plotted against x for several values of E_o. Inspection of Figure 4 and the equation for S(x) illustrates the following points:

1. $S(E_o, x)$ increases with x, slowly at first, before reaching a singularity as x approaches R.
2. The initial value of $S(E_o, x)$ decreases with increasing initial energy E_o.

Both of these observations are due to the decrease in electron-atom collision cross-section with increasing energy.

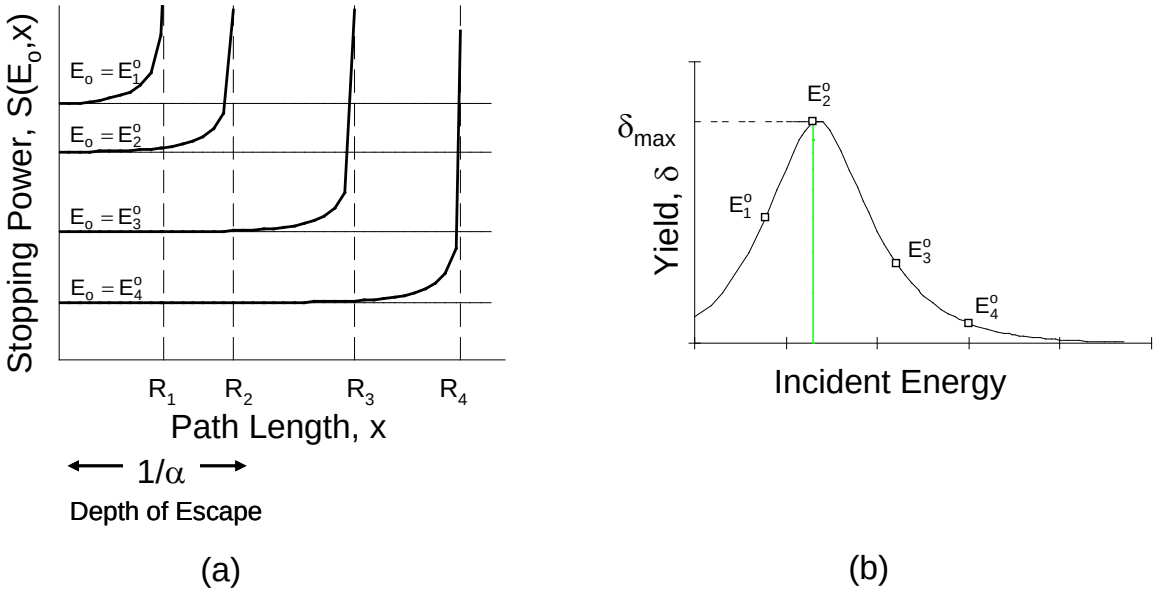

Figure 4. Energy Deposition Profiles of Normally Incident Primary Electrons for Four Incident Energies E_1^o, E_2^o, E_3^o, and E_4^o and Corresponding Yield Curve.

The yield is only sensitive to the details of the stopping-power depth-dependence for initial energies with ranges of the same order as the escape depth, $R \sim 1/\alpha$ (i.e., about the maximum of the yield curve). For lower energies, $R << 1/\alpha$, essentially all the primary energy is available for detectable secondary production, leading to a linear increase in yield with increasing E_o. At higher energies, where $R >> 1/\alpha$, $S(E_o,x)$ remains almost constant over the depth of escape. Therefore, along with $S(E_o,x)$, the yield decreases as E_o increases.

Taking this into account, the stopping power can be approximated by a linear expansion in x, about x = 0.

$$\frac{dE}{dx} = \left(\frac{dR}{dE_o}\right)^{-1} + \left(\frac{d^2R}{dE_o^2}\right)\left(\frac{dR}{dE_o}\right)^{-3} x \tag{21}$$

The simple power law does not adequately describe the available experimental data. The range has different exponents for low energy and high energy. A bi-exponential range law with four parameters b_1, b_2, q_1, q_2 fits the experimental data better.

$$R = b_1 E_o^{q_1} + b_2 E_o^{q_2} \tag{22}$$

Figure 5 shows CSDA (Continuous Slowing Down Approximation) range values for Aluminum for energies from 20 eV to 100 keV. Note the drastic change in behavior near 300 eV. The bi-exponential formula $R = 142.63E^{0.2335} + 245.15E^{1.7269}$ fits well throughout the range plotted.

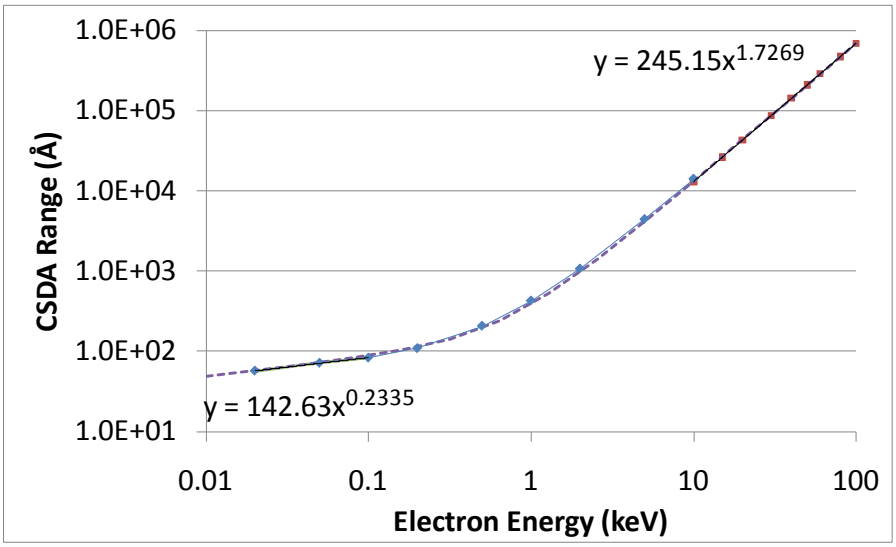

Figure 5. CSDA Range for Electrons in Aluminum. Low Energy Values (Blue Diamonds) from Ashley *et al*. (Reference 17). High Energy Values (Red Squares) from NIST ESTAR* Database. Dashed Line is Bi-exponential Fit.

For materials where no suitable data is available, a mono-exponential form can be generated using Feldman's empirical relationships[16], connecting b and n to atomic data.

$$b = 250W/\rho_{mass} Z^{q/2} \tag{23}$$

$$q = 1.2/(1 - 0.29\log_{10} Z) \tag{24}$$

where W is the atomic or molecular weight of the material, Z is the atomic number, and ρ_{mass} is the mass density in gm cm^{-3}. Then E is in keV and R is in angstroms. The stopping power is then

* National Institute of Standards and Technology Electron STopping power And Range database available at http://www.nist.gov/pml/data/star/index.cfm

obtained indirectly with the above equation. Theoretical estimates of the stopping power for a number of materials are available from Ashley et al.[17] Comparison of these values with those implied by the range data showed significant discrepancies, particularly for those materials fit using Feldman's formula. The best approach is to fit the four parameters in the equation for R directly to the stopping power data.

$$S = \left(q_1 b_1 E^{q_1 - 1} + q_2 b_2 E^{q_2 - 1} \right)^{-1} \tag{25}$$

The secondary electron yield depends on angular distribution of the incident electrons. For low energy electrons, all the energy is deposited near the surface regardless of incident angle, so the yield is independent of incident angle. For high energy electrons the stopping power is constant in the near-surface region, so the yield is proportional to the path length near the surface, or inversely proportional to $\cos\psi$. It follows that the yield for high energy isotropic electrons is double that for normally incident electrons of the same energy. The isotropic yield curve makes a transition from being equal to the normal incidence curve at low energy to double at high energy. The maximum yield for isotropic electrons is somewhat higher than for normal electrons, and occurs at somewhat higher energy.

2.2.2 Secondary Electron Emission Due to Ion Impact

Secondary emission of electrons due to ion impact can be treated in a way similar to that for electron impact. The yield is given by

$$Y_{ie}(\psi) = C \int_0^d \left| \frac{dE}{dx} \right| e^{-\alpha x \cos\psi} dx \tag{26}$$

The stopping power is assumed to be independent of path length x over the thickness, d, of the sample. Above 10 keV, the stopping power is approximately proportional to the velocity, and at higher energies (above ~200 keV) it is inversely proportional to the velocity[18]. Below 10 keV, it is lower.

$$\left| \frac{dE}{dx} \right| = \frac{\beta(E) E^{1/2}}{1 + E/E_{max}} \tag{27}$$

E_{max} is the energy at the maximum in the yield curve. This is approximately 100 keV for most materials.

$$\beta(E) = \begin{cases} 0.25 & E < 0.476 \text{ keV} \\ 2^{\left(\frac{1}{E} - 0.1\right)} & 0.476 \text{ keV} \le E \le 10 \text{ keV} \\ 1 & 10 \text{ keV} < E \end{cases} \tag{28}$$

As the CSDA range is at least comparable to the mean depth of secondary electron production for protons above 1 keV (140 angstroms of aluminum), we consider the proton yield to vary

inversely with the cosine of the incident angle, so that the isotropic incidence yield is double the normal incidence yield. This is usually an adequate treatment, because the ion fluxes are almost always low, and the effect of secondary emission is to mildly augment the incident ion flux, rather than canceling it as is the case with incident electrons.

The secondary emission properties due to the impact of ions other than protons are assumed to be identical to the proton values for the same energy.

The secondary electron yield curve for protons incident on aluminum is shown in Figure 6. As can be seen by comparison with Figure 7, the yield closely follows the stopping power.

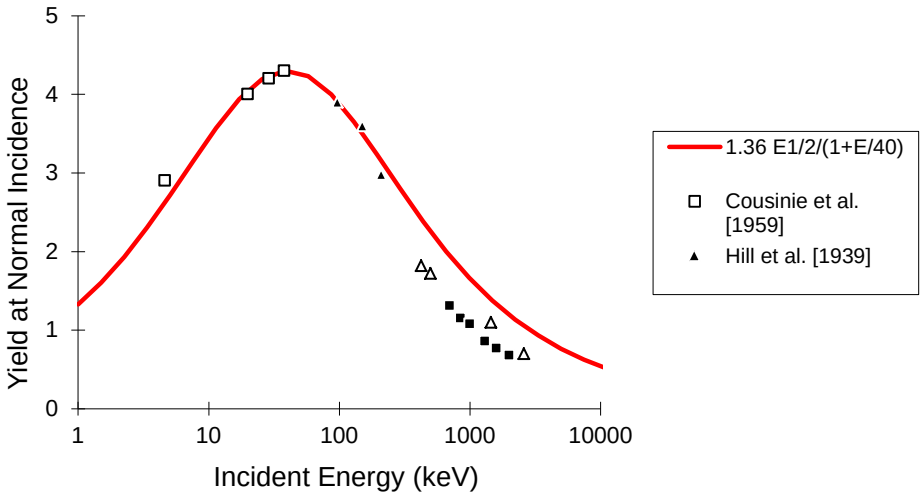

Figure 6. Secondary Electron Emission by Aluminum for Proton Impact at Normal Incidence; Experimental Points as Indicated in the References.[19, 20, 21, 22]

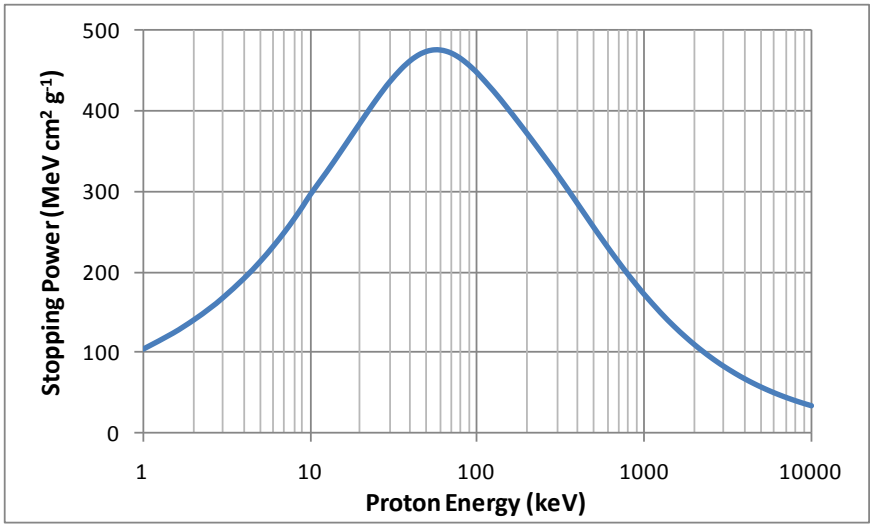

Figure 7. Stopping Power for Protons on Aluminum. (From NIST PSTAR Database.†)

2.2.3 Backscatter

Backscattered electrons are those emitted from the surface with energies above 50 eV. Their energy distribution is usually peaked close to the primary incident energy and they may be considered as reflected electrons.

Nascap-2k uses a backscattering theory[23] based on that of Everhart[24] as extended by McAfee[25]. It assumes a single scattering in accordance with the Rutherford cross-section and the Thomson-Widdington slowing down law,

$$\frac{dE}{dx} \propto E^{-1} \tag{29}$$

(valid for most metals for E > 10 keV). For normal incidence the backscattering coefficient is given by

$$\eta = 1 - \left(\frac{2}{e}\right)^{a} \tag{30}$$

where a is taken to be 0.0375 Z and where Z is the atomic number of the material. This expression matches the experimental data.

The large-angle scattering theory, together with Monte Carlo data and experiments by Darlington and Cosslett,[26] indicate that the angular dependence of backscattering is well-described by

$$\eta(\psi) = \eta_o \exp\left(\eta_1 (1 - \cos\psi)\right) \tag{31}$$

† National Institute of Standards and Technology Proton STopping power And Range database available at http://www.nist.gov/pml/data/star/index.cfm

where the value of η_1 is, within the uncertainty in the data, what would be obtained by assuming total backscattering at glancing incidence, $\eta_1 = -\log \eta_o$. The net albedo for an isotropic flux is then

$$A_o = 2\frac{1-\eta_o\left(1-\log\eta_o\right)}{\left(\log\eta_o\right)^2} \tag{32}$$

As the energy is decreased below 10 keV, the backscattering increases. Data cited by Shimizu[27] indicate an increase of about 0.1, almost independent of Z. This component of backscattering can be approximated by

$$\delta\eta_o = 0.1\exp\left[-E/5\text{ keV}\right] \tag{33}$$

At very low energies, the backscattering coefficient becomes very small and, below 50 eV, becomes zero by definition, as all emitted electrons are considered secondaries. This can be taken into account by a factor of

$$H\left(E-50\text{eV}\right)\left[\frac{1}{\log 20}\right]\log\left(\frac{E}{50\text{eV}}\right) \tag{34}$$

where H is the Heaviside step function. The formula for energy-dependent backscattering, incorporating these assumptions, is then

$$\eta_o = \left(H\left(1-E\right)H\left(E-0.05\right)\left(\frac{1}{\log 20}\right)\log\left(\frac{E}{0.05}\right)+H\left(E-1\right)\right)\times\left(\frac{e^{-E/5}}{10}+1-\left(\frac{2}{e}\right)^{0.037Z}\right) \tag{35}$$

where energies are measured in keV.

2.2.4 Photoemission

Photoelectrons are those ejected from the surface due to the solar ultraviolet radiation. Usually the quantity known is the yield, or number of electrons emitted for a surface normally exposed to the solar spectrum, at an "earth distance" from the sun (Y_{sun}). The photocurrent from a surface exposed to the sun at an angle ψ_{sun} is given by the formula

$$i_{photo} = \left(\text{Area exposed}\right)Y_{sun}\cos\psi_{sun} \tag{36}$$

This assumes that the yield per photon is, on average, independent of ψ_{sun}.

A surface element is taken to be sunlit if its centroid is sunlit, *i.e.*, if a vector from the centroid in the sun direction does not intersect any other surface element.

2.3 Surface Charging from Tracked Currents and/or Current Balance

In short Debye length environments, such as encountered in low-Earth orbit, the orbit-limited approximation greatly overestimates currents of attracted particles. This occurs because potentials that decay faster than inverse square (sheath potentials) lead to an effective potential barrier to attracted charged particles when angular momentum is taken into account. *Nascap-2k* can compute the charging of spacecraft surfaces using tracked currents, either by themselves or in conjunction with analytically computed currents. Calculations of typical interest include:

1. Floating potential and/or differential charging of a negative spacecraft, whose ion current may be enhanced and asymmetrized due to ram/wake effects.
2. Floating potential of a biased spacecraft that has both ion and electron sheaths. The electron current may be additionally limited by magnetic field effects.
3. Dynamic potential of a spacecraft with time-dependent bias.

In "Surface Charging" calculations with "Tracked Ion and Analytic Electron Currents" ("Auroral" environment only), the analytic electrons used are high energy electrons computed from the Fontheim formula. In "Time Dependent Plasma" calculations, the analytic electrons used are computed by the convected Maxwellian formula.

2.4 Potentials in Space

Nascap-2k uses a finite element method to solve Poisson's equation $-\varepsilon_o \nabla^2 \phi = \rho(\mathbf{x})$ for electrostatic potentials throughout space. *Nascap-2k* uses the variational form

$$0 = \frac{\delta}{\delta\phi}\left\{\int dV\left[\frac{1}{2}(\nabla\phi)^2 + \frac{\rho\phi}{\varepsilon_o}\right] + \int \phi \nabla\phi \bullet dS\right\} \tag{37}$$

The first term in the volume integrand corresponds to the Laplacian operator; the second term is the space charge contribution. As surface potentials are held fixed when solving for potentials in space, the surface term appearing in Equation (37) is not used in the potential solution, but may be used later to determine the normal component of electric field (and thus the surface charge) for each surface element.

The solution is subject to fixed potential boundary condition on the spacecraft surfaces and either zero potential or monopole potentials on the grid boundary.

Available Space Charge-Density Models

A number of models of the charge density are available to study different phenomena.

In the following, the symbol λ_D is the plasma Debye length and g is the plasma density reduction factor computed by geometric wake model ($0<g<1$).

Laplace. The Laplacian space charge option specifies that the charge density is zero and is appropriate for very low density plasmas.

$$\frac{\rho}{\varepsilon_o} = 0 \tag{38}$$

i.e., charge exists only on object surfaces and external boundaries, as determined by the boundary conditions. “Space charge” iterations may still be required, however, due to the treatment of surface electric fields.

Linear (Debye Shielding). The Linear space charge option solves the Helmholtz or Debye-Huckel equation. This model is rarely applicable to spacecraft because it assumes all potentials are much less than the plasma temperature, which is only true in low density plasma where the laplace approximation is valid.

$$-\nabla^2\phi = \frac{\rho}{\varepsilon_o} = -\frac{\phi}{\lambda_D^2/g} \tag{39}$$

Nonlinear. The Nonlinear space charge model is appropriate for most low-Earth-orbit type plasmas. It accounts for space charge acceleration and convergence in a manner based on spherical collection (Langmuir-Blodgett[28] problem). Poisson’s equation is solved with space charge given by:

$$-\nabla^2\phi = \frac{\rho}{\varepsilon_o} = -\frac{\phi}{\lambda_D^2/g}\left(\frac{\max\left(1, C\left(\phi, |\mathbf{E}|\right)\right)}{1+\sqrt{4\pi}\left|\phi/\theta\right|^{3/2}}\right) \tag{40}$$

This model smoothly interpolates between Debye screening at low potential and an accelerated distribution with particle convergence at high potentials. The convergence factor is computed in terms of local information and problem parameters. The convergence model was developed by numerically solving the Langmuir-Blodgett problem for collection by a high-voltage sphere and fitting the result to an analytic form. An excellent fit was found with

$$\left(R_{sh}/r\right)^2 = 2.29\left(|\mathbf{E}|\,\lambda_D/\theta\right)^{1.262}\left|\theta/\phi\right|^{-0.509} \tag{41}$$

$$C\left(\phi, |\mathbf{E}|\right) = \min\left(\left(R_{sh}/r\right)^2, 3.545\left|\phi/\theta\right|^{3/2}\right) \tag{42}$$

where **E** is the local electric field.

Frozen Ion. The Frozen Ion formulation is intended for short timescale (typically sub-microsecond) problems for which it is a good approximation to assume that ions remain stationary and at ambient density (“ion matrix” approximation), but electrons achieve barometric equilibrium. This approximation is intended primarily for negative potentials, for which the charge density is zero at zero potential and for which at negative potential (electrons repelled) the charge density becomes positive and asymptotically reaches the ion density. For computational convenience we extend the charge density linearly to positive potentials, as an exponential increase in electron charge would be unphysical.

$$\begin{aligned} \rho &= gne\left(1 - e^{\phi/\theta}\right) \quad \phi \le 0 \\ \rho &= -gne\frac{\phi}{\theta} \qquad \phi > 0 \end{aligned} \tag{43}$$

Considerations for implementing this formulation stably on a coarse mesh are discussed in Section 3.6.5.

Barometric. The barometric space charge model is for cases in which all the surfaces are at potentials comparable to or below the plasma temperature and there is a region of low density, such as a plasma wake. The total charge density is the sum of the ion and electron charge densities.

$$\rho = \rho_e + \rho_i \tag{44}$$

The ion density is the plasma density decreased by the wake factor.

$$\rho_i = g\,en \tag{45}$$

The electron density is expanded about barometric equilibrium:

$$\rho_e = -\rho_i \begin{cases} 1 + \left(\phi - \phi_b\right)/\theta & \phi > \phi_b \\ \exp\left(\left(\phi - \phi_b\right)/\theta\right) & \phi \le \phi_b \end{cases} \tag{46}$$

$$\phi_b = \theta \ln\left(g\right) \tag{47}$$

In a dense, short Debye length plasma, the requirement that the ion and electron densities be nearly equal gives strictly barometric potentials. In plasmas with a longer Debye length strict quasineutrality does not hold, so that, for example, the potential in a wake is considerably less negative than barometric, and the wake is therefore electron rich.

Note that this model differs from the “Nonlinear” model in that it lacks an approximation to attracted species density in sheaths and does not allow for ion depletion in positive potential regions.

Full Trajectory Ions. Ion densities are calculated from steady-state ion trajectories. Electrons are barometric. This approximation is used to model charge density for a moving spacecraft when current collection in the wake is important and the neutral wake approximation is inadequate—such as when high potential surfaces are in the wake.

$$\begin{aligned} \frac{\rho}{\varepsilon_o} &= \frac{\rho_i}{\varepsilon_o}\left(1 - \exp\left(\left(\phi - \phi_b\right)/\theta\right)\right) \\ \phi_b &= \theta \ln\left(\frac{\rho_i}{en}\right) \end{aligned} \tag{48}$$

Here, ρ_i is calculated by tracking ions.

Plume Ion Density. Ion densities are initially computed from an imported plume map file. Electrons are barometric. The quantity ρ/ε_o is computed using the same formula as for full trajectory ions, where ρ_i is computed by summing the contributions from the thruster plumes instead of computed by tracking macroparticles. After the initial iteration, ρ_i is computed by summing the main beam contribution from the thruster plumes and the charge exchange contribution from generating and tracking charge exchange ions.

Hybrid PIC. This algorithm is used for timescales (typically sub-millisecond) on which it is practical to treat ion motion, but electrons may be considered in barometric equilibrium. The total charge density is the sum of the ion and electron charge densities.

$$\rho = \rho_e + \rho_i \tag{49}$$

The ion density is computed from ion macroparticles that move in the local electric fields at each timestep. The electron charge density is given by the same formula as for the Barometric model above with the barometric potential given by

$$\phi_b = \theta \ln\left(\frac{\rho_i}{en}\right) \tag{50}$$

Full PIC. For this option, it is assumed that both the electron and ion-charge densities were stored during particle tracking.

$$\rho = \rho^{\text{tracked}} \tag{51}$$

2.5 Macroparticle Creation and Tracking

Particle tracking is used to study sheath currents, to study detector response, to generate steady-state charge densities, and to generate space charge evolution for dynamic calculations. The investigation of detector response is applicable in both tenuous and dense plasmas. However, the other phenomena are only applicable in plasmas with Debye lengths no more than the spacecraft size.

In a dense plasma with high potentials, the disturbed region is referred to as a sheath. The "sheath surface" represents a sharp demarcation between a low potential exterior region containing neutral "undisturbed plasma," and a high potential interior region from which one species (ions for positive potentials; electrons for negative potentials) is excluded.

In a dense plasma, the total current and its distribution over the spacecraft surface depend on the plasma environment, the surface potentials, the sheath structure, the spacecraft velocity, and ambient and spacecraft generated magnetic fields. For a large object (many Debye lengths in size) at low potential (at most, a few times the plasma temperature), Debye screening minimizes the extent of the object's influence on the plasma. Because the sheath is "thin," the sheath surface lies near the spacecraft surface. The current attracted to each surface element is then given by its area times the plasma thermal current of the appropriate species. For an object (not necessarily

large) at high potential, however, the extent of perturbed plasma is far greater. A first estimate of the sheath thickness is given by the Child-Langmuir[29,30] distance.

$$D_{CL} = \sqrt{\frac{8\varepsilon_o}{9en}\sqrt{\frac{\pi}{\theta}}} \tag{52}$$

The plasma thermal current then flows through an area much larger than the spacecraft surface. The current may be focused by the fields within the sheath, which affects the distribution of current over the spacecraft surface. This focusing causes the increase in space charge density due to particle acceleration modeled in the "Nonlinear" space charge density model.

Macroparticles are generated in the **Particle Generation** step of the script and tracked in the **Track** step of the script. Macroparticles can be generated at a well-defined sheath surface, at the boundary of the computational space, throughout the volume of space, at surface elements, or at user specified locations. As macroparticles are tracked, their charge density in the volume elements they pass through may or may not be retained, depending on user choices. The current to any surface element hit by the macroparticles is retained.

2.5.1 Generation of Macroparticles at Sheath Surface

The attracted species diffuses across the sheath surface at a rate given by the plasma thermal current.

$$j_{th} = en\sqrt{\frac{e\theta}{2\pi m}} \tag{53}$$

The current density to the sheath edge is computed by assuming the sheath to be a perfectly absorbing spherical surface.

The charged particles constituting this current undergo motion consistent with the electric and magnetic fields inside the sheath. The sheath surface is taken as the equipotential surface at $\phi = \pm\theta\ln 2$. This choice is made because the attracted species is absorbed by the sheath, so we have only the inward moving component, comprising half the ambient density. The repelled species, whose density satisfies $n = n_a \exp\left(-\left|\phi/\theta\right|\right)$, must also be at half the ambient density, leading immediately to the sheath potential.

Macroparticles representing this sheath current can be generated and tracked to determine the current to the spacecraft and its distribution. The initial velocity is the average velocity of a charged particle crossing the sheath boundary. In the absence of spacecraft motion or a magnetic field, this is $v = \sqrt{\frac{2e\theta}{\pi m}}$ in the direction of the local electric field. More precisely, for a sheath segment on the ram side

$$\mathbf{v} = \pm\frac{1}{2}\sqrt{8\frac{e}{m}\left(\frac{\theta}{\pi}+|\phi|\right)+v_x^2+v_x}\left(\frac{\mathbf{E}}{|\mathbf{E}|}\right)-V_{sc} \tag{54}$$

where the plus sign is for ions and the minus for electrons and v_x is the component of the spacecraft velocity along the local electric field. In the absence of spacecraft motion and for a sheath segment in the wake,

$$\mathbf{v} = \pm\sqrt{\frac{2e}{m}\min\left(\frac{\theta}{\pi},|\mathbf{E}|\lambda_D+|\phi|\right)}\left(\frac{\mathbf{E}}{|\mathbf{E}|}\right) \tag{55}$$

With a uniform magnetic field

$$\mathbf{v} = \pm\sqrt{\frac{2e(\theta\mp\phi)}{m}-v_{drift}^2}\left(\frac{\mathbf{E}}{|\mathbf{E}|}\right)+\mathbf{v}_{drift} \tag{56}$$

where the drift velocity term $\mathbf{v}_{drift}=\frac{\mathbf{E}\times\mathbf{B}}{B^2}$ is not included if it would make the argument of the square root negative.

This model is appropriate for high potentials. When either the thermal distribution of particle velocities or the spacecraft velocity is important, macroparticles should be tracked from the boundary of the computational space.

2.5.2 Generation of a Thermal Distribution at the Computational Space Boundary

There are two models for creation of macroparticles at the boundary of the computational grid. In both models, the plasma is assumed to be Maxwellian. The two models are inconsistent and should *not* be used together.

Boundary Injection

In the simplest model, macroparticles are created with charge equal to the plasma thermal current times the area times the time interval, $q = j_{th}A\Delta t$, and velocity equal to $\sqrt{\frac{2e\theta}{\pi m}}$ normal to the boundary, so that they represent a density of n/2. These can each be split into eight outwardly moving macroparticles, to approximate a thermal distribution. The split macroparticles have an additional velocity of $\pm 0.707\sqrt{\frac{e\theta}{m}}$ along each axis of a randomly generated coordinate system. The splitting is done in the plasma frame of reference in order to simulate the correct momentum and energy distribution for a drifting Maxwellian when transformed back to the spacecraft reference frame.

Boundary

In this model, macroparticles that represent a specified fraction of the thermal distribution in each of the three spatial directions are created. At each boundary emission point, several macroparticles are created that sample the velocity distribution function in each of the three spatial directions. The user specifies which fraction of the distribution function each macroparticle is to represent and the code computes the range of velocities $\left(v_{1,2}^{x,y,z}\right)$ which would give the specified fractions, η_i.

$$\eta_i = \int_{v_1^z}^{v_2^z}\int_{v_1^y}^{v_2^y}\int_{v_1^x}^{v_2^x} f(\mathbf{v})dv^x dv^y dv^z = \int_{v_1^z}^{v_2^z}\int_{v_1^y}^{v_2^y}\int_{v_1^x}^{v_2^x} \left(\frac{m}{2\pi e\theta}\right)^{3/2} \exp\left(-\frac{mv^2}{2e\theta}\right) dv^x dv^y dv^z \tag{57}$$

Several macroparticles are created, each with velocity the sum of the average velocity of its fraction of the distribution and the ram velocity (negative of the spacecraft velocity).

$$\mathbf{v}_i = \int_{v_1^z}^{v_2^z}\int_{v_1^y}^{v_2^y}\int_{v_1^x}^{v_2^x} \mathbf{v}\, f(\mathbf{v})dv^x dv^y dv^z = \int_{v_1^z}^{v_2^z}\int_{v_1^y}^{v_2^y}\int_{v_1^x}^{v_2^x} \mathbf{v} \left(\frac{m}{2\pi e\theta}\right)^{3/2} \exp\left(-\frac{mv^2}{2e\theta}\right) dv^x dv^y dv^z \tag{58}$$

2.5.3 Generation of Macroparticles Throughout the Computational Space

Initialization

Macroparticles can be created throughout the computational space to represent a uniform distribution of charge. The weight of these macroparticles is decreased by any geometric wake factor. Each macroparticle can be split into eight outwardly moving macroparticles so as to approximate a thermal distribution. The velocities have components of $\pm 0.707\ \sqrt{e\theta/m}$ along each axis in a randomly oriented coordinate system. The splitting is done in the plasma frame of reference in order to simulate the correct momentum and energy distribution of a drifting Maxwellian when transformed back to the spacecraft reference frame.

Charge Exchange

Macroparticles can also be created throughout the computational space to represent charge exchange current. Charge exchange ions are those created by a charge transfer collision between a fast ion and a slow neutral atom, such as occurs in ion thruster plumes. The current per unit volume associated with each macroparticle is the product of the charge exchange cross section, the neutral density, and the main beam ion current density.

$$j_{cex} = e\, \sigma_{cex}\, n_{neutral}\, n_{beam}\, v_{beam}. \tag{59}$$

Each component of the initial velocity is given by $\zeta\sqrt{\frac{2e0.3448}{m}}$, where 0.3448 is 4000 K in electron volts and ζ is a random number between -1 and 1.

The neutral density is the sum of the un-ionized propellant from the thrusters, the gas flowing through the neutralizers, and the background gas.

$$n_{neutral} = n_{thrusters}^{unionized} + n_{neutralizers}^{gas} + n_{a}^{neutral} \tag{60}$$

The contribution from each thruster is given by the solid angle subtended by the thruster grid, the flow rate and the temperature.

$$n_{thrusters}^{unionized} = \frac{\Omega_{grid}}{\pi} Flow_{thruster}^{neutral} \sqrt{\frac{\pi m_{thruster}}{8e\theta_{thruster}}} \tag{61}$$

The contribution from each neutralizer is given by the flow rate, the temperature, the angle between the neutralizer axis and the line of sight from the neutralizer, and the distance from the neutralizer.

$$n_{neutralizer}^{gas} = Flow_{neutralizer} \sqrt{\frac{\pi m_{neutralizer}}{8e\theta_{neutralizer}}} \frac{\cos\psi}{\pi r^2} \tag{62}$$

2.5.4 Generation of Macroparticles at Surface Elements

Macroparticles can be created on surface elements to determine if emitted current will return to a surface of the object or leave the computational space, or to determine the current incident to a detector from a convected Maxwellian plasma.

Emitted Current

Macroparticles that represent a user specified emitted current and range of angles and kinetic energies are created on surface elements. The macroparticles are emitted with a flat distribution in velocity, azimuthal angle, and cosine of the polar angle. A full distribution of macroparticles is created at a user specified number of points on each emitter surface element. The emitted current is subtracted from the total current to the emitting surface element.

Current to Detectors (Reverse Trajectory Tracking)

Another reason to create macroparticles on surface elements is to compute the current to those surface elements from a flowing thermal plasma. This technique is applicable when the current of interest is composed of charged particles with velocity (direction, magnitude, or both) far from the mean of the distribution function, the sheath is very large, or there is some other condition such that tracking particles inward from a sheath boundary does not work well. Under these conditions, reverse tracking can be used to determine the original velocity of the incident particles, or if they are blocked. The current is then given by an integral over the environment distribution function of the incident species.[31]

Macroparticles that represent a user specified field of view are created at a user specified number of points on each detector surface element. The user-specified number of macroparticles are

distributed evenly in velocity, azimuthal angle, and cosine of the polar angle. Each macroparticle has a weight appropriate to its fraction of the total incident current.

When these macroparticles exit the computational space, the plasma properties and each macroparticle's weight and final velocity are used to assign an incident current to the originating surface element.

2.5.5 Particle Tracking

Macroparticles are tracked until they leave the computational grid, hit a surface, exceed the number of allowed steps, or exceed the computational tracking time. They are tracked in the local electric field and the magnetic field (ambient uniform and spacecraft-generated dipoles) using a third order energy conserving algorithm.

As the macroparticles pass through volume elements, their charge and/or current can be optionally saved to volume elements and nodes. This charge and/or current can subsequently be used in the space charge formulas to compute potentials in space.

2.6 Geometric Wake

The exclusion of plasma in the wake of a rapidly moving spacecraft is also important. That portion of the sheath surface that lies in the wake region has a reduced current passing through it. The volume of space in the wake has a reduced charge density. Conversely, on the ram side of the spacecraft, there is enhanced current and charge density.

A spacecraft creates a wake when its velocity is comparable to, or larger than, the thermal velocity of the ambient ions. In low Earth orbit, the spacecraft velocity is 7500 ms^{-1}. The thermal velocity of a 0.3 eV oxygen ion is only about 2000 ms^{-1}. Thus the spacecraft travels a few of its own radii before ions can fill in behind it. The electrons fill in more rapidly. However, the density to which electrons can accumulate is limited by the space charge of the electrons already in the wake. Thus, except in regions where the density is extremely low, the electron density is only very slightly greater than the ion density.

For each point in space, the wake module calculates what fraction of the thermal distribution of velocities, (in the spacecraft frame, a Maxwellian displaced by the spacecraft velocity vector) is not blocked by the spacecraft.

The neutral wake density is given by

$$n_i(x) = \int g(x,\Omega)\left\{ \int f_{io}(v,\Omega) v^2 dv \right\} d\Omega \tag{63}$$

where $f_{io}(v,\Omega)$ is the unperturbed distribution function for a drifting Maxwellian, and $g(x,\Omega)$ has value "0" if a ray starting from x and going in the direction Ω would strike the spacecraft and "1" if it would not.

2.7 Plumes

The ion density and velocity due to an ion thruster main beam can be read into *Nascap-2k* and displayed. Multiple thrusters (each with its own location and axis direction) can be specified, although at present all thrusters have the same type of plume. Neutralizers can be specified as well. The plume currents are used in the computation of the potentials in space ("Plume Ion Density" space charge model) and charge exchange currents.

2.8 Transverse Surface Currents

The transverse surface current algorithm in *Nascap-2k* is used to calculate the current flowing along an antenna element or other object surface in response to time-varying applied potentials and/or active or passive current sources. The model accounts correctly for both local capacitance and incident plasma current. The change in charge on a surface element during a timestep is that which is needed to accomplish the change in surface electric field, which is obtained from the *Nascap-2k* potential calculation. The current to each surface element consists of the transverse surface current from neighboring surface elements and the current provided by the plasma, which is provided by the *Nascap-2k* PIC simulation. The current continuity equation is solved using a pseudopotential approach. As a boundary condition, one surface element of each conductive element (i.e., surfaces associated with a given *Nascap-2k* conductor) is specified as connected to the biasing power supply, and the solution provides the required current.

The basic equation to be solved is $\nabla \cdot \mathbf{J} + \frac{\partial \rho}{\partial t} = 0$, where $\mathbf{J}$ is the surface current density, and ρ is the surface charge density. Note that the solution for the current is non-unique to the addition of any divergence-free current field. We assume that, provided appropriate boundary conditions are implemented, such circulating currents are not of concern to the problem being solved.

2.9 Propagating Fields

The transverse surface currents, the volume ion currents computed during particle tracking, and the volume electron currents computed from tracking or saved in the database by an external code, are a source of propagating electromagnetic fields. *Nascap-2k* can compute the magnetic field, the vector potential, the transverse electric field (rate of change of the vector potential), and the Poynting vector from these currents.

$$\mathbf{A}(\mathbf{r}) = \oint dA_s \frac{\mathbf{j}^{trans}}{|\mathbf{r} - \mathbf{r}_s|} + \int dV \frac{\mathbf{j}^{ion} + \mathbf{j}^{elec}}{|\mathbf{r} - \mathbf{r}_v|} \tag{64}$$

$$\mathbf{B}(\mathbf{r}) = \oint dA_s \frac{\mathbf{j}^{trans} \times (\mathbf{r} - \mathbf{r}_s)}{(\mathbf{r} - \mathbf{r}_s)^2} + \int dV \frac{\left(\mathbf{j}^{ion} + \mathbf{j}^{elec}\right) \times (\mathbf{r} - \mathbf{r}_v)}{(\mathbf{r} - \mathbf{r}_v)^2} \tag{65}$$

$$\mathbf{P}(\mathbf{r}) = \varepsilon_o c^2 \frac{d\mathbf{A}(\mathbf{r})}{dt} \times \mathbf{B}(\mathbf{r}) \tag{66}$$

where the surface integrals are over the spacecraft surfaces and the volume integrals are over all space outside the spacecraft.

2.10 Electron Currents (Using Pseudopotential)

Nascap-2k includes an external code that provides a non-PIC method to calculate volume electron currents that satisfy the equation of continuity, along with other physical requirements, and are consistent with electron densities computed by an ion dynamics *Nascap-2k* simulation. The method can be used to calculate electron currents within and near the sheath about a VLF (Very Low Frequency) antenna or other high-voltage object at frequencies that are low compared with both the electron plasma frequency, ω_{pe}, and the electron cyclotron frequency, ω_{ce}. The currents can then be used to calculate electromagnetic radiation, ohmic heating, etc.

This external code uses a pseudopotential approach to the computation of volume electron currents. Local equilibrium electron densities are generated for each volume element as part of the Hybrid PIC ion dynamics simulation, or, if not available, may be calculated by the module as

$$\frac{n_{elec}}{n_a} = \begin{cases} 1 + \varphi / T_e & \varphi > 0 \\ e^{\varphi / T_e} & \varphi < 0 \end{cases} . \tag{67}$$

Time derivatives of the electron density are the main drivers of volume electron currents. Space outside the calculation boundary can act as either a source or a sink for electrons, and object surfaces may act as electron sinks.

The electron current, $\mathbf{j}_{elec}$, must satisfy $\nabla \cdot \mathbf{j}_{elec} + \frac{d\rho_{elec}}{dt} = 0$. To solve this we assume that $\mathbf{j}_{elec}$ is proportional to the gradient of a "pseudopotential," ψ: $\mathbf{j}_{elec} = \boldsymbol{\sigma} \nabla \psi$, where the conductivity tensor, $\boldsymbol{\sigma}$, depends on the electron density and magnetic field. Note that the solution for the current is non-unique to the addition of any divergence-free current field. The above equations can be combined as

$$-\nabla \cdot \boldsymbol{\sigma} \nabla \psi = \frac{d\rho_{elec}}{dt} . \tag{68}$$

By standard finite element treatment, this equation is equivalent to minimizing the function

$$\int dV \left(\frac{1}{2} \nabla \psi \cdot \boldsymbol{\sigma} \nabla \psi - \psi \frac{d\rho_{elec}}{dt} \right) . \tag{69}$$

The conductivity tensor to be applied to the pseudopotentials, $\boldsymbol{\sigma}$, is assumed to be the same as the normal conductivity tensor, which for $\mathbf{B} \| \mathbf{z}$ is given by

$$\boldsymbol{\sigma}_{\text{std}} = \frac{\sigma_0}{1+(\omega_c\tau)^2}\begin{pmatrix} 1 & -\omega_c\tau & 0 \\ \omega_c\tau & 1 & 0 \\ 0 & 0 & 1+(\omega_c\tau)^2 \end{pmatrix}. \tag{70}$$

We take $\sigma_0 = \frac{ne^2\tau}{m}$ and $\frac{1}{\tau} = \frac{\varpi_{pe}}{4}$, so that $\omega_c\tau = \frac{4\omega_c}{\omega_{pe}}$. The off-diagonal (Hall) terms are omitted for the pseudopotential solution and restored when calculating the currents. To obtain the conductivity tensor for an arbitrary magnetic field we apply the transformation

$$\boldsymbol{\sigma} = \mathbf{T}^{\mathrm{T}}\boldsymbol{\sigma}_{\text{std}}\mathbf{T}, \tag{71}$$

where the transformation **T** is given by

$$\mathbf{T} = \begin{pmatrix} \cos\theta\cos\phi & \cos\theta\sin\phi & -\sin\theta \\ -\sin\phi & \cos\phi & 0 \\ \sin\theta\cos\phi & \sin\theta\cos\phi & \cos\theta \end{pmatrix} \tag{72}$$

with $\cos\theta = \frac{B_z}{|\mathbf{B}|}, \tan\phi = \frac{B_y}{B_x}$.

3 NUMERIC MODELS

This section describes the numeric techniques *Nascap-2k* uses to implement the physics models described in the previous section.

- The orbit limited currents are computed by integrating over the distribution function. An implicitized version of the Boundary Element Method is used to compute the evolution of surface potentials.
- The finite element approach is used to solve Poisson's equation for the spatial potential. Implicitization and charge stabilization are used for stability. The finite element grid uses strictly continuous electric field interpolants for accurate particle tracking.
- Macroparticle tracking is used for computing surface and volume currents and volume densities. Macroparticle splitting is used for improved accuracy.

3.1 Environment Integrals

In section 2.1 we noted that the analytic current density to a surface at potential ϕ is given by

$$j = q\int_L^\infty \frac{2Ee^2}{m^2}\left(\frac{E}{E\pm\phi}\right)f(E\pm\phi)dE = q\int_L^\infty \left(\frac{E}{E\pm\phi}\right)F(E\pm\phi)dE \tag{73}$$

where L is 0 for the repelled species and $|\phi|$ for the attracted species, the "+" sign is for ions and the "-" sign is for electrons, f(E) is the distribution function at infinity, and F(E) is the flux at infinity.

Below we describe how these integrals are done.

The environment parameters used are those valid at the beginning of the timestep.

3.1.1 Maxwellian Currents

The Maxwellian integrals are simple.

$$j = q\int_L^\infty \left(\frac{E}{E \pm \phi}\right) F(E \pm \phi) dE = e\sqrt{\frac{e}{2\pi\theta m}} n \exp\left(\mp\frac{\phi}{\theta}\right)\int_L^\infty \frac{E}{\theta}\exp\left(-\frac{E}{\theta}\right)dE \tag{74}$$

which for the repelled species simplifies to

$$j = ne\sqrt{\frac{e\theta}{2\pi m}}\exp\left(\mp\frac{\phi}{\theta}\right) \tag{75}$$

and for the attracted species simplifies to

$$j = ne\sqrt{\frac{e\theta}{2\pi m}}\left(\frac{|\phi|}{\theta}+1\right) \tag{76}$$

The average yield requires a numeric integral.

$$\langle Y\rangle = \frac{\int_L^\infty Y(E) E \exp\left(-\frac{E \pm \phi}{\theta}\right) dE}{\int_L^\infty E \exp\left(-\frac{E \pm \phi}{\theta}\right) dE} \tag{77}$$

For the attracted species use the substitution $u = \exp\left(-\frac{E \pm \phi}{\theta}\right)$

$$\frac{-\theta\int_{1}^{0} Y\left(-\theta\ln u \mp \phi\right)\left(-\theta\ln u \mp \phi\right)du}{-\theta\int_{1}^{0}\left(-\theta\ln u \mp \phi\right)du} = \frac{\int_{0}^{1} Y\left(-\theta\ln u \mp \phi\right)\left(-\theta\ln u \mp \phi\right)du}{\theta \mp \phi} \tag{78}$$

For the repelled species use the substitution $u = \exp\left(-\frac{E}{\theta}\right)$

$$\frac{-\theta\exp\left(\frac{\mp\phi}{\theta}\right)\int_{1}^{0} Y\left(-\theta\ln u\right)\left(-\theta\ln u\right)du}{-\theta\exp\left(\frac{\mp\phi}{\theta}\right)\int_{1}^{0}\left(-\theta\ln u\right)du} = \frac{\int_{0}^{1} Y\left(-\theta\ln u\right)\left(-\theta\ln u\right)du}{\theta} \tag{79}$$

The numerator is calculated numerically using 200 points and Simpson's integration.

3.1.2 Fontheim Currents

The Fontheim distribution includes both a Gaussian and a power law term. This distribution is only applicable for electrons.

Gaussian Term

The Gaussian integrals are slightly more complex than the Maxwellian.

$$j = q\int_{L}^{\infty}\left(\frac{E}{E-\phi}\right)F\left(E-\phi\right)dE = q\int_{L}^{\infty}\left(\frac{E}{E-\phi}\right)\pi\zeta\left(E-\phi\right)\exp\left(-\left(\frac{E-\phi-E_o}{\Delta_{gauss}}\right)^2\right)dE \tag{80}$$

Use the substitution $u = \frac{E-\phi-E_o}{\Delta_{gauss}}$

$$\begin{aligned} j &= \pi\zeta q\int_{L}^{\infty}\left(\Delta_{gauss}u + \phi + E_o\right)\exp\left(-u^2\right)\Delta_{gauss}du \\ &= \pi\zeta q\Delta_{gauss}^2\int_{L}^{\infty} u\exp\left(-u^2\right)du \quad + \pi\zeta q\left(\phi + E_o\right)\Delta_{gauss}\frac{\sqrt{\pi}}{2}\operatorname{erfc}\left(L\right) \end{aligned} \tag{81}$$

where L is now $\max\left(\frac{-E_o}{\Delta_{gauss}}, \frac{-\phi - E_o}{\Delta_{gauss}}\right)$.

The substitution $x = \exp\left(-u^2\right)$ can be used to solve the remaining integral.

$$j = \pi\zeta q\Delta_{gauss}^2 \frac{1}{2}\exp\left(-L^2\right) + \pi\zeta q\left(\phi + E_o\right)\Delta_{gauss}\frac{\sqrt{\pi}}{2}\operatorname{erfc}(L) \tag{82}$$

The average yield requires a numeric integral. Using the same substitution and definition of L we have

$$\langle Y \rangle = \frac{\int_L^\infty Y\left(\Delta_{gauss}u + \phi + E_o\right)\left(\Delta_{gauss}u + \phi + E_o\right)\exp\left(-u^2\right)\Delta_{gauss}du}{\Delta_{gauss}^2\frac{1}{2}\exp\left(-L^2\right) + \left(\phi + E_o\right)\Delta_{gauss}\frac{\sqrt{\pi}}{2}\operatorname{erfc}(L)} \tag{83}$$

The integral in the numerator can be divided into three in order to isolate the peak at u = 0. If L > 0, then the first two terms are zero and $\xi = L$.

$$\int_L^\infty f(u)du = \int_L^{-\xi} f(u)du + \int_{-\xi}^{\xi} f(u)du + \int_{\xi}^{\infty} f(u)du \tag{84}$$

The first and third terms can be evaluated using the substitution $x = \exp\left(-u^2\right)$. Then $u = \pm\sqrt{-\ln x}$, where the "-" sign is used in the first term and the "+" sign in the third. Under the assumption that ξ is small, symmetry can be used to write the second term in terms of the error function. The numerator can be written as

$$\begin{aligned}\frac{\Delta_{gauss}}{2}&\int_{\exp\left(-L^2\right)}^{\exp\left(-\xi^2\right)} Y\left(-\Delta_{gauss}\sqrt{-\ln x} + \phi + E_o\right)\left(-\Delta_{gauss} + \frac{\phi + E_o}{\sqrt{-\ln x}}\right)dx + \Delta_{gauss}Y\left(\phi + E_o\right)\left(\phi + E_o\right)\sqrt{\pi}\operatorname{erf}(\xi) \\ &+ \frac{\Delta_{gauss}}{2}\int_o^{\exp\left(-\xi^2\right)} Y\left(\Delta_{gauss}\sqrt{-\ln x} + \phi + E_o\right)\left(\Delta_{gauss} + \frac{\phi + E_o}{\sqrt{-\ln x}}\right)dx\end{aligned} \tag{85}$$

Power Law

$$j = q\int_{L}^{\infty}\left(\frac{E}{E-\phi}\right)F(E-\phi)dE = q\int_{\max(0,E_L+\phi)}^{\max(E_U,E_U+\phi)}\left(\frac{E}{E-\phi}\right)\pi\zeta\ (E-\phi)^{-\alpha}\,dE \tag{86}$$

Using the substitutions x = E-ϕ and then z =$x^{-(\alpha-1)}$ and z =$x^{-\alpha}$ we get

$$j = q\pi\zeta\int_{\max(-\phi,E_L)^{-(\alpha-1)}}^{\max(E_U-\phi,E_U)^{-(\alpha-1)}}\frac{dz}{-(\alpha-1)} + q\pi\zeta\phi\int_{\max(-\phi,E_L)^{-\alpha}}^{\max(E_U-\phi,E_U)^{-\alpha}}\frac{dz}{-\alpha}$$

$$= \frac{q\pi\zeta}{-(\alpha-1)}\left(\max(E_U-\phi,E_U)^{-(\alpha-1)} - \max(-\phi,E_L)^{-(\alpha-1)}\right) + \frac{q\pi\zeta\phi}{-\alpha}\left(\max(E_U-\phi,E_U)^{-\alpha} - \max(-\phi,E_L)^{-\alpha}\right) \tag{87}$$

The same technique is used to evaluate the average yield.

$$\langle Y\rangle = \frac{q\pi\zeta\displaystyle\int_{\max(-\phi,E_L)^{-(\alpha-1)}}^{\max(E_U-\phi,E_U)^{-(\alpha-1)}}\frac{Y\left(z^{\left(\frac{1}{-(\alpha-1)}\right)}-\phi\right)dz}{-(\alpha-1)} + q\pi\zeta\phi\displaystyle\int_{\max(-\phi,E_L)^{-\alpha}}^{\max(E_U-\phi,E_U)^{-\alpha}}\frac{Y\left(z^{\left(\frac{1}{-\alpha}\right)}-\phi\right)dz}{-\alpha}}{j} \tag{88}$$

3.1.3 Kappa Distribution Currents

$$j = q\int_{L}^{\infty}\left(\frac{E}{E\pm\phi}\right)F(E\pm\phi)dE = qn\sqrt{\frac{e}{2\pi\kappa\theta m}}\,\frac{\Gamma(\kappa+1)}{\Gamma\left(\kappa-\frac{1}{2}\right)}\int_{L}^{\infty}\frac{E}{\kappa\theta}\left(1+\frac{E\pm\phi}{\kappa\theta}\right)^{-\kappa-1}dE \tag{89}$$

which for the repelled species simplifies to

$$j = qn\sqrt{\frac{e}{2\pi\kappa\theta m}}\,\frac{\Gamma(\kappa+1)}{\Gamma\left(\kappa-\frac{1}{2}\right)}(\kappa\theta)^{\kappa}\int_{0}^{\infty}E(E\pm\phi+\kappa\theta)^{-\kappa-1}dE$$

$$j = qn\sqrt{\frac{\kappa e\theta}{2\pi m}}\,\frac{\Gamma(\kappa-1)}{\Gamma\left(\kappa-\frac{1}{2}\right)}\left(1\pm\frac{\phi}{\kappa\theta}\right)^{1-\kappa} \tag{90}$$

for κ > 1.

For the attracted species the integral requires a substitution.

$$
\begin{aligned}
j &= qn\sqrt{\frac{e}{2\pi\kappa\theta m}}\,\frac{\Gamma(\kappa+1)}{\Gamma\left(\kappa-\frac{1}{2}\right)}(\kappa\theta)^{\kappa}\int_0^{\infty}(u\mp\phi)(\kappa\theta+u)^{-\kappa-1}du \\
&= qn\sqrt{\frac{\kappa e\theta}{2\pi m}}\,\frac{\Gamma(\kappa-1)}{\Gamma\left(\kappa-\frac{1}{2}\right)}\left(1\mp\frac{(\kappa-1)\phi}{\kappa\theta}\right)
\end{aligned}
\tag{91}
$$

The average yield requires a numeric integral.

$$
\langle Y\rangle = \frac{\int_L^{\infty} Y(E)E\left(1+\frac{E\pm\phi}{\kappa\theta}\right)^{-\kappa-1}dE}{\int_L^{\infty} E\left(1+\frac{E\pm\phi}{\kappa\theta}\right)^{-\kappa-1}dE}
\tag{92}
$$

Use the substitution $u = 1+\frac{E\pm\phi}{\kappa\theta}$

$$
\langle Y\rangle = \frac{\int_{L'}^{\infty} Y\left(\kappa\theta(u-1)\mp\phi\right)\left(\kappa\theta(u-1)\mp\phi\right)(u)^{-\kappa-1}du}{\int_{L'}^{\infty}\left(\kappa\theta(u-1)\mp\phi\right)(u)^{-\kappa-1}du}
\tag{93}
$$

where $L' = 1\pm\frac{\phi}{\kappa\theta}$ for the repelled species and $L' = 1$ for the attracted species.

Then use the substitutions $y = u^{\kappa-1}$ and $y = u^{\kappa}$ for an even distribution of points.

$$
\langle Y\rangle = \frac{\frac{\kappa\theta}{1-\kappa}\int_0^{L_1} Y\left(\kappa\theta\left(y^{-1/(\kappa-1)}-1\right)\mp\phi\right)dy - \left(\frac{-\kappa\theta\mp\phi}{\kappa}\right)\int_0^{L_2} Y\left(\kappa\theta\left(y^{-1/\kappa}-1\right)\mp\phi\right)dy}{\frac{\kappa\theta L_1}{1-\kappa}-\left(\frac{-\kappa\theta\mp\phi}{\kappa}\right)L_2}
\tag{94}
$$

where $L_1 = \left(1\pm\frac{\phi}{\kappa\theta}\right)^{-1/(\kappa-1)}$ and $L_2 = \left(1\pm\frac{\phi}{\kappa\theta}\right)^{-1/\kappa}$ for the repelled species and $L_1 = L_2 = 1$ for the attracted species.

3.1.4 Convected Maxwellian Currents

As the convected Maxwellian distribution depends on the velocity of the plasma with respect to the spacecraft and the angle between the bulk plasma velocity and the particle velocity, the full angular integral is needed.

$$j_s = j_s(\hat{n}, \Phi, \mathbf{U}) = q\iiint d^3v(\mathbf{v}\cdot\hat{n})f_s(\mathbf{v}) \quad . \tag{95}$$

The coordinate system is shown in Figure 8.

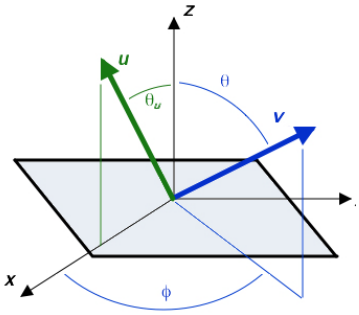

Figure 8. Coordinate System Used for Convected Maxwellian Environment, in Spacecraft Frame.

Written as an integral over the velocity at infinity, v_∞, we have

$$j_s = q_s n_s \sqrt{\frac{e\theta}{2\pi m_s}}\left(\frac{1}{2\pi}\right)\left(\frac{m_s}{e\theta}\right)^2 \int_0^{2\pi} d\varphi \int_0^{\pi/2} d\vartheta \int_L^{\infty} dv_\infty v_\infty \left(v_\infty^2 \pm \frac{2e\phi}{m_s}\right) e^{-\left(\frac{m_s}{2e\theta}\right)\left(v_\infty^2 - 2v_\infty U\cos\chi + U^2\right)} \sin\vartheta\cos\vartheta \tag{96}$$

where the lower velocity limit L=0 for an attractive potential and $L = \sqrt{\frac{2e\phi}{m_s}}$ otherwise. χ is the angle between the flow vector U and the incident velocity at infinity $\mathbf{v}_\infty$. χ is dynamically mapped to the incident angle ϑ and is given by

$$\cos\chi = \cos\vartheta_\infty \cos\vartheta_u + \sin\vartheta_\infty \sin\vartheta_u \cos\varphi \,. \tag{97}$$

where ϑ_u is the polar angle of the flow velocity vector and ϑ_∞ is the polar angle of $\mathbf{v}_\infty$. With this substitution, the azimuthal integrand has the form[‡] exp(-a cos(φ)), and noting that the zeroth-order modified Bessel function of the first kind I_0 is given by

$$2\pi I_0(a) = \int_0^{2\pi} d\varphi e^{-a\cos\varphi} \,, \tag{98}$$

we can write the current as

[‡] The evenness of the (even-order) Bessel function swallows a minus sign here.

$$j_s = A\int_L^{\infty} dv_\infty v_\infty \left(v_\infty^2 \mp \frac{2e\phi}{m_s} \right) e^{-\frac{m_s}{2e\theta} v_\infty^2} \int_0^{\pi/2} d\vartheta\, e^{\frac{m_s}{e\theta} v_\infty U \cos\vartheta_\infty \cos\vartheta_u} I_o\left(\frac{m_s}{e\theta} v_\infty U \sin\vartheta_\infty \sin\vartheta_u \right) \sin\vartheta\cos\vartheta$$
$$\text{with } A = q_s n_s \sqrt{\frac{e\theta}{2\pi m_s}} e^{-\frac{m_s}{2e\theta}(U^2)} \left(\frac{m_s}{e\theta} \right)^2 \tag{99}$$

The velocity and polar angle integrals are performed numerically. The angle and magnitude of the flow velocity vector (defined in the spacecraft frame) are specified by the user, and the angle at infinity θ_∞ is obtained from orbit relations in a 1/r potential, as a function of the total energy $E = \frac{mv_\infty^2}{2e}$ and launch angle ϑ_L. From reference 32 we obtain[§]

$$\frac{a}{r} = \frac{\phi}{2(E \mp \phi)\sin^2\vartheta} \times \left(1 + \sqrt{1 + \frac{4E(E \mp \phi)}{\phi^2} \sin^2\vartheta}\, \cos(\vartheta_L - \vartheta_o) \right) \tag{100}$$

Measuring orbital angles from the polar axis that is normal to the sphere at the launch point and setting a = r determines the angle ϑ_o

$$\cos\vartheta_0 = \frac{\left(-1 + 2\left(\frac{E}{\phi} \mp 1 \right) \sin^2\vartheta \right)}{\sqrt{1 + \frac{4E(E \mp \phi)}{\phi^2} \sin^2\vartheta}} \tag{101}$$

Setting $r = \infty$ ($\vartheta = \vartheta_\infty$) gives

$$\cos(\vartheta_\infty - \vartheta_0) = -1 \Big/ \sqrt{1 + \frac{4E(E \mp \phi)}{\phi^2} \sin^2\vartheta} \tag{102}$$

In the limit as $U \to 0$ we recover the expected isotropic/uniform flux density, while as the Mach number increases the flux approaches a cosine dependence on relative particle angle.[33]

For full consistency, the secondary electron emission current due to ion or electron impact and the backscattered current due to electron impact would be given by

[§] Starting from Goldstein eqn 3-46, substitute angular momentum l = r x p = r m v sin(ϑ), potential energy Φ = k/r, and $1/2mv^2 = E + \Phi$, then for a launch radius r = a).

$$j_s = A\int_{L'}^{\infty} dv_\infty v_\infty \left(v_\infty^2 \pm \frac{2e\phi}{m_s}\right) e^{-\frac{m_s}{2e\theta}v_\infty^2} \int_0^{\pi/2} d\vartheta\, Y_{i,e}^{sec,back}(v,\theta)\vartheta e^{\frac{m_s}{e\theta}v_\infty U\cos\vartheta_\infty \cos\vartheta_u} \times I_o\left(\frac{m_s}{e\theta}v_\infty U\sin\vartheta_\infty \sin\vartheta_u\right)\sin\vartheta\cos\vartheta \quad (103)$$

As this is a time consuming calculation and electron Mach numbers are always under 1, we compute the yields due to incident electrons using an isotropic Maxwellian distribution.

$$j_e^{sec,back} = \left\langle Y_{maxwellian}\right\rangle_e^{sec,back} j_e^{incident} \quad (104)$$

The secondary emission due to ions is computed using the full angular integral.

The effective density of each component is the expectation value of the distribution function. The techniques used to compute the average values of the square root of the inverse of the energy are the same as used to evaluate the current integrals above.

3.1.5 Measured Currents

If F(E)dE is the measured flux of ions or electrons striking a zero potential surface with energy between E and E+dE, after correction for the actual surface potential of the detector, then

$$j = q\int_L^{\infty}\left(\frac{E}{E\pm\phi}\right)F(E\pm\phi)dE = q\int_{L\pm\phi}^{\infty}\left(\frac{u\mp\phi}{u}\right)F(u)du \quad (105)$$

where the substitution $u=E\pm\phi$ was made.

If the measurement is expressed as a set of energy bins in ascending order with flux $F_i(u_{i+1}-u_i)$ in bin i which extends from u_i to u_{i+1}, the integral is discretized as

$$j = q\int_{L\pm\phi}^{\infty}\left(\frac{u\mp\phi}{u}\right)F(u)du \rightarrow q\left(\frac{\sqrt{\pm\phi\ u_{j+1}}\mp\phi}{\sqrt{\pm\phi\ u_{j+1}}}\right)F_j(u_{j+1}\mp\phi) + q\sum_{i>j}\left(\frac{\sqrt{u_i u_{i+1}}\mp\phi}{\sqrt{u_i u_{i+1}}}\right)F_i(u_{i+1}-u_i) \quad (106)$$

where u_{j+1} is the lower boundary of the first bin entirely within the domain of integration, $u_j < \pm\phi < u_{j+1}$.

The average yield is then given by

$$\langle Y \rangle = \frac{\int_{\max(0,\pm\phi)}^{\infty} Y(u \mp \phi)\left(\frac{u \mp \phi}{u}\right) F(u)du}{\int_{\max(0,\pm\phi)}^{\infty} \left(\frac{u \mp \phi}{u}\right) F(u)du} \tag{107}$$

$$\langle Y \rangle = \frac{Y\left(\sqrt{\pm\phi\, u_{j+1}} \mp \phi\right)\left(\frac{\sqrt{\pm\phi\, u_{j+1}} \mp \phi}{\sqrt{\pm\phi\, u_{j+1}}}\right) F_j\left(u_{j+1} \mp \phi\right) + \sum_{i>j} Y\left(\sqrt{u_i u_{i+1}} \mp \phi\right)\left(\frac{\sqrt{u_i u_{i+1}} \mp \phi}{\sqrt{u_i u_{i+1}}}\right) F_i\left(u_{i+1} - u_i\right)}{\left(\frac{\sqrt{\pm\phi\, u_{j+1}} \mp \phi}{\sqrt{\pm\phi\, u_{j+1}}}\right) F_j\left(u_{j+1} \mp \phi\right) + \sum_{i>j}\left(\frac{\sqrt{u_i u_{i+1}} \mp \phi}{\sqrt{u_i u_{i+1}}}\right) F_i\left(u_{i+1} - u_i\right)} \tag{108}$$

3.2 Space charge limiting of photoemission

For a barrier height of E_1, the escaping photocurrent for a surface exposed to the sun at an angle ψ_{sun} is given by the formula $j_{photo}^{escape}(E_1) = I_{sun} Y_{sun}(E_1) \max(\cos(\psi_{sun}), 0)$, where $I_{sun} Y_{sun}(E_1)$ is the yield of photoelectrons with energy greater than E_1 from the surface exposed to a normally incident solar spectrum. In the absence of electrostatic saddle-point or space charge barrier formation, the barrier to escape of photoelectrons is the surface potential for positive potentials and zero for negative potentials. Photoelectron space charge provides an additional possibility for increasing the barrier in excess of the surface potential or imposing a barrier in front of a negative potential surface. If the user requests that space charge limiting of the photocurrent be included in the charging calculation, the following algorithm is used to determine the barrier height, E_1.

First, if the ratio of the available photocurrent to the plasma density is less than 2% of the typical value for this ratio at Earth orbit, $\frac{j_{photo}^{escape}(0)}{78\times10^{-6}} \frac{7\times10^{6}}{n_a} < 0.02$ there is no barrier.

Otherwise, a "maximum barrier," B_{max}, is computed. B_{max} is the lesser of the barrier calculated in two different ways. The first estimate, $B_{max}^{(1)}$, is given by the condition that the barrier occurs no further from the surface than the distance at which the current drops by a factor of two, i.e., $R_{barrier}^2 \le 2R_c^2$, where the symbols represent the distance of the barrier from the local center of curvature and the effective radius of curvature of the surface. The second estimate, $B_{max}^{(2)}$, is given by the condition that the photoelectron density beyond the barrier must be no less than half the ambient plasma density. If either condition gives a negative value, the barrier is zero.

$B_{max}^{(1)}$ is found using an analytic fit to numeric calculations that assume only that the shape of the photoemission spectrum is the default shape specified in Section 2.1.3. Without loss of generality, the minimum potential is taken to be zero, therefore the surface potential is E_1. In a locally spherical geometry, the space charge between the surface and the barrier is given by

$$\rho(r,\phi(r)) = \sqrt{\frac{m_e}{2e}} \int_{E_1-\phi(r)}^{\infty} \frac{d}{dE}\left(j_{photo}^{escape}(E)\right)\left(\frac{R_c}{r}\right)^2 \frac{1+H(E_1-E)}{\sqrt{E-(E_1-\phi(r))}}\,dE \tag{109}$$

where the Heaviside step function has been used to reflect the fact that electrons with energy less than E_1 both leave and return, while those with energy greater than E_1 only leave. The surface potential can be found by integrating Poisson's equation inward from the barrier to the surface. For any combination of escaping photo current and effective radius of curvature there is a unique value of escaping energy E_1 for which the surface potential is also E_1. The fit to these self-consistent barrier calculations used in *Nascap-2k* is

$$B_{max}^{(1)} = (24.772 + 13.755R_c - 7.6419R_c^2)\left(j_{photo}^{escape}(0)\right)^{0.4291-0.1542R_c} \tag{110}$$

$B_{max}^{(2)}$ is found using an analytic fit to the solution of equating the charge density of the escaping photocurrent to half the ambient plasma density. Beyond the barrier in the ambient plasma, the charge density of the escaping photocurrent is

$$\rho_{escaping} = \int_{B_{max}^{(2)}}^{\infty} \frac{d}{dE}\left(j_{photo}^{escape}(E)\right)\frac{dE}{\sqrt{\frac{2e}{m_e}(E-\phi_s)}} \tag{111}$$

Equating $\rho_{escaping}$ to half the plasma density and rearranging gives

$$\int_{B_{max}^{(2)}}^{\infty} \frac{1}{j_{photo}^{escape}(0)} \frac{d}{dE}\left(j_{photo}^{escape}(E)\right)\frac{dE}{\sqrt{E-\phi_s}} = \frac{1}{2}\frac{e\,n_a}{j_{photo}^{escape}(0)}\sqrt{\frac{2e}{m_e}} \tag{112}$$

where the left hand side depends only on the shape of the photoemission spectrum and the surface potential, and the right hand side depends only on the problem parameters and incident angle. Again, when solving this equation, the shape of the photoemission spectrum is taken to be default shape specified in Section 2.1.3. The maximum barrier is given by zero surface potential. For zero surface potential, the solution is well-fit for barriers up to 12 volts by

$$1.436\times10^{-8}\,\frac{j_{photo}^{escape}(0)}{e\,n_a} = 10^{-3}\left(9.71 + B_{max}^{(2)}\left(0.199 + B_{max}^{(2)}\left(2.04 + 0.378\,B_{max}^{(2)}\right)\right)\right) \tag{113}$$

where the scaling is such that the left hand side is unity for typical 1 AU parameters. To simplify the solution of the cubic equation above, we obtain an initial guess by first solving the quadratic fit

$$1.436\times10^{-8}\,\frac{j_{photo}^{escape}(0)}{e\,n_a} = 10^{-3}\left(61.3 - B_{max}^{(2)}\left(39.7 - 9.41B_{max}^{(2)}\right)\right) \tag{114}$$

and then solve the cubic using Newton iteration.

Once the maximum barrier, $B_{max} = \min\left(B_{max}^{(1)}, B_{max}^{(2)}\right)$, has been determined, the actual barrier E_1 can be determined. If $\phi_s \geq B_{max} \geq 0$, the space charge is not sufficient to cause a negative potential in front of the surface, so the barrier is equal to the surface potential.

If the surface potential is less than the maximum barrier ($B_{max} > \phi_s$, including cases with negative surface potential) a final condition is used to determine the barrier. The escaping photocurrent must be sufficient to give photoelectron density comparable to the ambient density beyond the barrier in the ambient plasma. This condition is approximated as

$$j_{photo}^{escape}\left(E_1\right) \geq n_i e \sqrt{\frac{2e(E_1 - \phi_s)}{m_e}} \tag{115}$$

If $E_1 = B_{max}$ satisfies this inequality, the barrier equals the maximum barrier. If not, the equation is numerically solved for a lower barrier E_1 that gives the equality.

3.3 Shadowing

A surface element is shadowed from the sun if, either

(1) Its normal points anti-sunward, or
(2) Its centroid lies behind the projection of another sun-facing surface.

The determination of the second is handled in a coordinate system in which the z-axis is the direction to the sun. The unit vectors along the axes of the rotated coordinate system are given by $\mathbf{s}_x$, $\mathbf{s}_y$, $\mathbf{s}_z$. The position of a surface element along the z-axis in the rotated system is given by $r_z = \frac{1}{N}\sum_i \left(\mathbf{s}_z \bullet \mathbf{r}_i\right)$, where $\mathbf{r}_i$ are the nodes of element and N is the number of nodes. The projection of a surface element on the x-y plane of the rotated system is given by $\left(\mathbf{s}_x \bullet \mathbf{r}_i, \mathbf{s}_y \bullet \mathbf{r}_i\right)$.

Surface A is shadowed by surface B if, $r_z(A) < r_z(B)$ and the centroid of the projection of surface A is inside the projection of surface B.

3.4 Implicit Charging Using the Boundary Element Method

Among the difficulties of developing accurate and robust algorithms for spacecraft charging has been the inability to calculate electric fields accurately, let alone to predict how electric fields will change as a result of surface potential changes. *Nascap-2k* uses the Boundary Element Method (BEM)[34] to calculate accurate electric fields and as the basis for implicit charging equations.

3.4.1 Boundary Element Method Algorithm

The Boundary Element Method is a means for relating fields and potentials in a region to sources on the boundary of the region. It is comparable to a sum over the coulomb field of all the charges

in a region rather than an iterative field solution. In our case, the region is the space exterior to a spacecraft, and the boundary is the spacecraft surface. Also, we assume the "free space Green's function", *i.e.,* the potentials in the region obey Laplace's equation.

The sources are sheets of charge coincident with the spacecraft model's surface elements. We assume that each surface element, *j*, has a constant charge density, σ_j. The familiar relation for the potential of a point charge then generalizes to an integral over the object surface:

$$\phi = \frac{q}{4\pi\varepsilon_o r} \rightarrow (4\pi\varepsilon_o)\phi_i = \sum_j \int d^2 r_j \frac{\sigma_j}{r_{ij}} \tag{116}$$

where ϕ_i, which could be the potential at any point in space, is considered the potential at the center of a surface element. Similarly, the familiar relation for the electric field of a point charge generalizes to:

$$\mathbf{E} = \frac{q}{4\pi\varepsilon_o r} \rightarrow (4\pi\varepsilon_o)\mathbf{E}_i = \sum_j \int d^2 r_j \frac{\sigma_j}{r_{ij}^3}(\mathbf{r}_i - \mathbf{r}_j) \tag{117}$$

where $\mathbf{E}_i$ is the electric field at some point in space, the point again taken at the center of a surface element.

We express the relations of potential and electric field to charge density as matrices:

$$\phi_i = \left[C^{-1}\right]_{ij}\sigma_j \qquad (\mathbf{E}\cdot\mathbf{n})_i = \mathbf{F}_{ij}\sigma_j \tag{118}$$

These can be combined to obtain a relation between normal electric field and voltage:

$$(\mathbf{E}\cdot\mathbf{n})_i = \mathbf{F}_{ik}\mathbf{C}_{kj}\mathbf{V}_j \tag{119}$$

This last relation is the key to developing relations between surface charge, surface potential, and surface currents in order to derive charging equations.

3.4.2 Doing the Integrals

To get C^{-1} we need to do integrals of the form

$$\int d^2 r_j \frac{\sigma_j}{r_{ij}} \tag{120}$$

There are tricks to doing these integrals, which can be found in the literature. Denote the field point, r_i as P, and take the domain of integration as triangle ABC. Then, the vector from the field point to anywhere on the triangle can be parameterized as

$$\mathbf{r}_{ij} = PA + uAB + uvBC \tag{121}$$

where PA, AB, and BC are vectors between pairs of points, and u and v are parameters, each in the interval [0,1]. The square of the distance, r_{ij}, then becomes

$$r_{ij}^2 \equiv \mathbf{r}_{ij} \cdot \mathbf{r}_{ij} = \sum_{0 \le k,l \le 2} T_{kl} u^k v^l \tag{122}$$

where the coefficients T_{kl} are formed from pairwise scalar products of the three vectors above. Now, the integral can be expressed as

$$\int d^2 r_j \frac{\sigma_j}{r_{ij}} = \int_0^1 dv \int_0^1 udu \frac{\sigma_j}{\sqrt{V_0 + V_1 u + V_2 u^2}} \tag{123}$$

where the V_i coefficients are functions of v.

The inner integral (over *u*) may be found in standard integral tables[35]

$$\begin{aligned} \int xdx \frac{1}{\sqrt{c + bx + ax^2}} &= \frac{\sqrt{c + bx + ax^2}}{a} - \frac{b}{2a} \int dx \frac{1}{\sqrt{c + bx + ax^2}} \\ \int dx \frac{1}{\sqrt{c + bx + ax^2}} &= \frac{1}{\sqrt{a}} \log \left| 2\sqrt{a}\sqrt{c + bx + ax^2} + 2ax + b \right| \end{aligned} \tag{124}$$

We are left to do the outer integral (over v) numerically. To facilitate this, we select the vertex A such that the scalar product PA·BC is the minimum of the three choices. Then, very few integration points are needed in the outer integral (over v). (We use a 5-point Simpson's rule in the present implementation.)

The integrals for the electric field are similar, although there are more of them. The same techniques apply.

3.4.3 Test for Accuracy

We tested the algorithm for accuracy by calculating the electric fields on the surface elements of a uniform potential sphere. The sphere model in Figure 9 was originally defined using Patran, and has 90 surface elements and 92 nodes. It provides a fairly coarse mesh over the surface of the sphere.

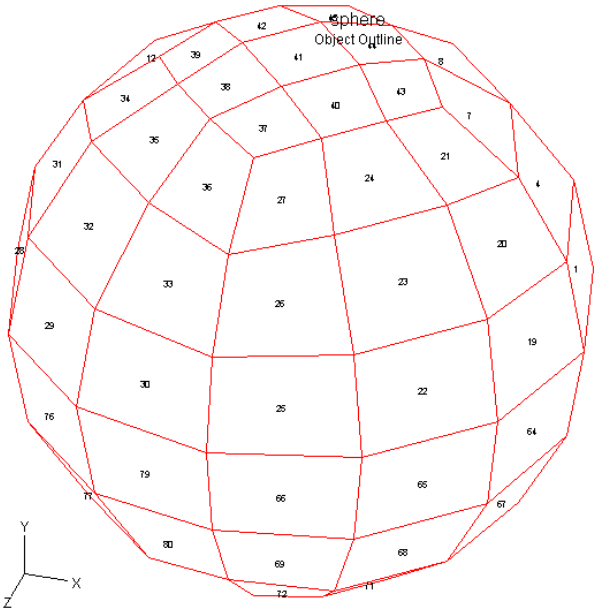

Figure 9. Sphere Defined Using Patran.

The next figure shows the result of the BEM calculation. Note that the total variation of electric field over the surface is only three percent. Also, the apparent radius of the sphere (given by V/E) is within three percent of the nominal radius.

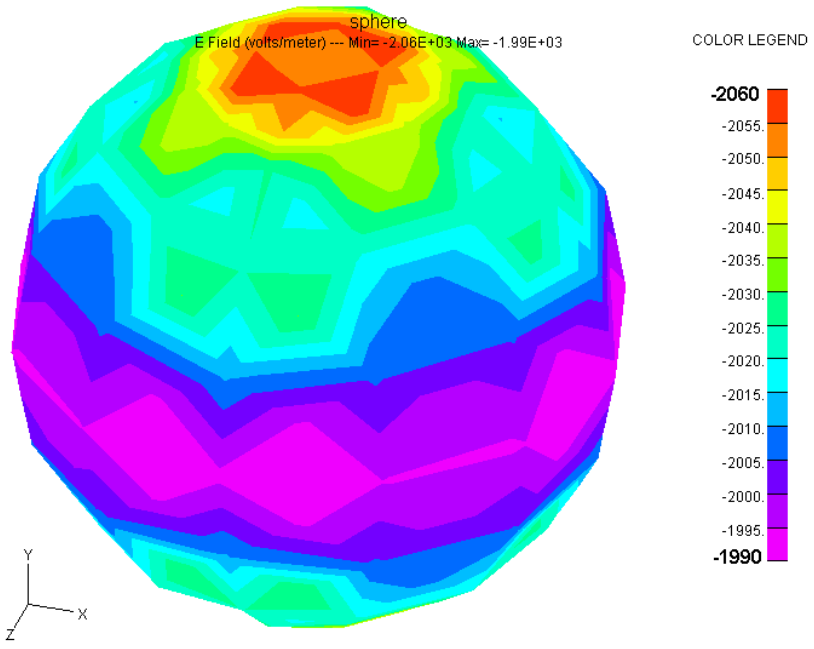

Figure 10. Normal Component of Electric Field at Surface of Sphere as Computed Using the BEM Approach.

By contrast, the same calculation using *Nascap-2k*'s finite element algorithm with higher order elements gives an electric field variation of seven percent, and a value of electric field that is about fifteen percent high. A finite element algorithm with linear elements gives an eight percent variation, and a value that is about twenty-five percent high.

3.4.4 Implicit Charging

To develop charging equations we need to express physical charges on physical surfaces in terms of the voltages on the same objects. We can then proceed to calculate what voltage changes will be produced by changes in charge (currents). Because the interior of a spacecraft is *not* free space, the physical charge densities bear no relation to the charge density σ's used in the derivation of the relation between the normal electric field and the voltage of Boundary Element Method.

To get the physical charges we use Maxwell's divergence equation in the form $\sigma = \nabla \cdot \mathbf{D}$. Figure 11 shows the "Gaussian pillboxes" used to calculate the actual surface charges on insulating surfaces and on conductors, as described below.

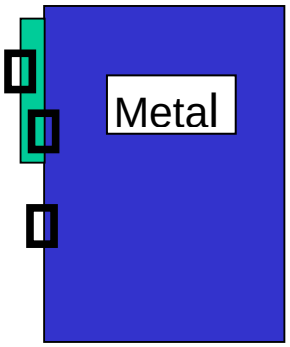

Figure 11. "Gaussian Pillboxes" Used to Calculate the Actual Surface Charges on Insulating Surfaces and on Conductors.

For an insulating surface (upper pillbox in Figure 11), the external field is $\mathbf{E}\cdot\mathbf{n}$, which we obtain from the BEM solution. The internal field is related to the capacitance between the insulating surface and its underlying conductor. Thus, the total charge, q_i on such a surface is given by:

$$q_i = A_i \left(\mathbf{E}\cdot\mathbf{n}\right)_i + C_{ic}\left(\phi_i - \phi_c\right) \tag{125}$$

where A is the surface area. For a conductor, since charges are mobile, it is not useful to know the charge on each individual surface, but we need to work with the total charge on the conductor. Conducting surfaces include the obvious "bare" surfaces (lower pillbox in Figure 11), as well as the surfaces that underlie the insulating surfaces (middle pillbox in Figure 11). In both cases, we have zero electric field internal to the metal. To obtain the total charge on all the surfaces of the conductor, we need to sum the external-field charge terms for the bare conducting surfaces, plus the capacitive-charge terms for the insulator-metal interfaces:

$$Q_c = \sum_{\text{bare}} A_i \left(\mathbf{E}\cdot\mathbf{n}\right)_i - \sum_{\text{insulators}} C_{ic}\left(\phi_i - \phi_c\right) \tag{126}$$

We previously found the BEM expression for the external fields in terms of the cell potentials:

$$\left(\mathbf{E}\cdot\mathbf{n}\right)_i = F_{ik}C_{kj}\phi_j \tag{127}$$

Substituting this into the equations for q_i and Q_c, performing the indicated sums, and adding the capacitive terms, we get the matrix equation:

$$\mathbf{Q}=\mathbf{G}\boldsymbol{\Phi} \tag{128}$$

where the vectors are composed of contributions from all the insulating surfaces and a term for each conductor representing all the bare conducting surfaces of that conductor. Conductors that are biased with respect to another conductor are treated as a single conductor at this point in the calculation.

$$\mathbf{Q} = \{q_1, q_2, \ldots, q_n, Q_c\} \tag{129}$$

$$\boldsymbol{\Phi} = \{\phi_1, \phi_2, \ldots, \phi_n, \phi_c\} \tag{130}$$

where **Q** and **Φ**, the charges and potentials, are related by the charging matrix, **G**.

We are looking for an equation that relates currents to voltage changes. So, we differentiate the charge equation in time:

$$\mathbf{I} \equiv \dot{\mathbf{Q}} = \mathbf{G}\dot{\boldsymbol{\Phi}} \tag{131}$$

Discretize to a finite time interval:

$$\mathbf{I}\Delta t = \mathbf{G}\left[\boldsymbol{\Phi}\left(t+\Delta t\right)-\boldsymbol{\Phi}\left(t\right)\right] \tag{132}$$

Implicitize by evaluating current at the final time (also, for simplicity, changing [t+Δt,t] to [t,0]):

$$\mathbf{I}\left(t\right)t = \mathbf{G}\left[\boldsymbol{\Phi}\left(t\right)-\boldsymbol{\Phi}\left(0\right)\right] \tag{133}$$

Linearize currents with respect to voltage (since we do not know the final voltages at which the current is to be evaluated):

$$\mathbf{I}\left(t\right) \approx \mathbf{I}\left(0\right)+\mathbf{I}'\left[\Phi\left(t\right)-\Phi\left(0\right)\right] \tag{134}$$

And, solve the equation:

$$\left[\mathbf{G}-\mathbf{I}'t\right]\boldsymbol{\Phi}\left(t\right)=\left[\mathbf{G}-\mathbf{I}'t\right]\boldsymbol{\Phi}\left(0\right)+\mathbf{I}\left(0\right)t \tag{135}$$

This gives us a straightforward matrix equation. Everything on the right-hand-side is known, and we can solve using standard linear algebra equation solver packages.

Any user specified values for the bias of one conductor with respect to another is reapplied each timestep. The $\mathbf{v}\times\mathbf{B}$ contribution to the surface potential is also reapplied each timestep.

Before proceeding to examples, it is worth commenting on the derivative of current, $\mathbf{I}'_{ij} = \partial I_i / \partial \phi_j$.

Consider three cases:

1. For current sources such as incident plasma current, we usually approximate the current as a function of the local voltage only. This gives a diagonal term in $\mathbf{I}'_{ij}$. Since such currents decay exponentially, some care must be taken not to underestimate the change in current if the voltage is changing in such a direction that a component of current is increasing (i.e., electron current for a surface whose potential is increasing (toward zero) from a large negative potential).

   For example, suppose we have $\dot{\phi} = I(\phi) = 1 - e^{-\phi}$ and $\phi(0)$=-2. The implicit solution for $\phi(t)$ is $\phi(t) = \frac{\phi(0)(1 - I't) + I(\phi(0))t}{(1 - I't)}$. If we use the actual derivative $I' = -\exp(\phi(0))$, we obtain the upper curve in Figure 12, which works satisfactorily for sensible timesteps like 0.1 or 1, but overshoots the solution $(\phi(\infty) = 0)$ badly for long timesteps like 10 or 1000. However, if we recognize that zero is a value we wish not to overshoot and accordingly set $I' = \frac{I(0) - I(\phi(0))}{0 - \phi(0)}$ we obtain the lower curve in Figure 12, which gives equally good results for short timesteps and does not overshoot the solution, even for a timestep of 1000.

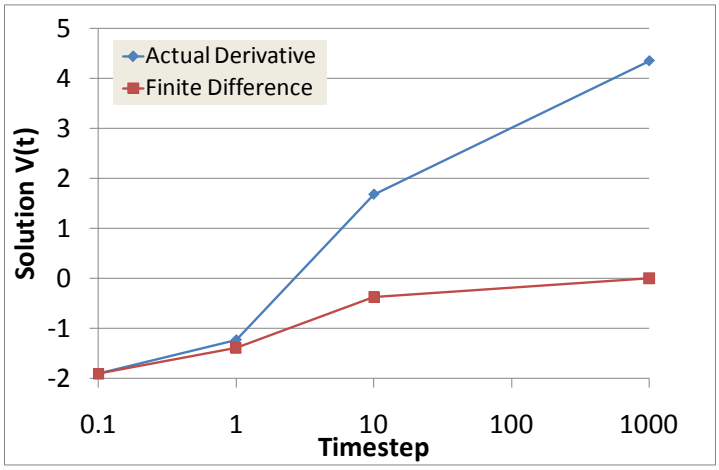

Figure 12. Example Problem Solutions for Short and Long Timesteps for Two Choices of Current Derivative.

2. Conductivity current, such as $I_i = \sigma(\phi_c - \phi_i)$, contributes off-diagonal as well as diagonal terms to the current derivative matrix. $\left(\frac{\partial I_i}{\partial \phi_i} = -\sigma; \frac{\partial I_i}{\partial \phi_c} = +\sigma \right)$. Surface conductivity contributes many more off-diagonal terms.

3. The case that is particularly problematic is $I_i = I_i(E \cdot n)$. This occurs for a photo-emitting surface at negative potentials. The problem is that the local electric field is a function of the potentials on all the surfaces. However, the BEM provides us with exactly that function. We can now compute the term

$$I'_{ij} \equiv \partial I_i / \partial \phi_j = \partial I_i / \partial E_i \times \partial E_i / \partial \phi_j \tag{136}$$

using the relation

$$(\mathbf{E} \cdot \mathbf{n})_i = \mathbf{F}_{ik} \mathbf{C}_{kj} \mathbf{\Phi}_j \tag{137}$$

derived from the BEM.

In *Nascap-2k* we impose some additional conditions on the current derivative in order to promote stability, some of which are related to the sharp cutoffs that occur with secondary and photoemission currents. The problem is illustrated by Figure 13. If we charge negative from point A and use the actual derivative we fail to anticipate the sharp increase in secondary emission current and overshoot negative. If we charge positive from point B and use the actual derivative we fail to anticipate the sharp drop in secondary emission current and overshoot positive. If we charge negative from point C, then the actual derivative predicts unphysically enhanced secondary emission current at negative potentials, with the result that negative charging becomes glacially slow. The rules summarized below are designed to promote reasonable behavior for charging of surfaces encountering suppressed emission current.

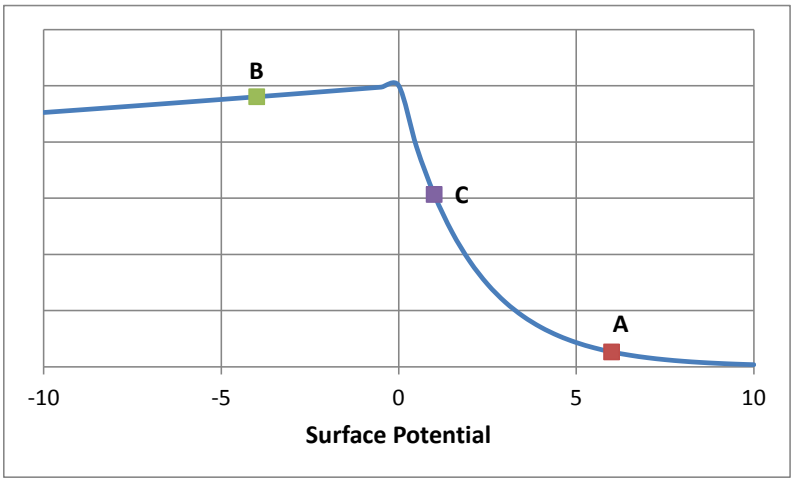

Figure 13. Notional Curve of Effective Secondary Emission Current versus Surface Potential.

1. If the secondary electrons are limited by positive potential or electric field barrier and the net current would be positive were they not limited, then the rate of increase of emission current with drop in potential is at least doubled, and for potential above 2 V the rate is adjusted such that emission is turned on fully should the potential drop to zero. This prevents (or, at least, minimizes) oscillations between high positive and high negative potential when the true current balance occurs at near zero potential.

2. For the Fontheim distribution, if the electric field is positive and the surface has negative current before any limiting of low energy currents, then the derivative is set to ignore the increase in emission due to decreasing potential. This allows the surface potential to decrease at a reasonable rate. Otherwise the low energy currents would go from suppressed to unphysically enhanced and prevent the correct negative charging.
3. If the electric field is negative and the surface has positive current before any limiting of low energy currents, then the derivative is set to turn off the emission when the potential reaches 2 V. Otherwise, the suppression of emission at positive potential would not be anticipated and the unsuppressed emission would drive the surface far above its true floating potential.
4. If a surface is negative but has positive current and positive normal electric field, the derivative is set so that the current is turned off after rising to a potential of no more than +5 V. This prevents charging from negative to unphysical positive values when emission is already suppressed.
5. The current derivative is set to allow a potential change of no more than 2 kV.
6. The current derivative is set to allow a potential change of at least the minimum of 1 V and one-one hundredth of the electron temperature.

3.4.5 Applicability at Finite Debye Length

The effect of using the BEM capacitances to calculate charging dynamics is that the "to space" capacitance is underestimated, and thus the "overall" (to space) charging rate of the spacecraft is too fast. For short Debye length and low temperature the capacitance is inversely proportional to the Debye length, whereas the BEM (vacuum) capacitance is inversely proportional to the spacecraft size. For typical cases the charging rate may be too fast by a factor of ~100. Note that even the "correct" charging rate is fast compared with the differential charging rate.

Two factors that mitigate the charging rate issue outlined above are;

1. At high potentials the capacitance is inversely proportional to the sheath size rather than to the Debye length, so that typical errors in charging rate are factors of ~2 to 10 rather than ~100;
2. Typically, in *Nascap-2k* calculations the timestep is far too long to resolve the vacuum charging rate, so that the charging rate in the simulation is determined by the choice of timestep rather than the actual capacitance.

Note that the rate of differential charging is not affected by the plasma, as the capacitances governing differential changing depend on material thicknesses and electronic component values rather than on spacecraft size and plasma effects. Also, the quasi-steady-state and equilibrium potentials are not affected, because these depend on currents which in turn depend on potentials and electric fields. The electric fields used to calculate currents are calculated from the finite element potential solution, and therefore do include the effects of a finite Debye length plasma.

3.4.6 Example: Sunlit Sphere

To illustrate the implicit charging model, we calculate the charging of a sunlit Teflon sphere in a 1 cm^{-3}, 20 keV plasma. The *NASCAP/GEO* version of this was published in 1978.[36] A version of

the original result is shown below in Figure 14. The sun direction is (1,1,1) (from the upper right). The dark side of the sphere gradually charges negative due to incident plasma electrons, while photoemission grounds the sunlit side. Eventually, however, the strong negative potentials due to the dark surfaces wrap around the sphere and form a barrier to photoelectron escape. The potential of each sunlit surface is subsequently determined by the condition that its electric field has a small, positive value (seen in Figure 14 by the coarse contour spacing near the upper right spacecraft surface), so that just the right fraction of photoelectrons can escape over the barrier.

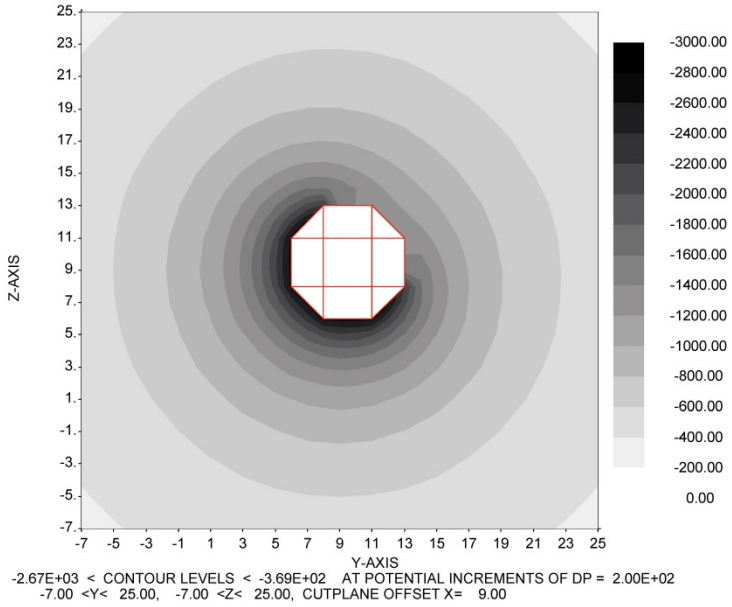

Figure 14. Potentials About Sunlit QSphere in Space as Computed By *NASCAP/GEO*.

Figure 15 and Figure 16 show the BEM solution of the same problem for a PATRAN sphere and a QSphere respectively. The point on the sphere furthest from the sun is the least negative point.

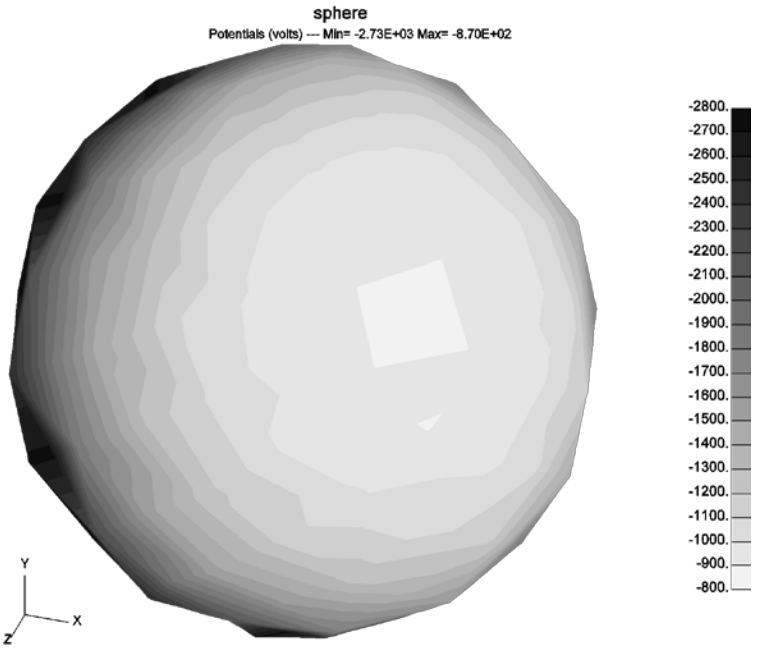

Figure 15. Potentials on Sunlit *PATRAN* Sphere in Space Viewed From Direction (1,2,3).

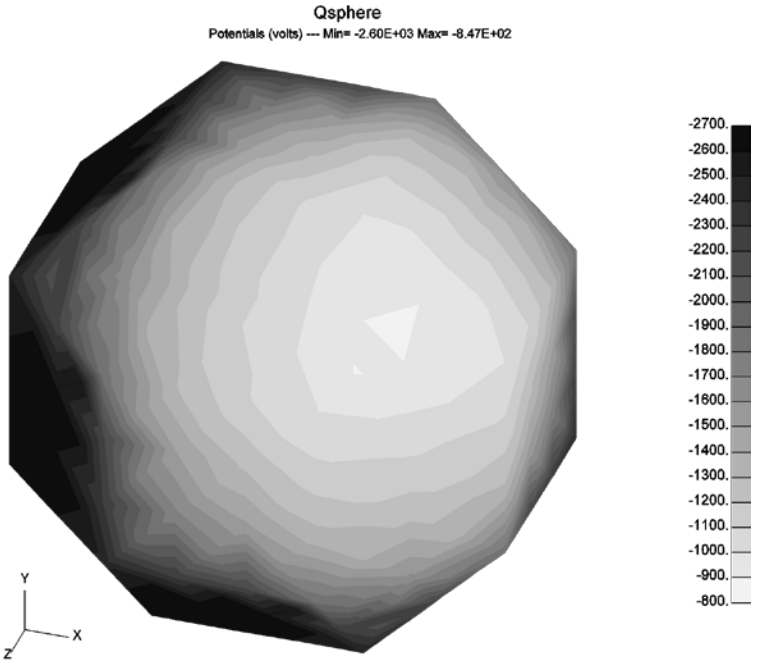

Figure 16. Potentials on Sunlit QSphere in Space Viewed From Direction (1,2,3).

Figure 17 is another view of the BEM solution, showing more of the dark side. Despite the fairly coarse gridding on the sphere, the gradual potential gradient on the sunlit side and the constant, large negative potential on the dark side are clearly seen in the BEM solution.

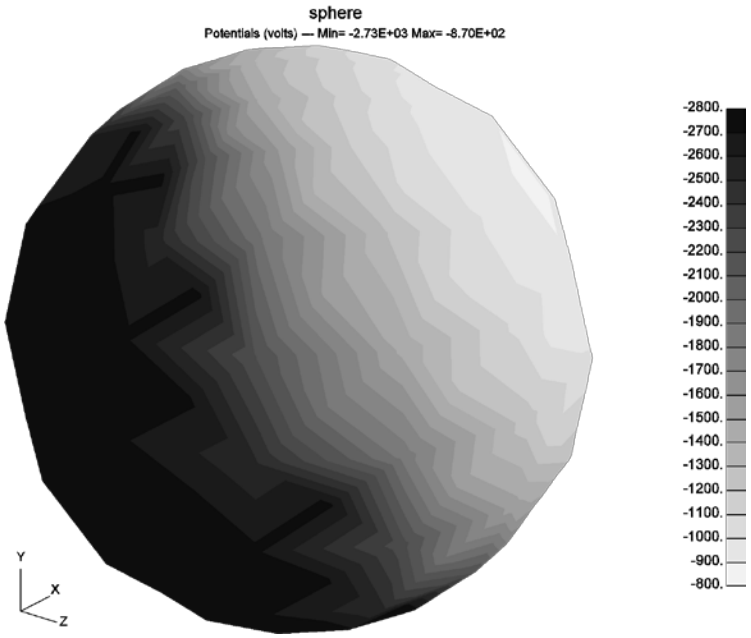

Figure 17. Potentials on Sunlit *PATRAN* Sphere in Space.

3.5 Finite Element Method to Compute Potentials in Space

In calculating the potential in three dimensions around an arbitrary object, *Nascap-2k* employs a finite element approach using right parallelepiped elements and nonlinear edge interpolants. Arbitrarily nested subdivision (up to seven levels) is used to resolve important object features while including a large amount of space around the spacecraft for determining accurate particle orbits and keeping memory requirements reasonable. Figure 18 shows an example of a computational grid with progressively finer subdivision to give fine resolution near an experiment.

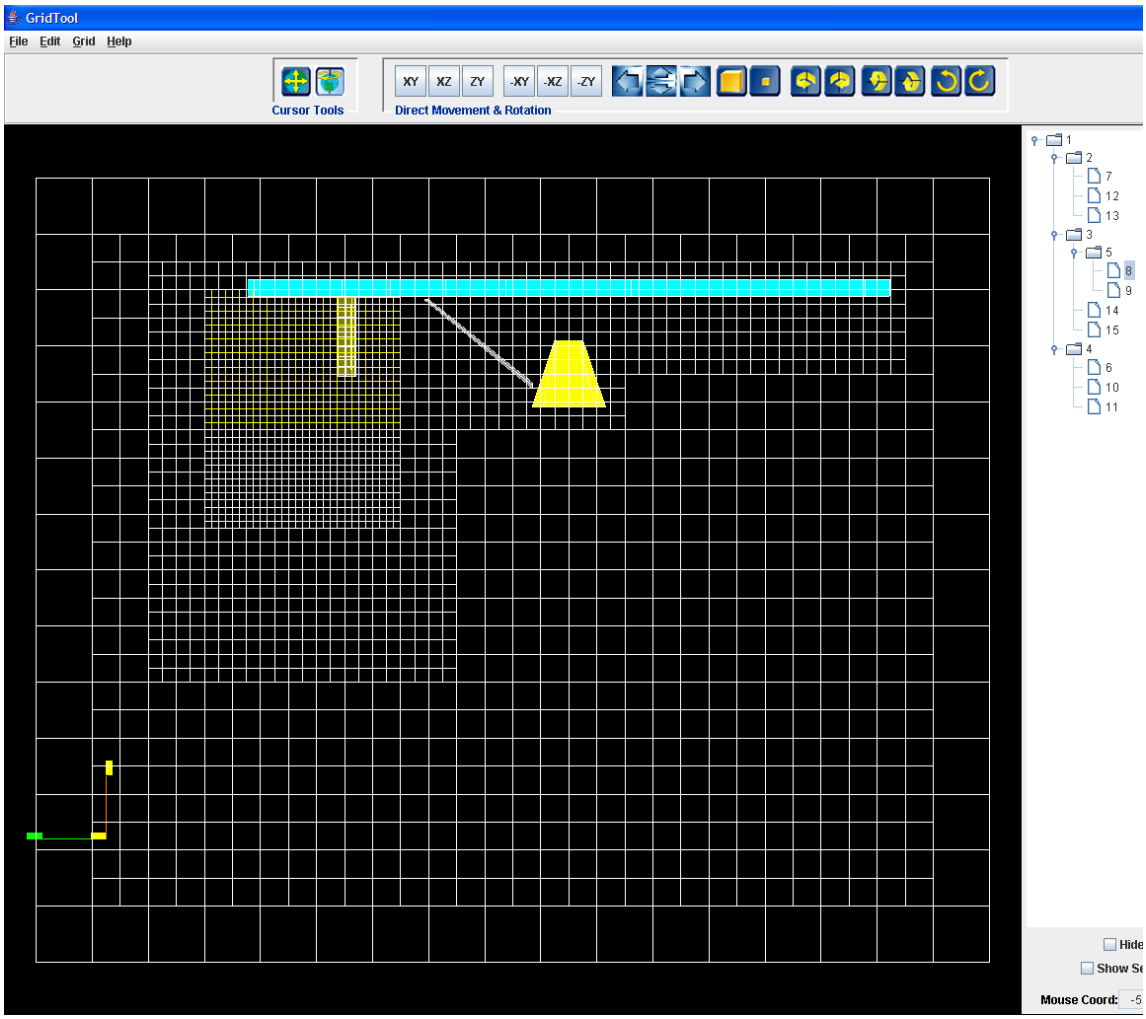

Figure 18. Computational Grid With Subdivision.

Nascap-2k solves Poisson's equation

$$-\nabla^2\phi = \rho/\varepsilon_o$$

by solving the associated variational principle

$$0 = \frac{\delta}{\delta\phi}\left\{\int dV\left[\frac{1}{2}(\nabla\phi)^2 + \frac{\rho\phi}{\varepsilon_o}\right] + \int \phi\nabla\phi \bullet dS\right\}. \qquad (138)$$

The first term in the volume integrand corresponds to the Laplacian operator; the second term is the space charge contribution. The surface contribution, given by the last term, is used to obtain the surface electric field.

Poisson's equation is solved with surface potentials fixed. To determine surface field values for fixed potential elements, we use the fact that the surface element electric field is conjugate to its potential, i.e., when the full conjugate gradient matrix multiplication is performed, the surface

element electric field (corresponding to the existing potentials and fields) is the residual corresponding to the surface element potential. This is an improvement over capacitance matrix methods in that it takes full account of the nonlinear space charge in the external space. In the variational calculation, we use locally defined basis sets, that is, interpolants within each cubic volume element. Fine mesh volumes are given the correct variational weight, ensuring the maintenance of accuracy through mesh transition regions. The potential and electric field are defined at each grid node. The potential inside each volume element is interpolated from the values at each of its vertices.

The volume integrals are solved volume element by volume element. The potential (and electric field) at each point in the element is the sum of interpolants times the values at the nodes.

$$\int\left[\frac{1}{2}(\nabla\phi)^2+\frac{\rho\phi}{\varepsilon_o}\right]dV=\frac{1}{2}\sum_e\int_{V_e}(\nabla\phi)^2\,dV_e\quad+\sum_e\int_{V_e}\frac{\rho\phi}{\varepsilon_o}dV_e\,. \tag{139}$$

The potential inside each element is given by

$$\phi^e(x,y,z)=\sum_i N_i(x,y,z)\phi_i \tag{140}$$

where "i" are the nodes of the element indexed by "e", and the N_i are the interpolants. Note that each element has four interpolants per node, whose coefficients are the potential and three components of electric field at the node, as discussed in Section 3.5.1.

We then have

$$\nabla\phi^e(x,y,z)=\sum_i\nabla N_i(x,y,z)\phi_i \tag{141}$$

which allows us to write

$$\int\frac{1}{2}(\nabla\phi)^2dV=\frac{1}{2}\sum_e\int_{V_e}\sum_{i\alpha}\sum_{j\beta}\nabla N_{i\alpha}(x,y,z)\nabla N_{j\beta}(x,y,z)\phi_{i\alpha}\phi_{j\beta}dV_e=\frac{1}{2}\sum_e\sum_{i\alpha}\sum_{j\beta}W^e_{i\alpha j\beta}\phi_{i\alpha}\phi_{j\beta} \tag{142}$$

Where the indices (α,β) run over the potential and three electric field components at the nodes and their corresponding interpolants. Note that the $W_{i\alpha j\beta}$ depend only on the shape of the volume element.

The second term can be written

$$\int\left[\frac{\rho\phi}{\varepsilon_o}\right]dV=\sum_e\int_{V_e}\frac{\rho\phi}{\varepsilon_o}dV_e=\sum_e\int_{V_e}\sum_{i\alpha}\frac{\rho}{\varepsilon_o}N_{i\alpha}(x,y,z)\phi_{i\alpha}dV_e=\sum_{i\alpha}\phi_i\frac{Q_{i\alpha}}{\varepsilon_o} \tag{143}$$

The minimization can then be written as the matrix equation

$$\frac{\delta}{\delta\phi}\left\{\sum_e \frac{1}{2}\sum_i\sum_j W_{ij}^e \phi_i\phi_j + \sum_e\sum_i \frac{Q_i}{\varepsilon_o}\phi_i\right\} = \frac{\delta}{\delta\phi}\left\{\frac{1}{2}\boldsymbol{\varphi}\mathbf{W}\boldsymbol{\varphi} + \frac{\mathbf{Q}}{\varepsilon_o}\boldsymbol{\varphi}\right\} = 0 \tag{144}$$

This function is then expressed in terms of the vector, **φ**, of all nodal values and a sparse, symmetric, positive definite matrix **W**. The conjugate gradient solution to this problem requires that we be able to form the matrix-vector product **Wφ**, which we can do by adding up the contribution to **Wφ** from each finite element without ever forming (or storing) the sparse but extremely large matrix **W**.

The resulting system of linear equations is solved using the Conjugate Gradient approach.

3.5.1 Continuous Field Interpolants

Nascap-2k uses a finite element interpolation scheme that has strictly continuous electric fields. This approach insures the continuity of the electric field used to compute particle trajectories. Tri-quadratic interpolants were also considered, but experience showed that the difference in weight between the corner nodes and the edge-center nodes leads to a poorly conditioned matrix.

The basic interpolation functions consist of functions (representing nodal potentials) that have unit value and zero slope at their home nodes, and zero value and slope at opposite nodes:

$$\begin{aligned} F_o &= \frac{(x-1)^2}{1-2x+2x^2} \\ F_1 &= 1-F_o = \frac{x^2}{1-2x+2x^2} \end{aligned} \tag{145}$$

and functions (representing nodal electric fields) that have zero value and unit slope at their home nodes and zero value and slope at opposite nodes:

$$\begin{aligned} G_o &= x(1-x)F_o \\ G_1 &= x(x-1)F_1 \end{aligned} \tag{146}$$

The coefficient of F corresponds to the potential at the home node, and the coefficient of G corresponds to the (negative of the) electric field at the home node. (In the element interior, both F and G are needed to calculate potential and potential gradient.)

The functions F_0 and G_0 are shown in Figure 19. It can be verified that these functions can exactly reproduce constant, linear, and quadratic potentials.

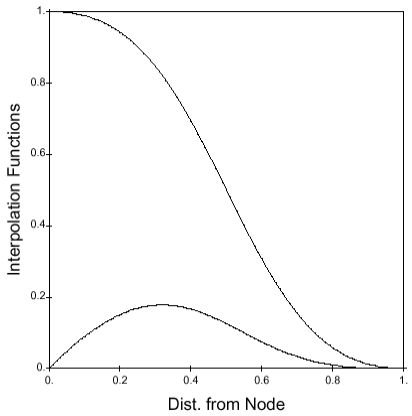

Figure 19. Interpolation Functions F_o and G_o.

We generalize to three dimensions by assigning to each corner of the unit cube four interpolation functions corresponding to the potential, x-component of potential gradient, y-component of potential gradient, and z-component of potential gradient for that node. The interpolants corresponding to node ijk are then given by

$$\begin{aligned} N^0_{ijk}(x,y,z) &= F_i(x)F_j(y)F_k(z) \\ N^1_{ijk}(x,y,z) &= G_i(x)F_j(y)F_k(z) \\ N^2_{ijk}(x,y,z) &= F_i(x)G_j(y)F_k(z) \\ N^3_{ijk}(x,y,z) &= F_i(x)F_j(y)G_k(z) \end{aligned} \tag{147}$$

The coefficients of the N^0 interpolants are the node potentials, and the coefficients of the $N^{1,2,3}$ interpolants are the negative Cartesian components of the nodal electric fields. We elect to omit the higher order terms of the form GFG or GGG.

The potential inside each element is given by

$$\phi(x,y,z) = \sum_{ijk\alpha} N^{\alpha}_{ijk}(x,y,z)\phi^{\alpha}_{ijk} \tag{148}$$

and the components of the electric field are given by

$$\mathbf{E}(x,y,z) = \sum_{ijk\alpha} \phi^{\alpha}_{ijk} \nabla N^{\alpha}_{ijk}(x,y,z) \tag{149}$$

3.5.2 Interpolating Potentials and Fields for Special Elements

Special elements are those elements which contain surfaces. Because surface-containing elements are not empty cubes, the potential interpolation functions described in the previous section cannot be straightforwardly applied. To develop finite element matrices for these elements, we require a prescription for calculating the potential and electric field in the element interior. Note that a special element is bounded by three types of surfaces: (1) square surfaces

bounded by grid edges and shared with adjacent (presumably empty) elements; (2) object surfaces; and (3) surfaces bounded by both object points or edges and grid points or edges. On type (1) surfaces we use the potential and field interpolation described in the previous section. On object surfaces, the potential and electric field must be expressed in terms of the object's surface element potentials and normal fields. Type (3) surfaces must smoothly blend between the two. We describe below an algorithm to express the potential and field at any point in the element volume in terms of the grid point potentials and fields, and the surface element potentials and normal fields. The algorithm has the property that, when applied to an element with six type (1) surfaces, it reproduces the empty cube result exactly.

Let **R** be a point in a volume bounded by a set of surfaces {S}, each of which may be a triangle or a planar convex quadrilateral. For a given S, let **P** be the point on S nearest **R,** let $\phi(\mathbf{P})$ and **E**(**P**) be the potential and electric field at **P**, and **n** be the unit normal (from the surface point **P** into the volume) to the surface. Let

$$\begin{aligned} \mathbf{d} &= \mathbf{R} - \mathbf{P} \\ d^2 &= \mathbf{d} \bullet \mathbf{d} \\ K_S &= A_s / d^2 \ \text{ for } \ \mathbf{d} \bullet \mathbf{n} > 0 \\ N &= \sum_{\{S\}} K_S \end{aligned} \tag{150}$$

where A_S is the area of surface S and K_S is its weighting function.

Let *l* be the distance from **P** in direction **n** to the next surface intersection. (In practice, it is adequate to extend *l* to the intersection with the surface of the rectangular parallelepiped bounding the volume.) Then the contribution of S to the potential at **R** is

$$\phi_S(\mathbf{R}) = (K_S / N)\left[\phi(\mathbf{P}) - (1 - \mathbf{d} \bullet \mathbf{n} / l)(\mathbf{d} \bullet \mathbf{n})(\mathbf{E(P)} \bullet \mathbf{n})\right] \tag{151}$$

and the total potential is found by summing the contributions from all surfaces.

The electric field is found by differentiating the above. The contribution of S to the electric field is

$$\mathbf{E}_S = \phi_S\left[\nabla N / N - \nabla K_S) / K_S)\right] + (K_S / N)\left[-\nabla\phi(\mathbf{P}) + (1 - 2\mathbf{d} \bullet \mathbf{n} / l)\mathbf{n}(\mathbf{E(P)} \bullet \mathbf{n})\right] \tag{152}$$

Where $\nabla\phi(\mathbf{P})$ is taken tangential to the surface, and is calculated using the continuous field interpolants if S is a full square in empty space, and otherwise using linear interpolation for triangles and bilinear interpolation for quadrilaterals.

This approach allows us to interpolate surface fields and potentials on bounding surfaces in a manner that maintains the continuous electric field property. Potentials and normal field components are defined at the centroids of the original object surfaces and area-weighted averaged at surface corners. Potentials, normal fields, and tangential field components at all

surface points that are vertices of bounding surfaces are expressed as linear combinations of centroid potentials and fields.

3.5.3 Boundary Conditions

Most often we use a zero potential boundary condition at the outer boundary of the computational grid. For some problems, specifically, Laplacian potential and linearly Debye screened potentials, a different approach is desirable. For these problems, we apply boundary conditions by extending the problem beyond the computational box using external elements whose inward boundary is a quarter-boundary-surface-element (QBSE) containing one problem node and which extends radially outward from the center of the computational box (to which we henceforth refer as "the origin"). (See Figure 20.) These elements are added to the sum over all volume elements. We ignore potential variation over the QBSE, assuming it to have the potential, ϕ_{node}, of its problem node, so that this element makes a diagonal contribution to **W**. Within that approximation the new external element subtends solid angle $\Omega=\frac{1}{4}x^2/R^2$, where the QBSE is normal to the x-axis at distance *x* from the origin, and *R* is the distance of the center of the QBSE from the origin. (R and x are measured in outer grid units.) The potential in the element is

$$\phi(r) = \phi_{node}\left(\frac{R}{r}\right)\exp\left(-\left(r-R\right)/\lambda_D\right), \tag{153}$$

for Debye length λ_D. We can now proceed to evaluate the needed integrals. For the Laplacian ($\lambda_D=\infty$) case we get

$$\int \frac{1}{2}\left(\nabla\phi\right)^2 dV = \tfrac{1}{2}\phi_{node}^2\Omega\int_R^\infty r^2 dr\left(\frac{R}{r^2}\right)^2 \tag{154}$$

so that after properly taking account of the mesh spacing, L, the external element's contribution to the matrix element is

$$W_{VV} = \tfrac{1}{4}L(x/R^2) \tag{155}$$

where *x* and *R* are measured in units of L.

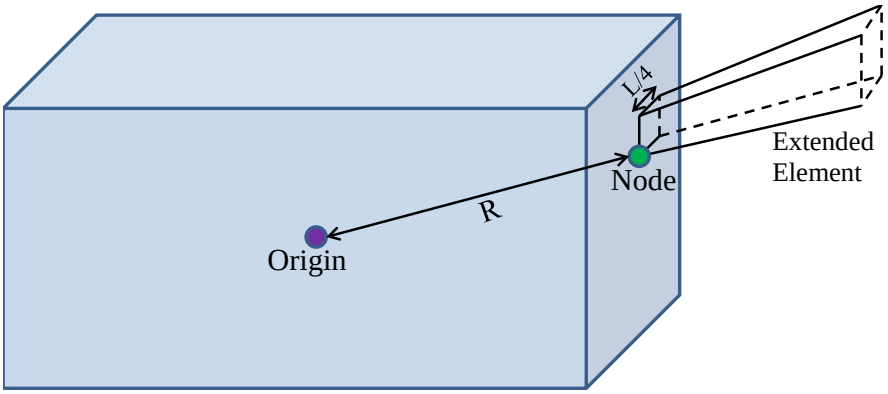

Figure 20. An Extended Element With Analytically Extrapolated Potential is Appended to Each Boundary Quarter-Square to Implement Non-Zero (Monopole) Potential Boundary Conditions.

For the case of finite Debye length, the evaluation contains more terms and involves integrals that cannot be expressed in closed form, so we approximate

$$\int_R^{\infty} dr \frac{e^{-r/\lambda}}{r^n} \approx \int_R^{R+\lambda} dr \frac{1}{r^n} \tag{156}$$

to eventually get

$$W_{VV} = \tfrac{1}{4} L(x/R^2)\left\{\frac{\rho}{2} + 2\rho \ln\left(1+\frac{1}{2\rho}\right) + \frac{1}{1+2\rho}\right\} + \frac{(L)^3 x}{8\rho\lambda^2} \tag{157}$$

where $\rho = R\, L/\lambda$.

It is recommended that zero potential boundary conditions be used if λ is comparable to or shorter than an outer grid mesh unit, and for most particle tracking problems for which no clear value exists for the Debye length.

3.6 Space Charge Stabilized Poisson Iteration

Poisson's equation can be written dimensionlessly as

$$-\nabla^2 \Phi = \left(n_i - n_e\right)/\Lambda^2 \tag{158}$$

where

$$\Phi = \frac{\phi}{\theta}, \text{ and } \Lambda^2 = \frac{\lambda_{Debye}^2}{L^2} = \varepsilon_o \frac{\theta}{N_o e L^2} \tag{159}$$

Λ is the dimensionless Debye length, N_o is the ambient plasma density, $n_i = N_i/N_o$, $n_e = N_e/N_o$, and the Laplacian is also normalized by L^2.

The traditional approach to the solution of Equation (158) has been an explicit iteration of the form

$$-\nabla^2\Phi^{\nu} = \Lambda^{-2}\left(n_i\left(\Phi^{\nu-1}\right) - n_e\left(\Phi^{\nu-1}\right)\right) \tag{160}$$

where ν is the iteration index and the charge density is determined using the potentials of the previous iteration. This method can be shown to be unstable[37] when the Debye length, λ_D, becomes small with respect to other scale lengths of the problem. This can be understood by considering that a smooth potential variation over a distance of, say, 1000, would require a smooth $\nabla^2\phi$ which is, in turn, given everywhere by the charge density. Maintaining a smooth charge density distribution is difficult when any errors in determining (n_e–n_i) are multiplied by a huge Λ^{-2}. There is one effective remedy to this dilemma described in Parker[37], but the process reported here appears to be more efficient in the short Debye length limit. This method involved the combination of two concepts. One uses a partial implicitization of the repelled density[38]. The other simply reduces the charge density to an acceptable level whenever the first method is inadequate. An "acceptable level" means a value not so great that it will cause spatial oscillations in the potential.

3.6.1 Implicitization

The right hand side of Equation (158) is the dimensionless charge density.

$$q\left(\mathbf{r}, \Phi^{\nu}(\mathbf{r})\right) = \Lambda^{-2}\left(n_i\left(\Phi^{\nu}\right) - n_e\left(\Phi^{\nu}\right)\right) \tag{161}$$

The charge density at the present iteration may be linearized about the previous potential iteration

$$q\left(\Phi^{\nu}\right) \cong q\left(\Phi^{\nu-1}\right) + q'\left(\Phi^{\nu-1}\right)\left(\Phi^{\nu} - \Phi^{\nu-1}\right)$$

where $q' = \dfrac{\partial q}{\partial \Phi}$, and the **r** dependence has been dropped for clarity. With this expression, we may write the implicit Poisson iteration scheme

$$-\nabla^2\Phi^{\nu} - q'\left(\Phi^{\nu-1}\right)\Phi^{\nu} = q\left(\Phi^{\nu-1}\right) - q'\left(\Phi^{\nu-1}\right)\Phi^{\nu-1} \tag{162}$$

Though it is not immediately obvious, the implicit character of Equation (162) makes it more stable than the scheme expressed in Equation (160) provided q' is constrained to be non-negative. This can be understood by realizing that in Equation (160) the charge density is treated as an independent variable, whereas in Equation (162) the charge density is determined simultaneously with the potential.

The finite element approximation to Equation (162) produces the matrix equation

$$\sum_{e}\left(\mathbf{W}^{e}-\overline{S}'^{e}\mathbf{V}^{e}\right)\boldsymbol{\Phi}^{\nu}=S-\overline{S}'^{e}\boldsymbol{\Phi}^{\nu-1} \tag{163}$$

where (e) refers to each element, W (which produces the square of the electric field) corresponds to the Laplacian operator, V (which produces the square of the potential) corresponds to the screening matrix, and the coefficient of the screening matrix, S, is derived from q by the following analysis.

3.6.2 Charge Limiting

For $\Lambda \geq 1$, S is simply the total charge associated with each node, Q. (Because the Debye length is longer than the grid resolution, an entire grid cube of plasma with one species eliminated alters the potential by no more than the temperature.) However, for $\Lambda << 1$, numerical noise and features like a sheath edge, which may span only a few λ_D, become incorrectly amplified when the q determined at a point becomes multiplied by the entire nodal volume. When it is not possible to reduce the volume element size, stability can be preserved by replacing Q (and Q´) with a reduced value S, (and S´) which is limited by the maximum allowable charge for the element.

Because of the artificial amplification argument, S is often the more realistic total for an element, in the sense that it produces potential variation appropriate to the spatial resolution rather than causing unphysical overshoots. Before deriving S, we define the barometric potential $\Phi_b = \ln(n_i)$, which (in cases where electron density is governed by the Boltzmann factor, e^{Φ}) is the potential for which Q = 0. (For the "Linear" and "Nonlinear" space charge density formulations, the ion charge density is also dependent on the potential. For these cases, the barometric potential as used here is zero, $\Phi_b = 0$.) Note that it is important that $S \rightarrow Q$ as $\Phi \rightarrow \Phi_b$ if quasineutral regions are to be modeled correctly. To determine S, consider a capacitor with potential difference $\Phi_b - \Phi$, area L^2, and a separation of L. The charge q_c on this capacitor is given by

$$Q_c = C\Delta V = \frac{\varepsilon_o L^2}{Le}\left(\Phi_b - \Phi\right)e\theta \tag{164}$$

We could then set the maximum allowable charge per element to be

$$q_{Limit} = \alpha\left(\Phi_b - \Phi\right) \tag{165}$$

with the parameter α, set to the maximum value consistent with the stability of the Poisson solver. Thus at each node, the charge would be

$$|S| = \min\left(|q_{Limit}|, |q|\right) \tag{166}$$

with

$$S' = \begin{cases} -\alpha, & \text{for } S = q_{Limit} \\ \dfrac{\partial q}{\partial \Phi}, & \text{for } S = q \end{cases} \tag{167}$$

However, this algorithm can easily give a discontinuous value for S′, which could lead to numeric instabilities.

In practice a different formulation is used. If a problem has been specified where a boundary potential would be screened in less than an element or two (the limit of any code's resolution), sufficient sheath charge is redistributed to allow the potential to be screened over the minimum number of elements that is consistent with stability. Consider the solution of the Helmholtz equation in a single, linear zone. The variational principle for the Helmholtz equation is

$$0 = \frac{\delta}{\delta \Phi}\left\{\int dV\left[\frac{1}{2}(\nabla\Phi)^2 + \frac{1}{2}\frac{\Phi^2}{\Lambda^2}\right]\right\} \tag{168}$$

The squared-gradient term is minimized by a constant potential, whereas the squared-potential term is minimized by going symmetrically through zero. So, there must be some minimum value of Λ for which the solution does not change sign. Minimizing the variational function on the interval [0, 1] with respect to $\Phi(1)$ when Φ (x) = (1-x) Φ (0)+x Φ (1) gives

$$\Phi(1) = \Phi(0)\frac{2 - \dfrac{1}{3\Lambda^2}}{2 + \dfrac{2}{3\Lambda^2}} \tag{169}$$

so that the condition for non-oscillatory potentials becomes $6\Lambda^2 > 1$. Thus if the charge is artificially constrained so that the Debye length is greater than $\sqrt{6}\,L = 2.45L$, the Poisson solution is stable.

For each charge density formulation, a computational temperature is defined and used so that the Debye length analog, λ, defined by $-\dfrac{\partial \rho}{\partial \phi} = \dfrac{\varepsilon_0 \phi}{\lambda^2}$, is no less than a user specified fraction (usually ½) of the local mesh spacing. The formulas for S and S′ for each charge density formulation appear in Section 3.6.5.

3.6.3 Analysis of the Space Charge Stabilized Poisson Method

The charge stabilized Poisson method calculates for each node the maximum allowable charge that is consistent with the stability of a linearly interpolating Poisson solver. This method is developed above, but a further analysis is presented here to help the user interpret its impact.

Nascap-2k's charge stabilization is accomplished through the process of charge limiting, illustrated in Figure 21. This figure shows two charge-versus-potential curves for the case where

the ion density is fixed (tracked or equal to the background density) and the electron density is barometric. Equation (162) is rewritten as

$$q = \alpha \exp\left(-\Phi_m\right)\left(\exp\Phi_b - \exp\Phi\right) \tag{170}$$

where $\Phi_m = \ln\left(\alpha\lambda_{Debye}^2 / L^2\right)$ α is user specified and Φ_b is the barometric potential, $\Phi_b = \ln(n_i)$. For curve q_1, $\Phi_b = -3.0$ ($n_i = 0.05$); for curve q_2, $\Phi_b = 0.0$ ($n_i = 1.0$) and for both curves $\Phi_m = -2.2$, and $\alpha = 1$. For each curve, the limiting charge as given by Equation (165) is also shown. The limiting charge is rewritten here as

$$q_{Limit} = \alpha\,(\Phi_b - \Phi) \tag{171}$$

which intersects the "natural" charge curves at Φ_c and Φ_b. The charge stabilization method reduces the charge to the limiting value when $\Phi > \Phi_c$ and uses the natural charge for $\Phi < \Phi_c$. The parameter Φ_m provides a good measure of the limiting process. From Figure 21 it can be seen that Φ_m is the point at which the slope of the natural charge curve equals that of the limiting charge line. Figure 22 shows a family of curves giving the dependence of the cutoff potential Φ_c on the barometric potential for various values of Φ_m. These curves were obtained by numerically solving for the zeros of the difference between q and q_{Limit}. This difference equation always has two solutions, one at Φ_c and one at Φ_b, with the exception of a degeneracy at $\Phi_c = \Phi_b = \Phi_m$, which is indicated in the figure. This figure shows that the charge limiting is minimal for $\Phi_m > -1$, and quite severe for $\Phi_m < -6$ or so.

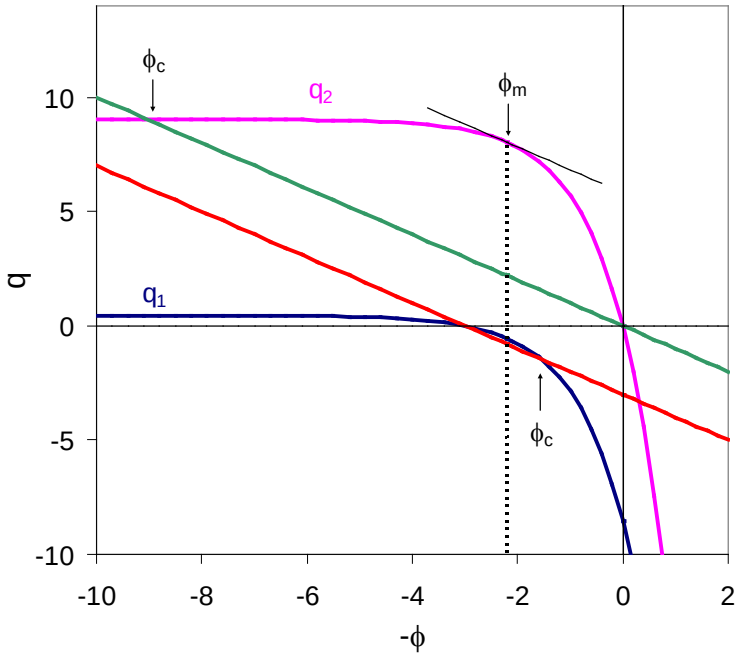

Figure 21. Plots of Space Charge (Curves q_1 and q_2) as a Function of Potential as Given by Equation (162). The Straight Lines Represent the Maximum Allowable Charge for Non-oscillatory Potentials. The "Natural" Space Charge, q_1 or q_2 is Acceptable for Cases for Which Slopes of the Curves and the Corresponding Line Are Equal.

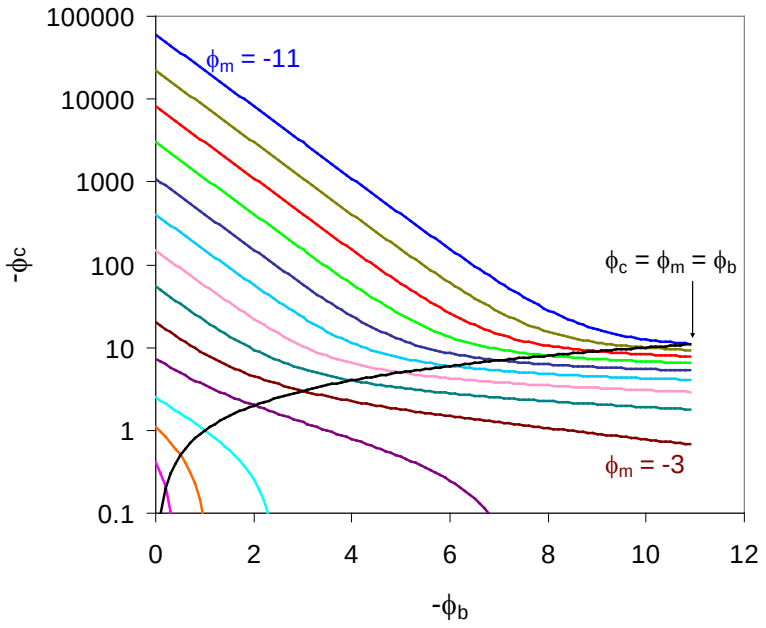

Figure 22. Plot of the Space Charge Cutoff Potential, Φ_c, Versus Barometric Potential ($\Phi_b = \ln n_i$) for a Series of Φ_m Values (-02, -0.5, -1.0, -2.0, -3.0, --4.0 … -11.0). The Point at Which $\Phi_m = \Phi_b = \Phi_c$ is Also Indicated.

3.6.4 Sheath Boundary Potential

Space charge limiting must be accounted for when choosing the sheath boundary potential. Space charge limiting limits the rate at which space charge can cause the potential to drop.

Consider the first volume element of a sheath to satisfy the laws of Child and Langmuir (planar space charge limiting). At the sheath edge (z=0) and one element in (z = L) the potential and electric field are given in Table 1.

Table 1. Potential and Electric Field Variation Given by Planar Space Charge Limiting.

Position	L
Potential	$K(L)^{4/3}$
Electric field	$(4/3)K(L)^{1/3}$

By Gauss's law, the charge per unit area in this element is given by

$$\frac{Q}{\varepsilon_o A} = \frac{4}{3} K(L)^{1/3} \tag{172}$$

Nascap-2k computes the charge density to be limited by (α/L^2) times the mean potential (assuming linear interpolation), and so gets

$$\frac{Q}{\varepsilon_o A} = L\left(\frac{\alpha}{L^2}\right)\frac{1}{2}\left(0 + K(L)^{4/3}\right) \tag{173}$$

Equating these two expression gives $\alpha = 8/3$.

Because of the requirements of disk space and computational time of three-dimensional codes, *Nascap-2k* is frequently operated at high Φ_m values, i.e., a coarse mesh with respect to the Debye length. In these cases charge is removed at almost all points. Ideally, the charge that was removed was excess charge generated by the coarse gridding. This is the artificial charge amplification argument. However, since *Nascap-2k* must be reliably stable, the result is that too much charge is often removed. This results in an enlarged sheath thickness for high negative Φ_m problems. In order to compensate for this sheath enlargement, the sheath boundary potential must be adjusted.

Equating the above equation to the code resolution, L, gives

$$\phi_x = 5.1\times10^{-6} L^{4/3}\theta^{1/3} n^{2/3} = 0.74\left(L/\lambda_D\right)^{4/3}\theta \tag{174}$$

The potential ϕ_x may be interpreted as the potential below which *Nascap-2k* underestimates screening. At best, beyond the ϕ_x contour, the potential drops about one order of magnitude per element. For $\theta = 0.1$ eV, $n = 10^{11} m^{-3}$, and L = 0.2 m, we find $\phi_x = 6$ V. If the 6 V contour is correctly placed, the 0.6 V contour lies at least one element beyond (at the approximate sheath location), and the default sheath contour (0.07 V) is yet another element farther. This would produce a sheath area that is too large. The suggested criterion for the sheath boundary potential is

$$\phi_{SB} = \mathrm{Max}\left(\theta \ln 2, 0.24\phi_x\right) \tag{175}$$

where $0.24 = e^{-1.0/0.7}$ is the planar screening per element allowed by *Nascap-2k*. Note, however, that ϕ_x depends strongly on the grid in which the sheath is found, so that if an increase in object potential moves the sheath from grid 3 to grid 2, a corresponding larger value of ϕ_{SB} should be used.

3.6.5 Charge Density and Derivative in *Nascap-2k*

Nascap-2k has a selection of eight different expressions to describe the charge density for different kinds of problems. Each expression uses implicitization and charge limiting to a different extent. As there is no space charge for the Laplace space charge option, the following discussion does not apply to that case. The expressions used for the space charge and its derivative including limiting are listed below.

The parameter D is the local mesh spacing, L, divided by the user provided Debye limiting value, which defaults to 2. The parameter g is the maximum of plasma density reduction factor computed by neutral wake model ($0<g<1$) and 10^{-6}.

Laplace. The Laplacian space charge option specifies that the charge density is zero and no space charge limiting is needed.

$$\frac{\rho}{\varepsilon_o} = 0$$
$$\frac{d(\rho/\varepsilon_o)}{d\phi} = 0 \tag{176}$$

i.e., charge exists only on object surfaces and external boundaries, as determined by the boundary conditions. Space charge iterations may still be required, however, for numerical reasons.

Linear (Debye Shielding). The Linear space charge option solves the Helmholtz or Debye-Huckel equation:

$$\frac{\rho}{\varepsilon_o} = -\frac{\phi}{\lambda_{nl}^2}$$
$$\lambda_{nl}{}^2 = \max(\lambda_D^2/g, D^2) \tag{177}$$
$$-\frac{d(\rho/\varepsilon_o)}{d\phi} = \frac{1}{\lambda_{nl}^2}$$

Nonlinear. Nonlinear space charge is appropriate for most low-Earth-orbit type plasmas in the presence of high applied potentials. Poisson's equation is solved with space charge given by:

$$\rho/\varepsilon_0 = -\left(\phi/\lambda_{nl}^2\right)\frac{\max\left(1, C(\phi, E)\right)}{1+\sqrt{4\pi}\left|\phi/\theta_{nl}\right|^{3/2}}$$
$$C(\phi, E) = \min\left(\left(R_{sh}/r\right)^2, 3.545\left|\phi/\theta_{nl}\right|^{3/2}\right)$$
$$\left(R_{sh}/r\right)^2 = 2.29\left|E\lambda_{nl}/\theta_{nl}\right|^{1.262}\left|\theta_{nl}/\phi\right|^{0.509} \tag{178}$$
$$\lambda_{nl}{}^2 = \max(\lambda_D^2/g, D^2)$$
$$\theta_{nl} = \theta(\lambda_{nl}^2 g/\lambda_D^2)^{2/3}$$

The term C(ϕ,E) (analytic focusing) comes from fitting a finite temperature spherical (Langmuir-Blodgett) sheath. If analytic convergence is turned off (on the Potentials Advanced screen) then C(ϕ,E) is set to zero. Additional adjustments are made to the convergence portion of this formula for significant values of velocity.

$$-\frac{d(\rho/\varepsilon_o)}{d\phi} = \mathrm{Max}\left(\left|\frac{\rho/\varepsilon_o}{\phi}\right|, \left(\frac{1}{\lambda_{nl}^2}\right)\left(\frac{\max(1, C(\phi, E))}{1+\sqrt{4\pi}\left|\phi/\theta_{nl}\right|^{3/2}}\right)\left(1-\left(\frac{3}{2}\right)\frac{\sqrt{4\pi}\left|\phi/\theta_{nl}\right|^{3/2}}{1+\sqrt{4\pi}\left|\phi/\theta_{nl}\right|^{3/2}}\right)\right) \tag{179}$$

Note that the derivative of the convergence contribution to the charge density with respect to the potential is assumed to be negligible.

Frozen Ion. The Frozen Ion formulation is intended for short timescale (typically sub-microsecond) problems for which it is a good approximation to assume that ions remain stationary and at ambient density ("ion matrix" approximation), but electrons achieve barometric equilibrium. The space charge function depends on the mesh-dependent potential, $\phi_1 < 0$, which satisfies

$$1-\exp\left(\phi_1/\theta\right)=-\left(\lambda/D\right)^2\left(\phi_1/\theta\right) \tag{180}$$

for $D>\lambda$. Otherwise, $\phi_1=-1\times10^{-6}$. The meaning of this quantity is that the charge density increases linearly at a stable rate for negative potentials between zero and ϕ_1, and then asymptotes to the ambient ion density for potentials more negative than ϕ_1.

The space charge is then given by

$$\rho/\varepsilon_0=\begin{cases}\left(\phi_1/D^2\right)\left(1-\exp\left(\phi/\phi_1\right)\right) & \phi\ge 0\\ -\phi/D^2 & 0\ge\phi\ge\phi_1\\ -\phi_1/D^2+\left(\theta/\lambda_{\text{Debye}}^2\right)\left(\exp\left(\phi_1/\theta\right)-\exp\left(\phi/\theta\right)\right) & \phi_1\ge\phi\end{cases} \tag{181}$$

$$-\frac{d\left(\rho/\varepsilon_o\right)}{d\phi}=\begin{cases}\text{Max}\left(-\dfrac{\rho/\varepsilon_o}{\phi},\exp\left(\phi/\phi_1\right)/D^2\right) & \phi\ge 0\\ 1/D^2 & 0\ge\phi\ge\phi_1\\ \text{Max}\left(-\dfrac{\rho/\varepsilon_o}{\phi},\exp\left(\phi/\theta\right)/\lambda_{\text{Debye}}^2\right) & \phi_1\ge\phi\end{cases} \tag{182}$$

The derivative of charge with respect to potential appears in the variational function as a coefficient of ϕ^2. If this is too large, then minimizing ϕ^2 means you oscillate from one grid point to the next in order to get lots of intermediate zeroes, which is not a satisfactory solution.

Barometric . The Barometric algorithm is appropriate for cases in which all the surfaces are at potentials comparable to or below the plasma temperature (or negative) and there is a region of low density, such as a plasma wake. The ion density is taken as the plasma density decreased by the wake factor g. If the ions are sufficiently dense, quasi-neutrality requires the potential to be the "barometric" potential, φ_b (defined below). However, because the plasma may be under-dense or influenced by nearby surfaces, the electron density must be allowed to differ from the ion density. We take the electron density to be given by the expression

$$\frac{\rho_e}{\varepsilon_o}=-\frac{\rho_i^b}{\varepsilon_o}\begin{cases}\exp\left(\min\left(10,\left(\phi-\phi_b\right)/\theta_b\right)\right) & \text{for } \phi-\phi_b<0\\ 1+\min\left(10,\left(\phi-\phi_b\right)/\theta_b\right) & \text{for } \phi-\phi_b>0\end{cases} \tag{183}$$

$$\rho_i^b = \max\left(g\,en, en_{min}\right)$$
$$\phi_b = \theta \ln\left(\frac{\rho_i^b}{en}\right)$$
$$\theta_b = \min\left(10\theta, \max\left(\theta, D^2\,\frac{\rho_i^b}{\varepsilon_o}\right)\right)$$

$$-\frac{d\left(\rho/\varepsilon_o\right)}{d\phi} = \begin{cases} \max\left(-\dfrac{\rho_i^b + \rho_e}{\varepsilon_o\left(\phi-\phi_b\right)}, -\dfrac{\rho_e}{\varepsilon_o\theta_b}\right) & \text{for } \phi-\phi_b < 0 \\ \dfrac{\rho_i^b}{\varepsilon_o\theta_b} & \text{for } \phi-\phi_b > 0 \end{cases} \tag{184}$$

Full Trajectory Ions. Ion densities are calculated from steady-state ion trajectories. Electrons are barometric.

$$\frac{\rho}{\varepsilon_0} = \frac{\rho_i^{ft}}{\varepsilon_0}\left(1-\exp\left(\min\left(10, \left(\phi-\phi_b\right)/\theta_{ft}\right)\right)\right) \tag{185}$$

$$\rho_i^{ft} = \max\left(\rho_{ion}^{tracked}, en_{min}\right)$$
$$\phi_b = \theta \ln\left(\frac{\rho_i^{ft}}{en}\right)$$
$$\theta_{ft} = \max\left(\theta, D^2\,\frac{\rho_i^{ft}}{\varepsilon_o}\right)$$

$$-\frac{d\left(\rho/\varepsilon_o\right)}{d\phi} = \begin{cases} \max\left(-\dfrac{\rho}{\varepsilon_o}\dfrac{1}{\phi-\phi_b}, -\dfrac{\rho-\rho_i^{ft}}{\varepsilon_o\theta_{ft}}\right) & \text{for } \left(\phi-\phi_b\right)/\theta_{ft} < 1 \\ -\dfrac{\rho}{\varepsilon_o}\dfrac{1}{\phi-\phi_b} & \text{otherwise} \end{cases} \tag{186}$$

Hybrid PIC. This algorithm is used for timescales (typically sub-millisecond) for which it is practical to treat ion motion, but electrons may be considered in barometric equilibrium. The ion density is computed from actual ion macroparticles. The electron charge density is barometric for negative potentials and increases linearly (orbit limited) for positive potentials.

$$\frac{\rho_e}{\varepsilon_o} = -\frac{\rho_i^{hp}}{\varepsilon_o}\begin{cases} \exp\left(\min\left(10, \left(\phi-\phi_b\right)/\theta_{hp}\right)\right) & \text{for } \phi \le 0 \\ \exp\left(\min\left(10, -\phi_b/\theta_{hp}^0\right)\right)\left(1+\phi/\theta_{hp}\right) & \text{for } 0 < \phi \end{cases} \tag{187}$$

$$\rho_i^{hp} = \max\left(\rho_{ion}^{tracked}, en_{min}\right)$$

$$\phi_b = \theta \ln\left(\frac{\rho_i^{hp}}{en}\right)$$

When the potential is near the barometric potential $\left(\left|\phi - \phi_b\right| < \theta_1\right)$, space charge limiting is not needed, and θ_{hp} is θ. When the potential is far from the barometric potential $\left(\theta_2 < \left|\phi - \phi_b\right|\right)$, the effective temperature used is the space charge limited value. At intermediate potentials, the effective temperature varies linearly.

$$\theta_{hp} = \begin{cases} \theta & \text{if } \left|\phi - \phi_b\right| \le \theta_1 \text{ and } \phi \le 0 \\ \theta_{scl} & \text{if } \theta_2 \le \left|\phi - \phi_b\right| \text{ and } \phi \le 0 \\ \dfrac{\theta_{scl} - \theta}{\theta_2 - \theta_1}\left|\phi - \phi_b\right| + \dfrac{\theta\theta_2 - \theta_{scl}\theta_1}{\theta_2 - \theta_1} & \text{if } \theta_1 < \left|\phi - \phi_b\right| < \theta_2 \text{ and } \phi \le 0 \\ \dfrac{\theta_{scl} - \theta_{hp}^0}{\theta_2}\phi + \theta_{hp}^0 & \text{if } \left|\phi_b\right| \le \theta_2 \text{ and } \phi \le \theta_2 \text{ and } \phi > 0 \\ \theta_{scl} & \text{if } \left(\left|\phi_b\right| > \theta_2 \text{ or } \phi > \theta_2\right) \text{and } \phi > 0 \end{cases} \tag{188}$$

θ_{hp}^0 is the value of θ_{hp} at $\phi = 0$ and is only needed for positive potentials.

$$\theta_{hp}^0 = \begin{cases} \theta & \text{if } \left|\phi_b\right| \le \theta_1 \\ \theta_{scl} & \text{if } \theta_2 \le \left|\phi_b\right| \\ \max\left(\theta, \dfrac{\theta_{scl} - \theta}{\theta_2 - \theta_1}\left|\phi_b\right| + \dfrac{\theta\theta_2 - \theta_{scl}\theta_1}{\theta_2 - \theta_1}\right) & \text{if } \theta_1 < \left|\phi_b\right| < \theta_2 \end{cases} \tag{189}$$

$$\theta_{scl} = \max\left(\theta, D^2 \frac{\rho_i^{hp}}{\varepsilon_o}\right)$$

$$\theta_1 = \theta/8$$

$$\theta_2 = \theta_{scl}/4$$

$$-\frac{d(\rho/\varepsilon_o)}{d\phi}=\frac{\rho^i_{hp}}{\varepsilon_o}\begin{cases}\max\left(\dfrac{\exp\left(\min\left(10,(\phi-\phi_b)/\theta_{hp}\right)\right)-1}{(\phi-\phi_b)},\dfrac{\exp\left(\min\left(10,(\phi-\phi_b)/\theta_{hp}\right)\right)}{\theta_{hp}}\right) & 0\le\dfrac{\phi-\phi_b}{\theta_{hp}}<1 \text{ and } \left(\theta_1>|\phi-\phi_b| \text{ or } |\phi-\phi_b|>\theta_2\right) \text{ and } \phi\le 0\\ \max\left(\dfrac{\exp\left(\min\left(10,(\phi-\phi_b)/\theta_{hp}\right)\right)-1}{(\phi-\phi_b)},\dfrac{\exp\left(\min\left(10,(\phi-\phi_b)/\theta_{hp}\right)\right)}{\theta_{hp}}\left(\dfrac{\theta\theta_2-\theta_{scl}\theta_1}{\theta_2-\theta_1}\dfrac{1}{\theta_{hp}}\right)\right) & 0\le\dfrac{\phi-\phi_b}{\theta_{hp}}<1 \text{ and } \theta_1\le|\phi-\phi_b|\le\theta_2 \text{ and } \phi\le 0\\ \left(\dfrac{\exp\left(\min\left(10,(\phi-\phi_b)/\theta_{hp}\right)\right)-1}{(\phi-\phi_b)}\right) & 1\le\dfrac{\phi-\phi_b}{\theta_{hp}} \text{ and } \phi\le 0\\ \dfrac{1}{\theta_{hp}} & \dfrac{\phi-\phi_b}{\theta_{hp}}<0 \text{ and } \left(\theta_1>|\phi-\phi_b| \text{ or } |\phi-\phi_b|>\theta_2\right) \text{ and } \phi\le 0\\ \dfrac{1}{\theta_{hp}}\left(\dfrac{\theta\theta_2-\theta_{scl}\theta_1}{\theta_2-\theta_1}\dfrac{1}{\theta_{hp}}\right) & \dfrac{\phi-\phi_b}{\theta_{hp}}<0 \text{ and } \theta_1\le|\phi-\phi_b|\le\theta_2 \text{ and } \phi\le 0\\ \dfrac{\exp\left(-\phi_b/\theta^0_{hp}\right)}{\theta_{hp}} & \left(|\phi_b|\ge\theta_2 \text{ or } \phi\ge\theta_2\right) \text{and } \phi>0\\ \dfrac{\exp\left(-\phi_b/\theta^0_{hp}\right)}{\theta_{hp}}\dfrac{\theta^0_{hp}}{\theta_{hp}} & |\phi_b|<\theta_2 \text{ and } \phi<\theta_2 \text{ and } \phi>0\end{cases} \tag{190}$$

Full PIC. For this option, it is assumed that the total charged density (electron and ion) was previously computed and stored.

$$\begin{aligned}\rho &= \rho^{\text{tracked}}\\ \frac{d(\rho/\varepsilon_o)}{d\phi} &= 0\end{aligned} \tag{191}$$

3.7 Macroparticles

Macroparticles represent either current or charge. Macroparticles that represent current are used for steady-state problems and ones that represent charge are used for dynamic problems. Macroparticles are also used for visualization.

3.7.1 Macroparticle Creation

When macroparticles are created at a sheath surface, the sheath surface is divided into triangles and a macroparticle representing the current from that section of the sheath is created at the center of the triangle.

When macroparticles are created at the problem boundary, the outer surface of each grid boundary volume element is divided into squares (of size requested by the user) and a macroparticle is created at the center of each square to represent either the current through that area (“Boundary” and “BField”) or the charge passing through that area during a user specified time (“Boundary Injection”).

When macroparticles are created throughout the volume (for uniform charge density initialization or charge exchange), they are created at points appropriate to the weighting functions.

When macroparticles are created at user specified locations with user specified velocities, each macroparticle represents current.

When macroparticles are created on surface elements, the surface is divided into the requested number of quadrilaterals and triangles and macroparticles are created at the center of each. The macroparticles are distributed evenly in velocity, azimuthal angle, and cosine of the polar angle.

For visualization only, macroparticles can also be created at the intersection of the sheath surface and a user specified plane.

3.7.2 Macroparticle Tracking

Macroparticles are tracked using a third order energy conserving algorithm.

$$\begin{aligned}\mathbf{x}(t+dt) &= \mathbf{x}(t)+\mathbf{v}(t)dt+\frac{\mathbf{x}_2}{2}dt^2+\frac{\mathbf{x}_3}{6}dt^3+\frac{\mathbf{x}_4}{24}dt^4\\ \mathbf{v}(t+dt) &= \mathbf{v}(t)+\mathbf{x}_2 dt+\frac{\mathbf{x}_3}{2}dt^2+\frac{\mathbf{x}_4}{6}dt^3\end{aligned} \tag{192}$$

where

$$\begin{aligned}\mathbf{x}_2 &= \frac{e}{m}(\mathbf{E}+\mathbf{v}\times\mathbf{B})\\ \mathbf{x}_3 &= \frac{e}{m}(\mathbf{v}\bullet\nabla\mathbf{E}+\mathbf{x}_2\times\mathbf{B})\\ \mathbf{x}_4 &= \frac{e}{m}(\mathbf{x}_3\times\mathbf{B})\end{aligned} \tag{193}$$

The electric field is that at the location of the macroparticle determined by interpolation from the nodes of the volume element. The magnetic field is the sum of a constant, uniform field supplied by the user and the sum of all the magnetic dipoles defined during object definition. As the field sources are not, in reality, point dipoles, if a macroparticle is within 1 cm (0.01 m) of a dipole, that dipole's contribution to the particle's magnetic field is calculated as if it were 1 cm away. If the macroparticle is within 1 mm (0.001 m) of a dipole, the contribution of that dipole is set to zero.

$$\mathbf{B}(\mathbf{r}) = \mathbf{B}_{\text{ambient}} + \sum_{\text{all dipoles}} \frac{3\hat{\mathbf{n}}(\mathbf{p}\cdot\hat{\mathbf{n}})-\mathbf{p}}{|\mathbf{r}-\mathbf{r_o}|^3} \tag{194}$$

Here, $\mathbf{p}$ and $\mathbf{r}_o$ are the dipole moment and location and $\hat{\mathbf{n}}$ is a unit vector from $\mathbf{r}$ to $\mathbf{r}_o$,

Macroparticles are tracked for a timestep, which can be as long as a minute for static problems or as short as microseconds for dynamic problems. The timestep is divided into substeps such that the macroparticle can travel no more than a fraction of the local mesh size in a single substep. By default the fraction is 0.1; the user may specify an alternative value. The particle's total energy is calculated at the beginning of the timestep and preserved during the timestep. Changes in potential between timesteps are reflected by a change in the particle's total energy.

If the macroparticle represents charge, at the end of each timestep and optionally at the end of each substep, the charge and current are assigned to the nodes of the element the macroparticle is in, using the same weights as the potential. The charge density (charge divided by element volume) is assigned to the element. If the assignment is performed at the end of each substep, the charge assigned is divided by the fraction of the timestep that the substep represents.

If the macroparticle represent currents, at the end of each substep its charge density (current times substep time) is optionally assigned to the element within whose bounds the macroparticle is located.

When a macroparticle impacts a surface element, its current or charge is assigned to the surface element.

3.7.3 Macroparticle Splitting

Macroparticles are split both to avoid having heavy macroparticles in well-resolved regions and to simulate a thermal distribution. Macroparticle splitting has been implemented for macroparticles read from an external file, for a uniform distribution of macroparticles for initialization, and for macroparticles injected from the boundary. Macroparticles can also be split when entering a more finely resolved grid.

The following general principles are used in generating the smaller replacement macroparticles.

1. Macroparticles are split in velocity space only. Because particles frequently need to be split in high-field regions, spatial splitting would raise problems with energy conservation.

2. To be split in velocity space, a macroparticle must carry a temperature. We assume the temperature is always isotropic. The fission products carry half the temperature of the original macroparticle, while the remaining thermal energy appears as kinetic energy of the split macroparticles.

3. For splitting purposes, we define the Z-axis to be along the direction of the macroparticle velocity, the X-axis randomly chosen in the plane normal to Z, and the Y-axis mutually perpendicular.

4. We split into two or three macroparticles with added velocity along each axis, except that we may elect not to split along the Z-direction if the kinetic energy exceeds the thermal energy. Not splitting along Z helps ameliorate macroparticle proliferation, but makes an error by not preserving the original macroparticle temperature along Z. We thus end up with eight, nine, or twenty-seven new macroparticles.

5. Macroparticle velocity is assumed to be acquired by acceleration rather than actual drift (i.e., spacecraft velocity). If there is actual drift (e.g., ram velocity), then the drift velocity is removed before splitting the macroparticle, and added back after.

6. If the macroparticle with speed u_0 is split by two along the X or Y axis, the new velocity is $\pm 0.707\sqrt{e\theta/m}$. Along the Z axis, the velocity increment is calculated as if the temperature were $\theta - 2mu_0^2\left(\sqrt{1+\frac{\theta}{mu_0^2}}-1\right)$.

7. If the macroparticle with speed u_0 is split by three along the X or Y axis, there is a zero-velocity central macroparticle and two "probe" macroparticles with velocity $\pm 0.866\sqrt{e\theta/m}$. Along the Z axis, the velocity increment is calculated as if the temperature were $\theta - 2mu_0^2\left(\sqrt{1+\frac{\theta}{mu_0^2}}-1\right)$.

Examples of the effects of macroparticle splitting appear in Reference 39.

3.7.4 Reverse trajectory technique to compute currents to detectors

In the reverse trajectory approach, the current is determined by an integral over the thermal distribution of the incident charged particles. The flux to a specific location between θ_{min} and θ_{max} of the normal and with speeds between v_{min} and v_{max} is given by the integral[40]

$$n\left(\frac{m}{2\pi e\theta}\right)^{3/2}\int_{v_{min}}^{v_{max}}\int_{\cos(\vartheta_{max})}^{\cos(\vartheta_{min})}\int_{0}^{2\pi} d\varphi\, d\cos\vartheta\, v^2 dv\,(v\cos\vartheta)\exp\left(-\frac{m}{2e\theta}(\mathbf{v}_\infty-\mathbf{U})^2\right) \qquad (195)$$

where **v**, the velocity incident on the detector, is expressed in spherical coordinates (v, ϑ, φ) with respect to the surface normal, $\mathbf{v}_\infty$ is the velocity at infinity, and **U** is the ram velocity. Portions of phase space for which $\mathbf{v}_\infty$ does not exist, do not contribute to the integral. The $\mathbf{v}_\infty$ value corresponding to a **v** exists only when the trajectory of the particle with incident velocity **v** connects with infinity, *i.e.*, exits the computational space. Energy conservation relates the magnitude of $\mathbf{v}_\infty$ to that of **v**,

$$\frac{m}{2}v_\infty = \frac{m}{2}v^2 + e\phi \qquad (196)$$

where ϕ is the detector surface potential. The exponent includes a dot product, and is therefore a function of the angle between the velocity vector at infinity and the ram vector. It is a complicated function of **v** and in this technique is determined by tracking macroparticles.

When written as a sum, the above integral is

$$n\left(\frac{m}{2\pi e\theta}\right)^{3/2}\sum_{v=v_{min}}^{v_{max}}\sum_{\cos\vartheta=\cos(\vartheta_{max})}^{\cos(\vartheta_{min})}\sum_{\varphi=0}^{2\pi}(\Delta\varphi\Delta\cos\vartheta\Delta v)v^2(v\cos\vartheta)\exp\left(-\frac{m}{2e\theta}(\mathbf{v}_\infty-\mathbf{U})^2\right) \qquad (197)$$

This quantity is computed by generating and tracking a distribution of macroparticles with initial velocities distributed in each of v, cosθ, and ϕ and with weight $n\left(\frac{m}{2\pi e\theta}\right)^{3/2}(\Delta\varphi\Delta\cos\vartheta\Delta v)v^2(v\cos\vartheta)$. The contribution of each macroparticle is the product of its weight and $\exp\left(-\frac{m}{2e\theta}(\mathbf{v}_\infty-\mathbf{U})^2\right)$ where $\mathbf{v}_\infty$ is the velocity when it exits the computation space. Those macroparticles that intersect the object do not contribute.

3.8 Particle-in-Cell Tools

3.8.1 Transverse Surface Currents

We developed a pseudopotential approach (similar to the velocity potential used to describe potential flow[41] in fluid dynamics) to the solution of the current continuity equation for the computation of transverse surface currents on a spacecraft acting as an antenna. As a boundary condition, one surface element of each antenna element is specified as connected to the biasing power supply, and the solution provides the required current. The vector transverse surface current in each surface element is that which provides the best fit to the edge currents.

A solution having no circulating currents is guaranteed if we assign a pseudopotential value to each element of surface and take the current across their common edge to be proportional to the difference in their pseudopotentials. (In that case, current that flows “downhill” would need to flow back “uphill” in order to circulate.) The current is also taken as proportional to the edge length and inversely proportional to the distance between the centers of the elements.

The result of the above treatment is a matrix that multiplies the vector of pseudopotentials to describe the buildup of charge in the surface elements, which is then set equal to the source vector generated from *Nascap-2k* results at each timestep. This system of equations is then solved using the ICCG (Incomplete Cholesky Conjugate Gradient)[42] algorithm.

Figure 23 shows graphically the quantities that make up the surface current equation for each surface element. Moving the surface currents to the left side of the equation, and all other (known) quantities to the right, and expressing the edge currents as proportional to pseudopotential differences, results in a sparse symmetric matrix that is amenable to solution using the ICCG algorithm once the surface element connected to the power supply (denoted the “injection element”) is set to a fixed pseudopotential. The current required to bias the conductor may be obtained by evaluating the equation associated with the injection element and can be verified to be the sum of the total change in charge less plasma currents for all the remaining surfaces of the conductor. Surface currents are solved separately for each electrically isolated component.

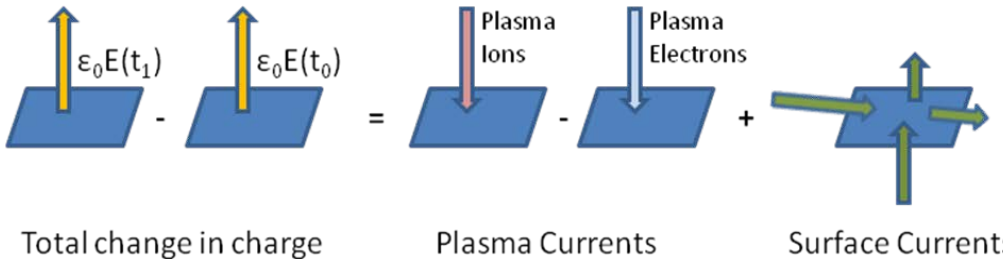

Figure 23. The Change in Charge on a Surface Element is Comprised of Plasma Currents and Surface Currents.

3.8.2 Propagating Fields

The transverse surface currents, the volume ion currents computed during particle tracking, and the volume electron currents computed from tracking or saved in the database by an external code, are a source of propagating electromagnetic fields. *Nascap-2k* can compute the magnetic field, the vector potential, and the rate of change of the vector potential from these currents.

$$\mathbf{A}(\mathbf{r}) = \sum_i \frac{\mathbf{j}_i^{\text{trans}} A_i}{|\mathbf{r}-\mathbf{r}_i|} + \sum_k \frac{\mathbf{j}_k^{\text{ion}} V_k}{|\mathbf{r}-\mathbf{r}_k|} + \sum_k \frac{\mathbf{j}_k^{\text{elec}} V_k}{|\mathbf{r}-\mathbf{r}_k|} \tag{198}$$

$$\mathbf{B}(\mathbf{r}) = \sum_i \frac{\mathbf{j}_i^{\text{trans}} \times (\mathbf{r}-\mathbf{r}_i) A_i}{(\mathbf{r}-\mathbf{r}_i)^2} + \sum_k \frac{\mathbf{j}_k^{\text{ion}} \times (\mathbf{r}-\mathbf{r}_k) V_k}{(\mathbf{r}-\mathbf{r}_k)^2} + \sum_k \frac{\mathbf{j}_e^{\text{elec}} \times (\mathbf{r}-\mathbf{r}_k) V_k}{(\mathbf{r}-\mathbf{r}_k)^2} \tag{199}$$

$$\mathbf{E}_{\text{trans}}(\mathbf{r}, t_m) = -\frac{dA(\mathbf{r}, t_m)}{dt} = -\frac{\mathbf{A}(\mathbf{r}, t_m) - \mathbf{A}(\mathbf{r}, t_{m-1})}{t_m - t_{m-1}} \tag{200}$$

$$\mathbf{P}(\mathbf{r}, t) = \varepsilon_o c^2 E(\mathbf{r}, t) \times \mathbf{B}(\mathbf{r}, t) \tag{201}$$

where the sums are over the surface elements (i) and volume elements (k) and t_m is the time at the present timestep, and P(r,t) is the Poynting vector.

3.8.3 Electron Currents (Using Pseudopotential)

The external code included with *Nascap-2k* provides a non-PIC (Particle-In-Cell) method to calculate volume electron currents that satisfy the equation of continuity and are consistent with an ion dynamics simulation. The volume electron current, $\mathbf{j}_{\text{elec}}$ is taken to be proportional to the gradient of a "pseudopotential," ψ: $\mathbf{j}_{\text{elec}} = \boldsymbol{\sigma} \nabla \psi$, where the conductivity tensor, $\boldsymbol{\sigma}$, depends on the electron density and magnetic field. The equation

$$-\nabla \cdot \boldsymbol{\sigma} \nabla \psi = \frac{d\rho_{\text{elec}}}{dt} \tag{202}$$

is solved by minimizing the function

$$\int dV\left(\frac{1}{2}\nabla\psi\cdot\boldsymbol{\sigma}\nabla\psi-\psi\frac{d\rho_{elec}}{dt}\right) \tag{203}$$

Like the solution to Poisson's equation, the integrals are calculated for each volume element. The pseudopotential is taken to be trilinear within each volume element, so it is given by

$$\psi^{e}(\mathbf{x})=\sum_{i}N_{i}(\mathbf{x})\psi_{i} \tag{204}$$

where "i" are the nodes of the element indexed by "e", and the N_i are the interpolants. Within each volume element, the integral is given by

$$\frac{1}{2}\sum_{ij}\psi_{i}\psi_{j}\int_{V_e}\sum_{\alpha\beta}\left(\sigma_{\alpha\beta}(\mathbf{B},\rho_{elec})\frac{dN_{i}(\mathbf{x})}{dx_{\alpha}}\cdot\frac{dN_{j}(\mathbf{x})}{dx_{\beta}}\right)dV-\sum_{i}\psi_{i}\int_{V_e}\left(N_{i}(\mathbf{x})\frac{d\rho_{elec}}{dt}\right)dV \tag{205}$$

As $\boldsymbol{\sigma}$ and ρ_{elec} are taken to be constant within each volume element, the integrals depend only on the volume size and shape. To minimize the volume integral in Equation (205), we set its derivative with respect to ψ equal to zero. Thus the equation to be solved is

$$\sum_{ej}A_{ij}^{e}\psi_{j}=\sum_{e}\frac{d\rho_{elec}}{dt}\int_{V_e}N_{i}(\mathbf{x})dV \quad , \tag{206}$$

with the finite element matrix for each element given by

$$A_{ij}^{e}=\frac{1}{2}\sum_{\alpha\beta}\sigma_{\alpha\beta}(\mathbf{B},\rho_{elec})\int_{V_e}\frac{\partial N_{i}}{\partial x_{\alpha}}\frac{\partial N_{j}}{\partial x_{\beta}}dV \tag{207}$$

The 576 (8 × 8 × 3 × 3) matrix elements of $\int\frac{\partial N_{i}}{\partial x_{\alpha}}\frac{\partial N_{j}}{\partial x_{\beta}}dV$ are precomputed for the unit cube. For each element, A_{ij} is an 8×8 matrix depending on **B** and ρ_{elec}. Because the conductivity tensor is anisotropic for $\mathbf{B}\neq 0$, matrix elements that are zero in the scalar case become nonzero in the presence of magnetic field.

The right hand side is formed by adding one-eighth of the charge density derivative (formed by differencing the present electron charge density with that at the previous timestep) for each volume element to each of its nodes after multiplying by the cube of the mesh size. The matrix elements are accumulated using a sparse matrix storage scheme for eventual solution using ICCG.

3.8.3.1 Boundary Conditions

Inner Boundary Conditions (Object Currents)

The solution is not extended to the special elements (those containing surfaces). Rather, the following boundary condition is applied: Electron current flows through the boundary between an empty and a special cell if the electric field points away from the special cell, and no electron current flows in the opposite polarity.

If an empty volume element neighbors a special element and has its electric field pointing away from the special element, then electrons are assumed to flow across the interface to the special element at the local plasma thermal current. Each of the four nodes on the corresponding face has its right hand side augmented by $\frac{1}{4}(\Delta x)^2 j_{th} \frac{\rho_{elec}}{\rho_a}$, where j_{th} is the electron plasma current in the ambient plasma and ρ_a is the ambient plasma density. If the electric field points toward the special element, then no electron current crosses the interface, and no action is taken.

Outer Boundary Conditions

The pseudopotential is assumed to vary inversely with radius (measured from the grid center) outside the computational space. As a consequence, for each outer boundary square, each of its nodes is assigned an additional diagonal matrix element given by $\sum_{\alpha\beta} \frac{\Omega}{4r} \sigma_{\alpha\beta} r_\alpha r_\beta$, where Ω is the solid angle subtended by the outer boundary square relative to the grid center, **r** is the vector from the grid center, and **σ** is the conductivity tensor.

3.8.3.2 Grid Interface

Grid interfaces are constrained to have the resolution of the coarser grid. The dislocations at grid interfaces can make convergence to a stable solution difficult.

Since the matrix elements for the entire computational grid are accumulated in order to use an ICCG solver, the matrix must be modified to place constraints on inner grid boundary nodes and assign matrix elements generated in the boundary volumes of the inner grid to outer grid nodes.

3.8.3.3 Upwind Correction

An upwind technique is used to reduce discontinuities at grid interfaces. The input current to each element is calculated, and then the magnitude of the cell current (now redefined as output current) is adjusted (after accounting for the known charge accumulation rate) to maintain charge conservation. The current direction calculated by the finite element solution is preserved. The following algorithm is used.

Conservation of charge in volume element i can be written as $(I_{in} - I_{out})\Delta t = \Delta q$, where I_{in} is the current of electrons flowing into element i from neighboring volume elements, I_{out} is the current of electrons flowing from element i to neighboring volume elements, and Δq is the change in electron charge observed in the simulation: $I_{in} = \sum_{j \ni \mathbf{J}_j \cdot \mathbf{n}_{ij} > 0} \mathbf{J}_j \cdot \mathbf{n}_{ij} A_{ij}$, where J_j is the calculated

electron current density in neighboring cell j, $\mathbf{n}_{ij}$ is the outward normal from cell i into cell j, A_{ij} is the interface area between the two cells, and the inequality restricts the sum to volume elements j from which electrons flow into element i. Similarly, $I_{out} = -\sum_{j \ni \mathbf{J}_i \cdot \mathbf{n}_{ij} < 0} \mathbf{J}_i \cdot \mathbf{n}_{ij} A_{ij}$, where the inequality now restricts the sum to volume elements *j* to which electrons flow from element *i*. We can make conservation of charge true by scaling the current in volume element i: $\mathbf{J}_i \rightarrow \mathbf{J}_i \frac{I_{in}\Delta t - \Delta q}{I_{out}}$. However, this affects the conservation of charge in "downwind" cells, so an iterative "relaxation" process must be implemented to achieve an improved solution.

Five iterations of this algorithm are applied.

REFERENCES

1. J.R. Stevens, A.L. Vampola, Eds., *Description of the Space Test Program P78-2 Spacecraft and Payloads*, USAF Space Division, El Segundo, CA, SAMSO TR-78-24, 1978.

2. I. Katz, G.A. Jongeward, V.A. Davis, M.J. Mandell, R.A. Kuharski, J.R. Lilley, Jr., W.J. Raitt, D.L. Cooke, R.B. Torbert, G. Larson, and D. Rau, Structure of the bipolar plasma sheath generated by SPEAR I, *JGR, 94*, A2, p. 1450, 1989.

3. M.J. Mandell, G.A. Jongeward, D.L. Cooke, W.J. Raitt, SPEAR 3 flight analysis: Grounding by neutral gas release and magnetic field effects on current distribution, *JGR 101*, A1, p. 439, 1998.

4. V.A. Davis, M.J. Mandell, D.L. Cooke, and C.L. Enloe, High-voltage interactions in plasma wakes: Simulation and flight measurements from the Charge Hazards and Wake Studies (CHAWS) experiment, *JGR, 104*, A6, p. 12445, 1999.

5. S. A. Brebbia, *Boundary Element Methods*, Springer Verlag, New York, 1981.

6. C.K. Purvis, H.B. Garrett, A.C. Whittlesey, N.J. Stevens, *Design Guidelines for Assessing and Controlling Spacecraft Charging Effects*, NASA TP 2361, 1984.

7. V.A. Davis, L.W. Duncan, *Spacecraft Surface Charging Handbook*, PL-TR-92-2232, Maxwell Laboratories, Inc., La Jolla, CA, Nov 1992.

8. H.B. Garrett, The charging of spacecraft surfaces, *Rev. of Geophysics and Space Physics, 19*, 4, p. 577, 1981.

9. E.C. Whipple, Potentials of surfaces in space, *Reports on Progress in Physics, 44*, p. 1197, 1981.

10. R. L. Guernsey and J. H. M. Fu, Potential Distribution Surrounding a Photo-Emitting Plate in a Dilute Plasma, *J Geophys Res, 75*, 3193, 1970.

11. R. E. Ergun, D. M. Malaspina, S. D. Bale, J. P. McFadden, D. E. Larson, F. S. Mozer, N. Meyer-Vernet, M. Maksimovic, P. J. Kellogg, and J. R. Wygant, Spacecraft charging and ion wake formation in the near-Sun environment, *Physics of Plasmas 17*, 072903, 2010.

12 T. Nakagawa, T. Ishii, K. Tsuruda, H. Hayakawa, T. Mukai, Net current density of photoelectrons emitted from the suface of the GEOTAIL spacecraft, *Earth Planets Space, 52*, p. 283, 2000.

13. M.J. Mandell, P.R. Stannard, I. Katz, *NASCAP Programmer's Reference Manual*, NASA CR 191044.

14. I. Katz, D.E. Parks, M.J. Mandell, J.M. Harvey, D.H. Brownell, Jr., S.S. Wang, M. Rotenberg, *A Three Dimensional Dynamic Study of Electrostatic Charging in Materials*, NASA CR 135256, 1977.

15. O. Hackenberg and W. Brauer, Secondary electron emission from solids, *Advances in electronics and electron physics*, edited by L. Marton, Academic Press, New York, P. 413, 1959.

16. C. Feldman, Range of 1 -10 keV electrons in solids, *Phys. Rev 117*, p. 455, 1960.

17. J.C. Ashley, C.J. Tung, V.E. Anderson, R.H. Richie, Inelastic interactions of electrons with polystyrene: calculations of mean free path, stopping powers and CSDA ranges, *IEEE Trans Nucl Sci, NS-25*, p. 1566, 1978.

18. E.J. Sternglass, Theory of secondary electron emission by high speed ions, *Phys Rev, 108*, 1, p. 1, 1957.

19. B. Aarset, R.W. Cloud, and J.G. Trump, Electron emission from metals under high-energy hydrogen ion bombardment, *J App Phys, 25*, p. 1365, 1954.

20. P. Cousinie, N. Colombie, C. Fert., and R. Simon. Variation du coefficient e'emission electronique secondaire de qualques metaux avec l'energie des ions incidents, *Comptes Rendus, 249*, p. 387, 1959.

21. G. Foti, R. Potenza, and A. Triglia, Secondary-electron emission from various materials bombarded with protons at Ep < 2.5 MeV, *Lettere al Nuovo Cimento, 11*, p. 659, 1974.

22. A.G. Hill, W.W. Buechne, J.S. Clark, and J.B. Fisk, The emission of secondary electrons under high-energy positive ion bombardment, *Phys Rev, 55*, p. 463, 1939.

23. I. Katz, D.E. Parks, M.J. Mandell, J.M. Harvey, S.S. Wang, and J.C. Roche, NASCAP, A three-dimensional charging analyzer program for complex spacecraft, *IEEE Trans on Nucl Sci, NS-24*, 6, p. 2276, 1977.

24. T.E. Everhart, Simple theory concerning the reflection of electrons from solids, *J Appl Phys, 31*, p. 1483, 1960.

25. W.S. McAfee, Determination of energy spectra of backscattered electrons by use of Everhart's theory, *J Appl Phys, 47*, p. 1179, 1976.

26. E.H. Darlington, and V.E. Cosslett, Backscattering of 0.5 - 10 keV electrons from solid targets, *J Phys D5*, 22, p. 1969, 1972.

27. R. Shimizu, Secondary electron yield with primary electron beam of kilo-electron-volts, *J Appl Phys, 45*, 5, p. 2107, 1974.

28. I. Langmuir, K.B. Blodgett, Currents limited by space charge between concentric spheres, *Phys. Rev., 24*, p. 49, 1924.

29. D.D. Child, Discharge from Hot CaO, *Physical Review, 32*, p. 492, 1911.

30. I. Langmuir, The effect of space charge and residual gases on thermionic currents in high vacuum, *Physical Review 2*, p. 450, 1913.

31. V.A. Davis, M.J. Mandell, F.J. Rich, D.L. Cooke, Reverse Trajectory Approach to Computing Ionospheric Currents to the Special Sensor Ultraviolet Limb Imager on DMSP, *IEEE Trans Plasma Sci, 34*, p. 2062, 2006.

32. H. Goldstein, *Classical Mechanics,* Addison-Wesley, 1959.

33. V.A. Davis, M.J. Mandell, G.A. Jongeward, *Computing Surface Charging In The Auroral Environment Using Nascap-2k*, AFRL-VS-TR-2003-1606, Leidos, Inc. San Diego, CA, May 2003.

34. S. A. Brebbia, *Boundary Element Methods*, Springer Verlag, New York, NY, 1981.

35. S. M. Selby, *Standard Mathematical Tables*, CRC Press, Cleveland, OH, 1975.

36. M. J. Mandell, I. Katz, G. W. Schnuelle, P. G. Steen, J. C. Roche, The decrease in effective photocurrents due to saddle points in electrostatic potentials near differentially charged spacecraft, *IEEE Trans. Nucl. Sci. NS-25*, 1978.

37. L.W. Parker and E.C. Sullivan, NASA Report No. TN-D-7409, 1974.

38. L.W. Parker, Calculation of sheath and wake structure about a pillbox-shaped spacecraft in a flowing plasma, *Proceedings of the Spacecraft Charging Technology Conference*, AFGL-TR-77-0051, NASA TMX-73567, 1977.

39. V.A. Davis, M.J. Mandell, S.L. Huston, B.M. Gardner, *Plasma Interactions with Spacecraft*, Vol 1, AFRL-RV-PS-TR-2011-0089, Leidos, Inc., San Diego, CA, 2011.

40. L.W. Parker, Calculation of sheath and wake structure about a pillbox-shaped spacecraft in a flowing plasma, Proceedings of the spacecraft charging technology conference, 1977, AFGL-TR-77-0051, NASA TMX-73537, p. 331, 1977.

41. Author unknown, Potential flow, Wikipedia entry, http://en.wikipedia.org/wiki/Potential_flow, accessed on February 20, 2014.

42. D.S. Kershaw, The incomplete Cholesky-conjugate gradient method for the iterative solution of systems of linear equations, *J Comp Phys, 26*, p. 43, 1978.

LIST OF SYMBOLS

The symbols in the following table are used in this document.

b_i	Range parameters
d	Thickness or distance
e	Magnitude of the electron charge (1.60×10^{-19} C)
f	Distribution function
g	Reduction in plasma density in wake in the absence of surface potentials
i and j and k and m	Indices
j_{th}	Plasma thermal current
j_x	Component of the current
l	Length
m	Particle mass
n	Component density
n_a	Ambient plasma density
n	Surface normal or unit vector
p	Magnetic moment
q	Charge on a surface or particle charge
q_i	Range parameters
r	Distance or location in space
$\mathbf{r}_o$	Location of magnetic moment
s	Axes of sun pointing coordinate system
t	Time
v or **v**	Velocity
u or *v*	Parameters in BEM
x or **x**	Position or path length
y	Substitute integrand

A	Area or Point of triangle in BEM discussion
A	BEM or pseudopotential matrix
B and B	Magnetic field and magnetic field magnitude or point of triangle in BEM discussion
B_{max}	Estimate of maximum possible barrier height to the escape of photoelectrons
C	Capacitance or point of triangle in BEM discussion or Convergence factor or coefficient
D_{CL}	Child Langmuir distance
D	Electric field (in Maxwell equation)
E	Particle energy in eV
E and E	Electric field and electric field magnitude
E_o	Parameter of Gaussian component of Fontheim distribution function
E_1	Barrier height to escape of photoelectrons
E_{max}	Energy at which secondary yield due to normally incident electrons peaks
F	Flux or interpolant
F	BEM matrix
G	BEM matrix
H	Heaviside step function
G	Interpolant
I	Current (amperes)
I	Current vector
I_{sun}	Relative sun intensity
J	Current density vector
L	Mesh spacing or lower limit of energy or velocity integral
N	Number of nodes of surface element
N_i	Interpolant
P or **P**	Point of triangle in BEM discussion or point in volume or Poynting vector
Q	Finite element matrix

R	Resistance or Sphere radius or Escape depth (range) or point in volume
S	Surface area or Stopping power or Surface index or reduced charge density
ΔT	Time interval
T	Pairwise scalar products in BEM
U	Velocity of plasma with respect to spacecraft, $-V_{sc}$
V	Volume or BEM coefficients
V_{sc}	Spacecraft velocity
W	Finite element matrix
Y	Yield
Z	Atomic number
α	Parameter used in ion secondary yield or Parameters used in space charge limiting or parameter used to specify power law component of Fontheim distribution function
β	Parameter used in ion secondary yield
χ	Angle between flow vector and the particle velocity
δ_{max}	Peak yield for normal incidence
ε_o	Permittivity of vacuum (8.854×10^{-12} F m^{-1})
ε	Relative dielectric constant
ϕ	Surface potential or Space potential
ϕ_b	Barometric potential
η	Backscatter coefficient or Fraction of the distribution
κ	Parameter used in kappa distribution function
λ_D	Debye length
ν	Iteration index
θ	Plasma temperature in eV
ρ	Resistivity or Charge density
σ or $\boldsymbol{\sigma}$	Surface charge density or conductivity tensor

σ_{CEX}	Charge exchange cross section
ξ	Small number used to evaluate current integral
ψ	Incident angle or Angle between neutralizer axis and look direction or pseudopotential
ζ	Coefficient in Fontheim formula
Δ_{gauss}	Parameter of Gaussian component of Fontheim distribution function
$\Delta\phi$	Difference in potential across dielectric layer
$\mathbf{\Phi}$	Potential vector
Ω	Solid angle

DISTRIBUTION LIST

DTIC/OCP
8725 John J. Kingman Rd, Suite 0944
Ft Belvoir, VA 22060-6218 1 cy

AFRL/RVIL
Kirtland AFB, NM 87117-5776 2 cys

Official Record Copy
AFRL/RVBXR/Adrian Wheelock 1 cy